Fall 2009

Near-Infrared Analysis and Process Control of Pharmaceutical Pelletization Processes

David J. Wargo

NEAR-INFRARED ANALYSIS AND PROCESS CONTROL OF PHARMACEUTICAL PELLETIZATION PROCESSES

A Dissertation

Submitted to the Graduate School of Pharmaceutical Sciences

Duquesne University

In partial fulfillment of the requirements for

the degree of Doctor of Philosophy

By

David J. Wargo

December 2009

NEAR-INFRARED ANALYSIS AND PROCESS CONTROL

OF PHARMACEUTICAL PELLETIZATION PROCESSES

By

David J. Wargo

Approved June 21, 2005

James K. Drennen, III, Ph.D.
Associate Professor of Pharmaceutics
Associate Dean for Graduate Programs & Research
Mylan School of Pharmacy
(Committee Chair)

Lawrence H. Block, Ph.D.
Professor of Pharmaceutics
Graduate School of Pharmaceutical Sciences
(Committee Member)

Carl A. Anderson, Ph.D.
Associate Professor of Pharmaceutics
Graduate School of Pharmaceutical Sciences
(Committee Member)

Peter Wildfong, Ph.D.
Assistant Professor of Pharmaceutics
Graduate School of Pharmaceutical Sciences
(Committee Member)

Mitchell E. Johnson, Ph.D.
Associate Professor of Chemistry
Bayer School of Natural & Environmental Sciences
(Committee Member)

David A. Johnson, Ph.D.
Director of Graduate Studies
Associate Professor of Pharmacology-Toxicology
Graduate School of Pharmaceutical Sciences

J. Douglas Bricker, Ph.D.
Dean, Mylan School of Pharmacy and the
Graduate School of Pharmaceutical Sciences

ABSTRACT

NEAR-INFRARED ANALYSIS AND PROCESS CONTROL
OF PHARMACEUTICAL PELLETIZATION PROCESSES

By

David J. Wargo

December 2009

Dissertation supervised by James K. Drennen, III, Ph.D.

This study explored the potential of near-infrared spectroscopy in the determination of pharmaceutical pellet characteristics and to predict desired process endpoints during fluidized bed drug suspension layering and coating operations. Various strengths of diltiazem HCl pellets were prepared via a tangential-spray rotogranulation process and subsequently coated Eudragit RS30D in a Wurster column. In-line and at-line near-IR process monitoring methods were evaluated. Quantitative calibrations for potency, applied polymer solids and dissolution were developed using several different regression models. Both in-line and at-line determinations of pellet potency were effectively accomplished with average standard errors of prediction of 1.11% and 0.63%, respectively. Near-IR prediction of pellet potency of pilot-scale batches was also achieved using data from laboratory-scale experiments. For Wurster coating operations,

in-line and at-line near-IR regression models for predicting applied polymer solids were developed which demonstrated R^2 values of 0.98 or greater and standard errors of calibration less than 0.6%. Prediction of a t50% dissolution metric within 7 minutes of actual values was possible for pellets exhibiting 8 to 12 hour release characteristics. Qualitative assessment of applied polymer solids was also accomplished using Mahalanobis distance and bootstrap pattern recognition algorithms. This study has demonstrated the potential of near-IR spectroscopy in quantitative and qualitative assessment of pelletized pharmaceutical product characteristics and in the identification of process endpoints. Future implementation of these techniques could potentially reduce production cycle-times associated with the acquisition of laboratory test results and ensure product quality compliance throughout various stages pellet manufacturing.

DEDICATION

To my wife, my parents, and all those who have supported and believed in me

ACKNOWLEDGEMENT

I would like to acknowledge many people for helping me during my doctoral work. I would especially like to thank my advisor, Jim Drennen, for his generous time, flexibility, understanding and commitment. Throughout my graduate experience, Jim encouraged me, stimulated my analytical thinking and provided an excellent atmosphere for doing research. It has been a great pleasure to develop scientific skills under his guidance. I would also like to thank Dr. Lawrence Block, Dr. Carl Anderson, Dr. Peter Wildfong, Dr. Mitch Johnson, Dr. David Johnson, and Dean Douglas Bricker for serving on my defense committee. Special thanks goes to Dr. Block for many enjoyable and thought provoking scientific discussions and for long ago instilling in me the desire to pursue graduate education and an industrial pharmacy career.

I would like to thank Mylan Pharmaceuticals and Merck & Co., both which provided support for my research efforts at Duquesne and for Mylan's support while I completed my dissertation.

I would also like to thank John Kirsch, who, as a good friend and colleague, was always willing to help and give his best suggestions. It would have been a lonely lab without him.

I wish to thank my parents who always supported and encouraged me in both personal and professional endeavors. I am also grateful to my children – Jacob, Natalia, and Liam – for allowing me many hours of seclusion as I completed this manuscript. Finally, I would like to thank my wife, Debbie, who has always stood by me through good times and bad. This would not have been possible without her love and support.

TABLE OF CONTENTS

Page

Page

Page

Page

Page

LIST OF TABLES

Page

LIST OF FIGURES

Page

Page

Page

1 INTRODUCTION

1.1 Statement of the Problem

Multiparticulate drug delivery systems have become increasingly popular due to their ability to provide unique release profiles and offer potential clinical benefits. A variety of pelletization technologies have provided the pharmaceutical scientist with tremendous flexibility during solid oral multiparticulate dosage form development. Of the technologies available to produce the particles comprising these systems, layering a suspension or solution of drug onto a seed material can produce pellets that are spherical in shape, have a smooth surface, and are uniform in size and size distribution. These characteristics are especially desirable when the pellets will be subsequently coated to provide some degree of controlled drug release.

The concentration of drug in the core pellet, and the quantity or thickness of the functional polymeric coating present on controlled release pellets are both critical factors affecting the physical integrity of these systems as well as drug release rates. Unfortunately, controlled release pellet production often involves lengthy and expensive manufacturing operations in which there are no simple in-process methods for accurately monitoring drug product potency or the extent of applied coating solids. Typically, researchers and manufacturing personnel must rely on theoretical determinations of applied solids to predict drug layering and coating process endpoints. An assay of the

pellets is necessary prior to encapsulation to determine the fill weight needed to deliver the desired dose. Additionally, dissolution testing of the final dosage form is essential to ensure uniformity of the drug release rate. The development of rapid analytical methods to evaluate pellet core and coating characteristics may reduce production-cycle time associated with the acquisition of laboratory test results and allow product quality to be assessed at various stages of processing prior to completing the manufacture of an entire batch.

The objective of this research was to develop and evaluate new applications of near-IR analysis for monitoring and controlling pharmaceutical pellet production operations, and to investigate the practical limits of the applications described. Both at-line and in-line near-IR spectroscopic methods for evaluating core and coated pellet characteristics, and predicting desired process endpoints were investigated. At the core of this research was the quantitative assessment of core pellet potency and applied polymer solids during rotor drug layering and Wurster coating operations, respectively. This includes modification of processing equipment and the application of a method to permit on-line monitoring of drug layering and polymer film coating processes, as well as the development of a reference technique for the quantification of an ammonio methacrylate sustained-release polymer. The ability of pattern recognition methods to qualitatively predict coating process endpoints was also determined. In addition, this research evaluated the use of near-IR spectroscopy to nondestructively predict drug release (dissolution) characteristics of controlled release pellets. Finally, the ability to utilize laboratory-scale data to assess pellet potency during production scale drug layering operations was investigated, obviating the need to rely on theoretical

determinations of applied drug layering suspension solids for process endpoint identification.

1.2 Literature Review

1.2.1 Pharmaceutical Pellet Dosage Forms

The term "pellet" has been used to define a number of different types of manufactured agglomerates. Pellet products are used in many industries, but in the pharmaceutical industry pellets are generally described as granular or spherical drug containing entities. Pharmaceutical pellets generally range in size from 0.5 to 1.5 mm in diameter (1).

1.2.1.1 Pelletization Rationale

Pelletized products offer flexibility in dosage from design and development, and can be utilized to improve safety and efficacy of bioactive agents. Pellets are attractive as components of dosage forms or as dosage forms themselves. They can be produced by a number of methods and can be incorporated into a number of different traditional dosage forms including capsules (2,3), conventional tablets (4,5), rapidly disintegrating tablets (6), or suspensions (7). Pellets composed of separate drug entities can be blended and formulated in a single dosage form either for simultaneous drug delivery or for delivery to different sites along the gastrointestinal tract. Additionally, combinations of pellets can be utilized to avoid drug substance incompatibilities. Because of their spherical

shape and low surface area to volume characteristics, pellets are excellent substrates for application of immediate or modified release coatings.

Pellets are also advantageous from an *in vivo* perspective. Because pellets disperse freely in the gastrointestinal tract, they provide increased surface area for dissolution and absorption. When coated with modified-release polymers, pellet systems can reduce peak plasma fluctuations, and minimize potential side effects without appreciably lowering bioavailability (8). Pellets also reduce variations in gastric emptying rates and overall transit times thereby minimizing intra- and inter-subject variability of plasma profiles as compared to single-unit dosage forms (9,10). Additionally, because a large number of pellets are administered per dose, the likelihood of dose dumping is dramatically reduced. If several individual pellets were to fail and "dump" their drug content, only a minimal effect on the overall release characteristics of the dosage form would be observed.

1.2.1.2 Pelletization Techniques

Pelletization has been defined as an agglomeration process that converts fine powders or granules of bulk drugs and excipients into small, free-flowing, spherical or semi-spherical units, referred to as pellets (8). A number of methods are available for the manufacture of pellets. The most common pelletization processes used in the pharmaceutical industry are extrusion/spheronization, solution/suspension layering, and powder layering (11). Other processes may include spray drying, spray congealing, and compression of dry powders into spherical compacts. "Balling" is another older process for pelletization in which dry powders are tumbled in a coating pan or drum with

simultaneous application of a binding liquid. In 1949, Smith, Kline & French (SKF) borrowed a process used in the confectionery industry to make pharmaceutical pellets (1). This process used sugar granules as seed cores for the application of powders upon which spherical particles were ultimately built. In the confectionary industry, spherical sugar seeds manufactured by this process, called nonpareils, are still used as decorative toppings for candies and pastries. This same procedure was adapted by SKF for the creation of drug containing pellets. Nonpareils themselves were also used as a starting core in this earliest drug layering technique, a practice still used today.

1.2.1.2.1 Fluid Bed Technology

Fluid bed technology has been used in the pharmaceutical industry for about forty years. It was first employed as an efficient drying technique, which was a dramatic improvement over traditional tray drying. Fluid bed processing now includes drying, granulation, coating and layering. Although pan and fluid bed technology can both be used to coat either tablets or pellets, modified pan coating is generally reserved for tablets, and pellets are almost exclusively processed using fluid bed techniques. The major advantage of these systems over traditional pan coating is enhanced air flow. In the past twenty years, few changes have been made to fluid bed technology other than the introduction of tangential drug layering and coating processes (12-14), and the emergence of fine particle coating techniques (15-17). Unit shape and geometry has, in some applications, become more specialized (18,19).

1.2.1.2.2 Drug Layering

Application of drug and excipients onto a seed material from a solution or suspension can produce pellets that are spherical in shape, have a smooth surface, and are uniform in size and size distribution. This process is similar to traditional coating, in that it involves the application of a dispersed solid onto a core. The dispersion is atomized using a nozzle that produces droplets that hit and spread over the surface of the core. Fluidization air, usually warmer than ambient conditions, aids in evaporation of the dispersion medium which results in deposition of the solid material.

In recent years, tangential-spray pelletization processes have gained considerable attention. This technology utilizes a fluid bed equipped with a rotating disc in the bottom of the fluid bed product container. Originally this technology had been conceived for high-density fluid bed granulation and is now frequently used to produce high-dose pellets by layering drugs on nuclei. A controlled release film may be subsequently applied (12-14).

The rotor processor, as depicted in **Figure 1,** consists of a cylindrically shaped product bowl and an expansion chamber (20). The rotor disk sits at the base of the product bowl seated along the circumference of the chamber when not in motion. The disk is raised during processing to create a slit between the edge of the rotor disk and the conical bottom of the rotor product bowl. The adjustable disk height allows control of air volume through the slit, independent of velocity. This key feature permits very low drying rates for direct pelletization, and pellet growth by powder layering. For coating applications requiring quick evaporation of a medium, the air volume can be significantly

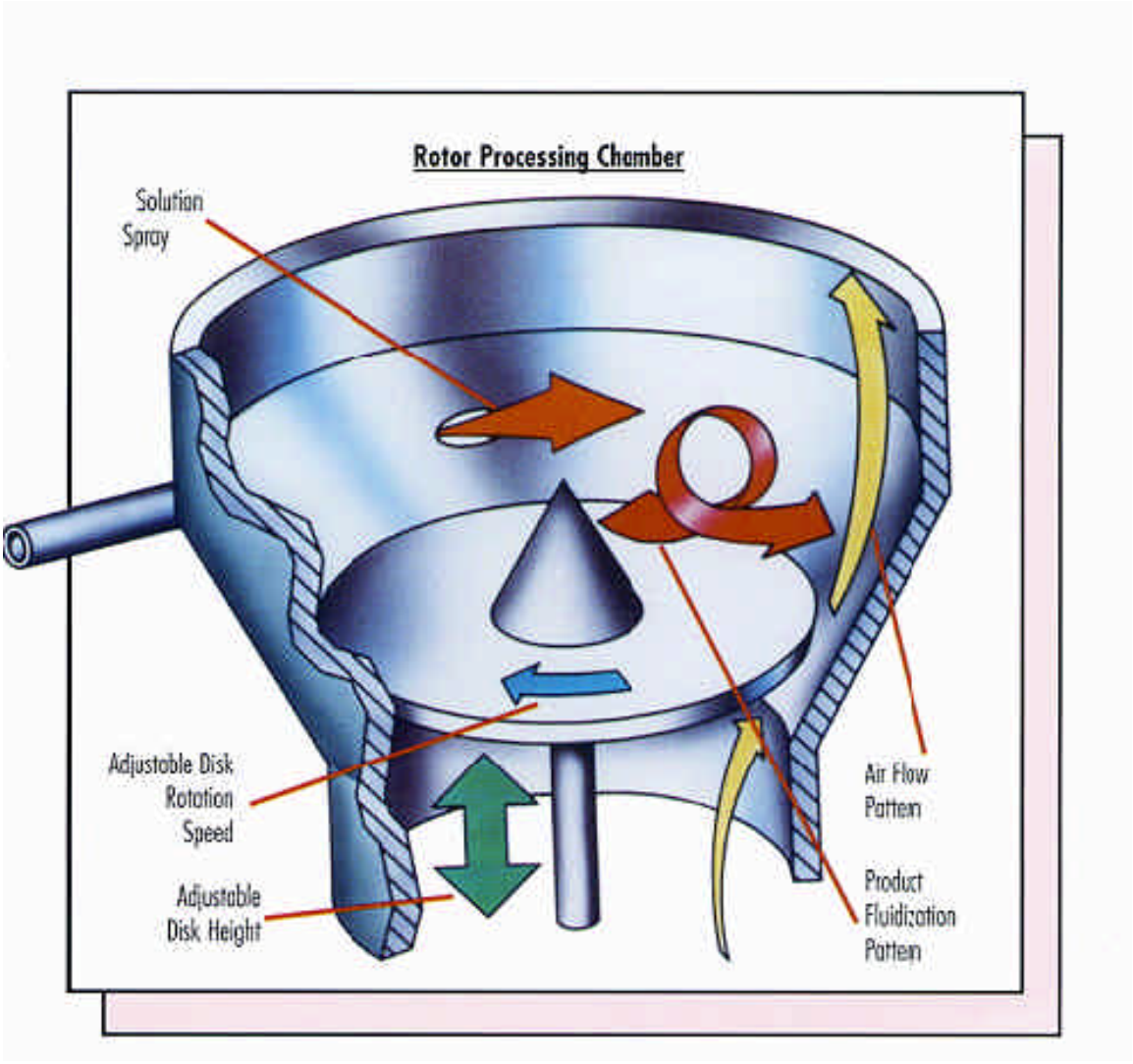

Figure 1. The rotor processor.

Glatt Gmbh. Fluid Bed Coating. http://www.glatt.com /e/01_technologien/ 01_04_08.htm (accessed 09/06/08). part of The Glatt Group. http://www.glatt. com/ (accessed 09/06/08).

increased while keeping air velocity constant. This flexibility results in a single unit processor capable of both layering and coating.

The fluidization pattern in the rotor processor can best be described as a spiraling helix. Three factors act on the product to create this flow pattern. The rotating disk provides centrifugal force which forces the pellets toward the wall of the processing chamber at the periphery of the rotor, while airflow through the slit creates a vertical force causing the product to become fluidized. The fluidization air pushes the product upward into the expansion chamber until gravity overcomes the air velocity and the material falls toward the center of the disk where there is little air movement (12,13). The cycle is repeated many hundreds of times until the appropriate quantity of solids are applied to the core substrate. Liquids or powdered solids can be added to the process through air atomizing nozzles located on the side wall of the product bowl. The nozzles spray tangentially into the processing chamber in the same direction as the fluidization pattern. Using this technique, weight gains of up to 400% w/w relative to the initial bowl charge can be achieved (21-23).

1.2.1.2.3 Wurster Coating

Perhaps one of the most important improvements to fluid bed equipment, especially for the coating of pellets, was the advent of the bottom spray Wurster column (24). The Wurster process is an industry recognized coating technique for precision application of a film coat to particulate materials such as powders, crystals, or granules. This technology can be used to encapsulate solid materials having diameters ranging from approximately 50 μm to several centimeters.

Wurster coating technology, as depicted in **Figure 2**, is characterized by the location of a spray nozzle at the bottom of a fluidized bed of solid particles (20). The particles are suspended in the fluidizing air stream that is designed to induce cyclical flow of the particles past the spray nozzle which delivers atomized coating solution or suspension. The process has a greater drying capacity than other coating systems due to a relatively high fluidizing air velocity. Since the particles actually separate as they are carried away from the nozzle, it is possible to coat small particles without agglomeration (15, 16).

During processing, the atomized coating material collides with the particles as they are carried away from the nozzle. The temperature of the fluidizing air is set appropriately to evaporate solution or suspension vehicle or solidify the coating material shortly after impingement on the particles. All coating solids remain on the particles as a part of the developing film or coating. This process is continued until each particle is uniformly coated to a desired film thickness.

For coating applications, the Wurster system compares favorably to the tangential-spray system, since the three main physical criteria are the same: (i) concurrent spraying, with the nozzle being buried inside the product resulting in minimal droplet travel distance; (ii) uniform exposure of the particles to the spray mist; and (iii) high product density in the spraying zone.

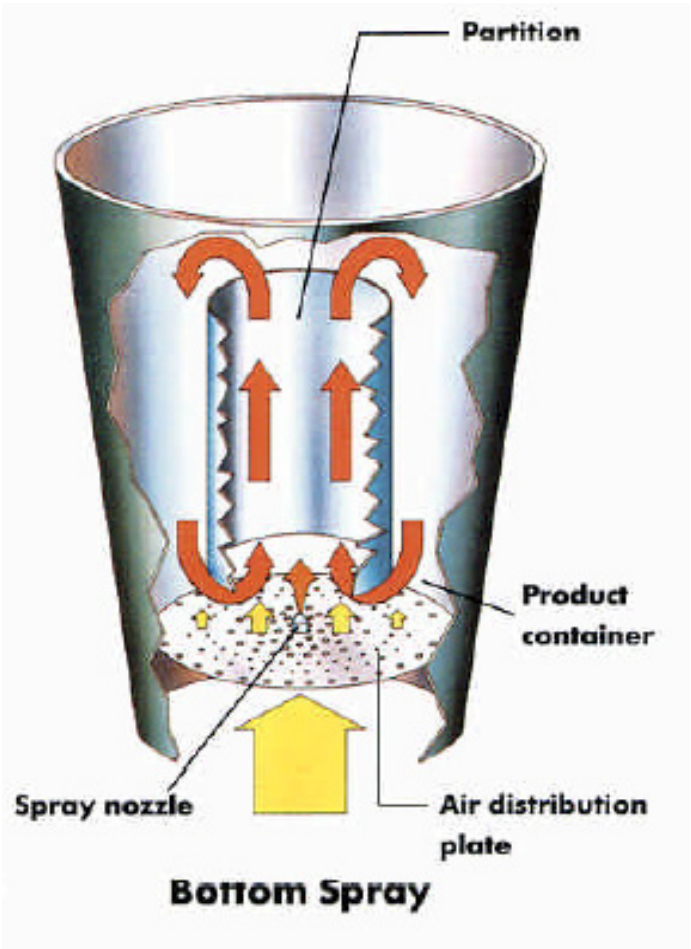

Figure 2. The Wurster Column

Glatt Gmbh. Fluid Bed Coating. http://www.glatt.com /e/01_technologien/ 01_04_08.htm (accessed 09/06/08). part of The Glatt Group. http://www.glatt. com/ (accessed 09/06/08).

1.2.2 Process Analytical Technology

Recently, there has been significant interest in process analytical technology (PAT) within the pharmaceutical industry following the issuance of an FDA guidance document on this subject (25). The FDA's PAT initiative is a push to bring the efficiency of pharmaceutical manufacturing in line with that of other specialty chemical production standards (26). PAT can be described as a system for designing, analyzing, and controlling manufacturing through timely measurements (i.e., during processing) of critical quality and performance attributes of raw and in-process materials and processes, with the goal of ensuring final product quality. The term *analytical* in PAT is broadly viewed and integrates chemical, physical, microbiological, and production mathematical risk analyses. Implementation of PAT should provide a means for better understanding and controlling pharmaceutical manufacturing operations, which is consistent with the FDA's perspective on drug quality systems: *quality cannot be tested into products; it should be built-in or should be by design* (25).

1.2.2.1 Process Analytical Chemistry – History and Concepts

Pharmaceutical PAT has essentially evolved from the concept of Process Analytical Chemistry (PAC), which has gained considerable attention since the mid-1980s because of opportunities presented by technological, methodological, and chemometric advancements, as well as changing needs within the chemical and allied products industries (27-30). Although Callis *et al.* (27) presented a conceptual framework to describe five areas of PAC, the boundary between it and the usual practice of laboratory analysis is still somewhat ambiguous. Nevertheless, the terms at-line, in-

line, off-line, on-line, and non-invasive are referred to throughout PAC and PAT literature. At-line analysis refers to manual sampling with local transport to an analyzer located within a manufacturing area, while in-line methods involve a sample interface located in the process stream (27). Off-line often refers to manual sampling with transport to a remote or centralized laboratory, while on-line analysis usually involves automated sampling and sample transfer to an automated analyzer (27). Callis *et al.* (27) also classified non-invasive sampling as a separate PAC area, however, today it is generally desirable that all process analytical sampling be as non-invasive as possible.

1.2.2.2 Near-infrared Spectroscopy

Although the near-IR region of the electromagnetic spectrum has been studied since the 1800s (31), it was not recognized for its analytical potential until after the Second World War. Modern concepts of this technology were developed in the 1950s at the USDA in an analytical group headed by Karl Norris, who evaluated the potential of near-IR for rapid quality control of agricultural commodities. This work, which demonstrated that non-destructive reflectance near-IR spectra of biological samples could be used for analytical purposes, lead to the widespread use of near-IR in the agricultural field (32).

Near-infrared spectroscopy (near-IR) has become the method of choice for many industrial process analytical applications because it is rapid, nondestructive and noninvasive. The widespread growth of this technology has primarily been the result of significant advancements in high speed computing. Additional developments in optical instrumentation, chemometric methods and spectral data analysis software have lead to

various applications of this technique in the petrochemical, pulp, paper, biomedical, and pharmaceutical industries. A number of books (33-35) and review articles (36-39) have been published on the theoretical aspects of near-IR and its applications. Additional papers devoted to pharmaceutical applications of near-IR spectroscopy have also been published (40-45).

1.2.2.2.1 Near-IR Theory

When molecules are irradiated with an external source of energy, they acquire the potential for energy changes. The electromagnetic spectrum consists of energy vibration ranging from wavelengths several meters in length to those less than 10^{-2} nm. The near-infrared region of the electromagnetic spectrum lies between about 750 – 2600 nm (46).

Murray and Williams (46) have provided an excellent description of near-infrared energy absorption. When photon energy (energy related to the wavelength at which the irradiation is emitted) is absorbed by a molecule, the rotational, vibrational, or electromagnetic energy of the molecule is elevated by a discrete amount that is equivalent to the energy applied. Molecules can only absorb energy that is coincident with the characteristic vibrations of the molecule and that can result in the molecule being excited to a higher energy level. When infrared radiation is absorbed by a molecule, the energy status of the molecule changes. The vibrational and rotational quantum numbers are representative of these changes. The magnitude of the rotational energy is lower than that of vibrational energy, but the energy level of a molecule is the sum of the vibrational and rotational energies. Most of the molecules in a substance are normally in the lowest energy level, or ground state, however, when an external source of energy is applied, the

molecules absorb photon energy and jump from the ground state to the next highest vibrational or rotational energy level, constituting the absorption process. Fundamental absorptions usually occur in the mid-infrared region between 2,500 and 15,000 nm. Other molecules will absorb enough energy to reach the next second energy level, represented the first overtone band. Since fewer molecules reach this level, the first overtone band is generally much weaker in intensity than the fundamental absorption. Still fewer molecules reach the third energy level, which is the second overtone. First and second overtones occur at approximately one-half and one-third of the wavelength of the fundamental. Higher energy levels are available, but fewer and fewer molecules attain these levels, therefore the third and higher overtones appear as even weaker bands relative to the fundamental. Deviation in the overtone absorption band frequencies from theoretical frequencies is due to anharmonicity (deviation from the law of harmonic vibration) of the chemical bonds involved (46). Vibrational energy changes are usually accompanied by a larger number of rotational changes and, therefore, appear as bands.

All molecules and parts of molecules have vibrations at characteristics wavelengths. In each model of vibration, all of the functional groups of atoms of the same type in a molecule vibrate with the same frequency. The two main modes of molecular vibrations are stretching and bending (46). Stretching is movement along the axes, so that the distance between the atoms changes rhythmically. Bending involves changes in bond angle between atoms. Only vibrations that result in rhythmic changes in the dipole moment of a molecule can cause absorbance in the infrared (46). Most fundamental resonant molecular vibrations occur at frequencies outside the near-infrared region, with bands seen in the near-infrared being the overtones or combinations of the

fundamentals, which are usually of higher intensity than the overtones (46). The intensity of overtone and combination bands depends on the degree of anharmonicity, and these different modes of vibration give rise to the bands observed in the near-IR region. The majority of overtone peaks arise from the R -H stretching mode (i.e., C-H, O-H, N-H, S-H) since vibrations of the hydrogen atom appear to be particularly susceptible to anharmonicity (46, 47). Therefore, the absorption bands observed in the near-IR region arise from overtones of stretching vibrations involving functional groups with hydrogen atoms or combinations involving stretching and bending modes of vibrations of these groups.

The majority of active pharmaceutical ingredients and excipients possess functional groups (i.e., -C-H, -O-H, -N-H, etc.) that absorb in the near-infrared region. In addition, the low molar absorptivity of most of these compounds in the near-IR region allows samples to be analyzed in their native state, requiring little or no preparation or dilution prior to analysis. Broad overlapping bands observed using this technique also provide a means for performing both quantitative and qualitative analyses.

1.2.2.2.2 Diffuse Reflectance

Reflectance spectroscopy measures the light reflected from a sample. The incident beam of light is divided into two parts: transmitted light and reflected light. The reflected light is comprised of both specular and diffuse components. The specular component, described by Fresnel's law, contains little information about sample chemical composition, consequently, its contribution to measurements is minimized by adjusting the detector's position relative to the sample (48,49). It can be eliminated through

appropriate optic designs. Diffuse reflection, however, is the result of the simultaneous absorption and scattering of light from the sample and contains information regarding physicochemical properties of potential interest. In practical applications, a simple relationship between the concentration of a component and reflected intensity, which is a direct analog of Beer's law, is

$$Log(\frac{1}{R}) = a * C \qquad \text{(Eq. 1)}$$

where R is the intensity of diffusely reflected light, a is the absorptivity of the material, and C is the concentration.

In reflectance mode, the sample must be sufficiently thick to present an infinite pathlength. All incident light is absorbed or reflected, and only the reflected light is measured. In reflectance mode, both specular and diffuse components are superimposed so that the path length cannot be kept constant and will vary with sample packing. Reflectance, refraction, transmittance, and absorbance will take place depending on both the chemical and physical properties of the sample pack (46). This scattering alters the proportion of absorbed and reflected radiation so that path length becomes an additional unknown along with concentration in Beer's law. Thus, even if only one component were known to absorb at just one wavelength, it would be necessary to solve a pair of simultaneous equations relating path length and concentration to optical density at the two wavelengths (46).

Several factors affect the linearity of Beer's law in near-IR diffuse reflectance analysis (46). One is the difference in the linearity of response of the lead sulfide (PbS)

detectors that are responsible for making the measurement and differences in path length caused by particle characteristics. Another factor is the influence of temperature, which at different wavelengths, can cause shifts to longer or shorter wavelengths, depending on the temperature and position of the band. Such factors can be compensated for by instrument design, and residual deviations from linearity are corrected by log 1/R transformation of the spectra.

1.2.2.3 Chemometrics

Chemometrics is a term used to describe the application of mathematics, statistics, and logic-based methods to derive meaningful chemical information from complex samples. The theoretical foundations of many commonly employed chemometric techniques were developed decades ago. However, the practical application of these methods has relied on advancements in computer technology and the availability of chemometric software.

Unlike other more traditional aspects of analytical chemistry, chemometrics is not associated with any particular instrumental method for measuring chemical data. Chemometric models have been employed to resolve analytical problems in a variety of scientific disciplines ranging from organic synthesis to electrical engineering. Although the breadth of this field makes it difficult to comprehensively review all aspects of chemometric research, Brown *et al.* (50) have published an extensive review of this topic. Review articles discussing chemometric applications to pharmaceutical and biomedical analysis have been presented by several authors (51,52). The following discussion

examines several chemometric techniques commonly employed in the near-infrared analysis of pharmaceuticals.

1.2.2.3.1 Spectral Preprocessing

Most near-IR instruments measure relative reflectance, *R*. Relative reflectance is computed as the ratio I_s/I_r, where I_s is the intensity of radiation reflected from the sample and I_r is the intensity of radiation reflected from a reference standard. Reflectance standards are commonly manufactured as flat disks composed of materials such as ceramic or PTFE (Spectralon®), both of which are highly reflective to near-IR radiation.

The depth of penetration of near-IR radiation into a sample is dependent on the absorption and scattering characteristics of the sample matrix. Variations in particle size, density, and sample positioning, as well ambient temperature and humidity conditions, may affect subtle changes in measured spectral characteristics. Various mathematical treatments have been suggested for modeling particle size effects on near-IR spectra (53-57). In addition, Berntsson *et al.* (58) evaluated methods for determining minimum effective sample size for near-IR reflectance analysis. To eliminate undesirable spectral attributes, several signal preprocessing techniques may be employed.

1.2.2.3.1.1 Linearization

Linearization of reflectance spectra is typically accomplished by either a log (1/R) or Kubelka-Munk transformation. Log (1/R) values are preferred instead of units of reflectance because there exists an almost linear relationship between the concentration of an absorbing component and its contribution to the log (1/R) value at the wavelength

absorbed. A more rigorous and theoretically satisfying approach to spectral linearization is presented by the Kubelka-Munk (K-M) transformation. K-M theory has three simplifying assumptions: (i) the scattered radiation is isotropically distributed; (ii) the particles in the layer are randomly distributed and very much smaller than the thickness of the layer; and (iii) the layer is subject to only diffused reflection (59). Radiation passing through a scattering medium can be divided into radiation passed forward in the direction of the incident beam (*I*), and radiation scattered back toward the illuminated surface (*J*) (60). An equation can be written describing the change in intensity (*dI*)of the beam (*I*), as it passes through a small sample layer of thickness, (*dx*). The amount of radiation absorbed is considered to be proportional to an absorption constant, *K*, and to the intensity of the beam itself. Since this represents a decrease, a minus sign is included such that $dl = -KIdx$. Loss to scatter is represented through a second constant, S, and the total decrease in intensity is thus $dI = -KIdx - SIdx$. The radiation that is scattered from the *I* beam augments the *J* beam, and vice versa. Therefore, the change in intensity of the *I* beam is:

$$dI = -(K + S)Idx + SJdx \qquad \text{(Eq. 2)}$$

and the equation for the J component is:

$$dJ = -(K + S)Idx + SIdx \qquad \text{(Eq. 3)}$$

These equations may be solved to obtain expressions for the intensities of the beams *I* and *J* anywhere within the samples as a function of certain boundary conditions, such as on an ideal black background, on an ideal white background, without backing, etc. The boundary conditions of the principal interest are $I = I_o$ at $x = 0$ and $J = 0$ at $x = d$ (60).

The K-M theory treats all beams passing through the layer *dx* in the general direction of *x*=0 as a part of *I* , and all beams passing through *dx* in the general direction of *x*=0 as part of *J*, however, their actual path length will be longer unless they are traveling exactly perpendicular to the surface (60). The deviations are probably due to the effects of total internal reflection, which tend to increase the path length more for large angles of incidence, but may also involve factors such as relative refractive index, particle size, and shape (61). The scattering coefficient, S, is likewise, the result of complex interaction of many factors (61).

Assuming that sample thickness is sufficiently large such that no light passes through it entirely, the K-M theory leads to the following equation:

$$\frac{(1-R)^2}{2R} = \frac{K}{S} = f(R) \qquad \text{(Eq. 4)}$$

where *R* is diffuse reflectance, and *K* and *S* are the respective absorption and scattering constants for a particular material. The quantity *f*(R) is known as the K-M function.

The Kubelka-Munk equation creates a linear relationship for spectral intensity relative to sample concentration. It requires a reference standard that is essentially non-absorbing. However, the log 1/R expression of reflectance does not require the standard to be 100% reflecting because each application involves the use of a unique empirically

derived equation. The standard, must, however, be stable with time and not affected by typical environmental changes. Furthermore, the K-M approach assumes an infinite sample dilution in a non-absorbing matrix, a constant scattering coefficient and an "infinitely thick" sample layer. The difficult variable to determine in this equation is the scattering factor, *S*, which depends on the particle size and shape distribution, and the packing density of the material (62). For these reasons it is critical that the samples are packed identically each time. Despite the sophistication the K-M transformation, log 1/R is more commonly utilized because of its simplicity and broad applicability.

1.2.2.3.1.2 Smoothing

Smoothing is used to remove noise from spectra without altering the important chemical information present. The most common techniques for smoothing spectra include boxcar smoothing, polynomial (Savitzky-Golay) smoothing, and Fourier transformation. Boxcar smoothing begins by defining subsets containing a fixed number of data points across the spectrum. The center point of each subset is replaced by the average value of the subset members, and the averages are connected by a smooth curve. The degree of smoothing can be modified by altering the number of points in the Boxcar interval. The greater number of points averaged, the greater the degree of smoothing. Although one advantage of this technique is its ease of computation, an increase in distortion of the signal and subsequent loss of spectral information may occur if too many points are averaged in the calculation (63).

Polynomial smoothing involves fitting, by least-squares methods, a polynomial equation to subsets of data points across a spectrum. From the derived equations, the

center point of each interval is computed. The points are then connected by a smooth curve (63).

The Fourier Transform (FT) is a mathematical operation for decomposing a time function into its frequency components (amplitude and phase). This process converts a raw spectrum (e.g., a time series) into two frequency domain spectra, one which is called a real spectrum and the other imaginary (this terminology comes from complex numbers) by performing cosine and sine functions, respectively, on the original data. An inverse transform then converts the real and imaginary pairs into a real series that is different from the original spectrum in some desirable way (64). For example, points corresponding to noise can be eliminated from the Fourier spectrum without altering essential chemical information. FT is considered to be both a filtering and a noise reduction technique (65).

1.2.2.3.1.3 Multiplicative Scatter Correction

Multiplicative scatter correction (MSC) is a technique used to remove baseline shifting due to linear additive and multiplicative scatter effects. MSC assumes that, for a given set of spectra, light scatter and chemical information can be mathematically differentiated. The first step in MSC involves regressing spectral variables x_i against an average spectrum $\bar{x}$ over k wavelengths using the following model:

$$x_{ik} = a_i + b_i \overline{x_k} = e_{ik} \qquad \text{(Eq. 5)}$$

The constants *a* and *b* are estimated from the regression and used to obtain the scatter corrected spectrum by:

$$x_{k,new} = \left(x_{k,old} - a\right)/b \qquad \text{(Eq. 6)}$$

Isakkson and Naes (66) have described the advantages of using MSC, indicating that prediction results are improved through better fit to a multivariate linear model (a more linear relationship between constituent and spectral values) and less irregularity in the scatter corrected data. As a result, quantitative and qualitative calibration and prediction errors may be minimized. An additional advantage of this technique for removing baseline shifting is that, following correction, the MSC spectra maintain the appearance of the original log (1/R) spectra.

1.2.2.3.1.4 Derivatization.

Derivatives are useful for resolving overlapping absorption bands and removing spectral baseline shifting. Although a variety of derivatization techniques have been used to resolve near-IR spectra, the second derivative has gained widespread acceptance for pharmaceutical analysis (67). Second derivative calculations yield absorption peaks pointing in a negative direction relative to the positive absorption peaks seen in log 1/R spectra. The appearance of the derivative spectra are highly dependent on the width or "gap" of data points over which the derivative calculations are performed. Higher-order derivative spectra may also be employed to resolve overlapping peaks and remove baseline shifting, however, they are more sensitive to noise, may be more difficult to

interpret, and have, in many instances, not been shown to improve calibration or prediction results (63).

1.2.2.3.2 Principal Component Analysis

The analysis of complex samples usually requires several measurements in order to define the different variables that make each sample unique. There are usually many variables that can influence the spectral data acquired from a sample, and it can be very difficult to determine what information is necessary in order to produce the correct correlation for sample classification.

Dimensionality reduction of spectral information should provide a simplistic representation of the data for visualization and understanding yet retain sufficient detail for thorough mathematical analysis. If executed properly, it should also encourage the consideration of meaningful relationships between the variables. Although several techniques for reducing the dimensionality of large data sets are well documented in the statistical literature, one such technique, principal component analysis, has gained widespread acceptance in near-infrared analysis.

Principal component analysis (PCA) involves the rotation of a spectral array of n points in p-dimensional space to introduce a new set of orthogonal linear coordinates so that the sample variances of the given points with respect to the derived coordinates are in decreasing order of magnitude (68). The first principal component is such that projections of the given points onto it have maximum variance among all possible linear coordinates; the second principal component has a maximum variance subject to being

orthogonal to the first. All subsequent axes are orthogonal to any preceding axes and follow in order of decreasing variance.

Mathematically, PCA corresponds to the decomposition of the data matrix X, which contains $I = 1, 2, \ldots, I$ spectra of $k = 1, 2, \ldots, K$ wavelengths, into means ($\bar{x}_k$), scores (t_{ia}), loadings (p_{ak}) and residuals (,ik):

$$x_{ik} = \bar{x}_k + \sum_{a=1}^{A} t_{ia} * p_{ak} + \varepsilon_{ik} \qquad \text{(Eq. 7)}$$

The loadings are an indication of the intra-spectrum variation. The absolute value of the loading describes how much a certain wavelength contributes to the *a*th principal component, whereas the sign provides information as to whether a particular wavelength is positively or negatively correlated with the principal component. Scores show the location of the spectral information for spectrum *i* along the a^{th} principal component and, hence, describe the inter-spectra variation. Spectra that are similar will, therefore, have a similar score value.

A simplistic representation of principal axis transformation can be expressed by the matrix equation:

$$T = XE \qquad \text{(Eq. 8)}$$

where *E* is a square matrix of *a* eigenvectors, each with *k* loadings elements. The matrix of new variables, *T*, is composed of score elements which form column vectors called principal components. The first principal component describes the largest systematic variation in the data matrix *X*, the second principal component the next largest, and so on.

One result of the principal axis transformation procedure is that the covariance between any two new variables for all samples is zero, which may not necessarily be true for the original variables. This allows the total variance of the spectra to be expressed as a summation of the variance for each of the new variables. A second result is that the total variance is now concentrated into the first few principal components. Therefore, higher order principal components, which primarily account for random spectral noise, can be easily removed from principal component models without the loss of significant chemical information (68).

1.2.2.3.3 Quantitative Analysis

Quantitative analysis involves a variety of statistical methods that relate near-IR absorbance values at specific wavelengths to measurable analyte qualities via Beer's law. Establishing this relationship by using a set of samples of known composition and a statistically sound regression technique is referred to as calibration. Global calibrations utilize full spectral data, while models using only a few selected wavelengths are referred to as local. The development of a calibration model should involve the following steps:

(i) Prepare a set of standards that will represent the expected range of samples to be encountered in a typical test environment.

(ii) Determine sampling and reference test errors (a spectral method cannot correlate to a reference method better than the method correlates to itself).

(iii) Choose a data treatment that provides an acceptable standard error of calibration (SEC) and acceptable coefficient of correlation (r). The SEC,

also referred to as the standard error of estimate (SEE), is calculated according to the following equation:

$$SEC = \sqrt{\frac{1}{N-k-1}\sum_{i=1}^{N}(y_i - \hat{y}_i)^2} \qquad \text{(Eq. 9)}$$

where N is the total number of samples in the model, k is the number of wavelengths used in the calibration, $\hat{y}_i$ is the estimated concentration from the calibration model for the ith sample, and y_i is the actual concentration of the ith sample.

The SEC statistic is the standard deviation for the residuals due to differences between actual and predicted values within the calibration set. It is an indication of the total residual error due to the particular regression equation to which it applies. The SEC will decrease with the number of wavelengths (independent variable terms) used within an equation, indicating that increasing the number of terms will allow more variation within the data to be explained (69). This statistic is a useful estimate of the theoretical maximum accuracy obtainable for a specified set of wavelengths used to develop a calibration. The residual for each sample is equal to the actual chemical value minus the near-IR predicted value for all samples within the calibration set.

The correlation of coefficient (r) provides an indication of the degree to which the calibration fits the data, and is determined according to:

$$r = 1 - \sqrt{\frac{\sum_{i=1}^{N} (y_i - \hat{y}_i)^2}{\sum_{i=1}^{N} (y_i - \bar{y})^2}} \qquad \text{(Eq. 10)}$$

where $\bar{y}$ is the average concentration.

(iv) Validate the calibration model and test for overfitting. For example, a calibration model demonstrating an SEC that is much less than the reference test error may be the result of too many terms in the calibration regression (too much random noise fit by the model) or too few samples.

(v) Attempt to understand why the calibration model works, why certain preprocessing techniques and regression methods provide better results than others, and why certain factors are included in the model. To gain practical acceptance, the model must be mathematically and spectroscopically justifiable.

Following the development of a statistically sound calibration model, the prediction of unknown sample properties may be accomplished by applying the calibration model to the near-IR spectra of the test samples. An indication of the predictive power of the model is provided by a standard error of prediction (SEP) calculation. This term, also referred to as the standard error of performance, provides a comparison between reference method results and the near IR predicted values for samples outside the calibration set used to develop the model. The SEP calculation is similar to that used in determining SEC, however, SEP has only N -1 degrees of freedom.

Although there exist numerous methods for performing quantitative near-infrared analysis, the following discussion will briefly examine methodologies commonly employed in pharmaceutical applications of near-infrared spectroscopy.

1.2.2.3.3.1 Multiple Linear Regression

One of the most elementary statistical approaches to quantitative near-infrared calibration and prediction is multiple linear regression (MLR). This technique uses the absorbance information at a number of wavelengths to isolate the effect of a single analyte and to normalize the baseline (63) . MLR is based on the following relationship:

$$\hat{Y} = a + b_1 X_1 + b_2 X_2 + ... + b_k X_k \qquad \text{(Eq. 11)}$$

where Y is the response variable, b_m is the absorptivity at the k^{th} wavelength, and X_k is the log 1/R value at that wavelength. An entire spectral data array or a selected number of wavelengths may be used in the estimation of the b_k coefficients. Calibrations based on narrow spectral regions are typically less complicated than global models, however, the performance of such localized models is highly dependent on the proper choice of wavelengths. To assist in wavelength selection, procedures such as "step-up" and "step-down" regression are often employed (70).

Several MLR algorithms have been described by Hruschka (63). The step-up or forward-stepwise regression procedure picks the wavelength to add as a second variable in a two-term regression, and so on until some stopping criterion is met. The step-down procedure starts with a multi-term regression using all available wavelengths and eliminates variables by some criterion. The all-possible combinations procedure tests all

possible linear regressions on all subsets of the available wavelengths and reports the subsets giving the lowest SEC. This procedure is usually limited to all subsets containing only two or three wavelengths. As an alternative, each step in the step-up method can be followed by one step of the step-down method, to check for wavelengths that can be safely eliminated when a new wavelength is added. Proper selection of subset of available variables is necessary to avoid overfitting (63). However, with respect to near-IR, correlation of absorbances of adjacent wavelengths may lead to collinearity, and there are usually fewer calibration samples available than there are recorded wavelengths of the log 1/R spectra (71). Consequently, MLR often leads to unstable estimates of *b*. Therefore, although the model may fit a calibration set well, an unstable regression vector may magnify small random errors in future samples and lead to large prediction errors.

1.2.2.3.3.2 Principal Component Regression

Principal component regression (PCR) is a robust technique for developing global calibrations. PCR utilizes principal component spectra derived from principal axis (PCA) transformation as previously discussed. Because most of the spectral variation of the calibration set is usually described by the first few principal components, the number of regression variables necessary to adequately model the data is dramatically reduced. Data reduction also allows for sources of spectral variation, other than those related to the sample attributes being evaluated, to be eliminated from calibration. One weakness of PCR is that, because chemical information is not included in principal axis transformation, regression factors are determined solely on the basis of near-IR data. Therefore, the development of a calibration model using PCR may rely on good

correlation between the principal components and the chemical data, which may or may not exist. In addition, there may also remain y-correlated variance proportions in the higher order PCs that never get into the PC-regression stage, simply because the magnitudes of the other **X**-structure parts (which are irrelevant in an optimal (X,Y) regression sense) dominate (72).

1.2.2.3.3.3 Partial Least Squares Regression

The partial least squares (PLS) technique, developed by Svante Wold, considers errors in both independent (spectroscopic data) and dependent (sample analyte information) variables in the calculation of PLS factors (73). Such factors are analogous to principal components. Since both spectral and sample analyte variance are taken into account in determining PLS factors, the significance of the factors with respect to the analytical problem at hand is increased because the factors are oriented in accordance with the target analyte. Basically, PLS attempts to explain as much of the variation in the dependent variable as possible using only relevant factors contained in the spectral data.

The mathematics of PLS are quite rigorous and have been thoroughly described in the literature (74). For a system of n samples, PLS simultaneously resolves matrices **X** (n x k) and **Y** (n x p), which contain spectral absorbance values recorded at k wavelengths and the concentrations of the p analytes to be determined. Each matrix is resolved into the product of a scores and loadings matrix. The loadings for matrix **X** are determined from the scores of the dependent variable matrix, and the loadings for matrix **Y** are calculated from the scores of the independent variable (spectral data) matrix, **X**. The

covariance between *y*, the dependent variable, and the PLS component is maximized for component *p* according to:

$$c_p = \sum_{n=1}^{n=N} x''_{pn} y'_n / N \qquad \text{(Eq. 12)}$$

where y'_n is the centered value of the *y* sample for *n*, there are *N* samples in the dataset and x''_{pn} is the PLS score of the centered p^{th} component for this sample.

Erbensen (72) has provided a concise comparison of PCR and PLS regression. As opposed to performing two independent PCA-analyses on two spaces, **X** and **Y**, PLS uses y-variance to guide the decomposition of the **X**-matrix, so that the outcome constitutes an optimal validated regression. Instead of performing independent PCA analysis on **X** and **Y** spaces, PLS actively connects these spaces by specifying the **u**-score vector(s) to act as the starting points for the **t**-score vectors in the decomposition of **X**. Thus the starting proxy-$\mathbf{t_1}$ is actually $\mathbf{u_1}$ in the PLS method, thereby letting the **Y**-data structure directly guide the decomposition of **X**. Subsequently, $\mathbf{u_1}$ is substituted by $\mathbf{t_1}$ later in the algorithm. By this method, $\mathbf{u_1}$ influences the decomposition of **X** and the calculation of the **X**-loadings (**w**). The **X**-space **t**-vectors are then calculated based on the newly determined **w**-vector, and are subsequently used in **Y**-space decomposition. The PLS-algorithm is specifically designed around these interdependent $\mathbf{u_1 \rightarrow t_1}$ **and** $\mathbf{t_1 \rightarrow u_1}$ substitutions in an interactive way until convergence, at which time a final set of vectors has been calculated for the current PLS-component for both the X-space and the Y-space. Thus, what first appears as two sets of independent PCA decompositions is, in fact, based on these interchanged score vectors (72). In this way, the **X-** and **Y-** spaces are interdependently

modeled. By balancing both **X-** and **Y-** information, PLS reduces the influence of large **X**-variations which do not correlate with **Y**, and thereby removes the problem of the two-stage PCR weakness (72). Since PLS focuses as much on the **Y**-variance as well as the **X**-variance, and there is particular interest in the co-varying relationship between these samples, simpler models (those with fewer components) can be developed.

Perhaps, the most critical step involved in PLS calibration involves the selection of the number of factors used to construct the regression model. Too few factors can leave important spectral information unmodelled, while too many factors may result in the inclusion of a significant amount of noise included in the model. Martens and Naes (75) suggested a cross-validation procedure to determine the optimum number of factors to be included in the PLS calibration. This technique calculates a root mean square error of prediction (RMSEP) for a series of PLS calibration models containing 1 to *n* factors. The optimal number of factors to be included in the calibration model is determined as the number of factors after which there is no significant decrease in the RMSEP.

1.2.2.3.4 Qualitative Analysis

In addition to being a powerful tool for quantitative pharmaceutical analysis, near-IR spectroscopy has gained recognition for its qualitative analysis capabilities. Qualitative analysis involves classifying samples by comparing their spectral characteristics to those of a reference group. Unlike quantitative methods, qualitative spectral analysis does not always rely on the existence of a direct correlation between spectral characteristics and chemical information.

Qualitative near-IR analysis is typically performed in one of two ways. The first method involves a visual examination of the spectrum followed by sample identification or classification by matching the location and strength of absorption peaks with those of known substances. Although this technique may provide satisfactory results in certain cases, the broad overlapping nature of near-IR absorbance bands combined with extraneous sources of spectral variation, greatly limits the usefulness of this method.

The second, and more widely accepted method for qualitative near-IR analysis, utilizes pattern recognition techniques. Such methods classify samples according to their similarity to a training set. Because pattern recognition techniques can only recognize the variability to which they are accustomed, it is necessary to develop a training set that represents all expected sources of spectral variability. After training the computer to recognize the spectral qualities of acceptable material, pattern recognition algorithms can be employed to quickly identify and classify unknown test samples. The following discussion will describe several popular pattern recognition methods.

1.2.2.3.4.1 Mahalanobis Distance

Mark and Tunnell (76) suggested a Mahalanobis distance (D^2) calculation to qualitatively classify near-infrared spectra. The Mahalanobis distance is a standardized Euclidean distance that describes the distance between point X and the center of a group of spectra X_i through the following relationship

$$D^2 = \left(X - \overline{X}_i\right)' M \left(X - \overline{X}_i\right) \qquad \text{Eq. (13)}$$

where X is the multidimensional vector describing the location of the spectrum X, $\overline{X}_i$ is a multidimensional vector describing the location of the mean spectrum of the *i*th group, $\left(X-\overline{X}_i\right)'$ is the transpose of vector $\left(X-\overline{X}_i\right)$ and M is the matrix describing the distance measures of the multidimensional space involved. A spectrum is typically classified as "acceptable" if its distance falls inside the 99% probability (less than three standard deviations) level. Multiple wavelengths or principal component spectra may be used to calculate D^2, however, the use of principal components ensures that all spectral information is retained for classification.

1.2.2.3.4.2 Soft Independent Modeling of Class Analogies

Soft Independent Modeling of Class Analogies (SIMCA) is a pattern recognition technique that uses principal component analysis of near-IR spectra to develop mathematical models for each training set (77). The number of principal components used determines the dimensionality of the class model and may affect the performance of the SIMCA calculation.

SIMCA begins by calculating the sum of squares of the difference (s_i^2) between the original spectrum and the reproduced spectrum according to

:

$$s_0^{\,2} = \sum s_i^{\,2} / (n-k-1) \qquad \text{(Eq. 14)}$$

where a_{ij} is the raw absorbance spectrum, a_{ij} is the transformed spectrum following PCA, p is the number of wavelengths and k is the number of significant principal components. The total variance between samples within a class (s_0^2) is determined by the equation:

$$F = \frac{s_i^{\,2}}{s_o^{\,2}} \cdot \frac{1}{(n-k-1)} \qquad \text{(Eq. 15)}$$

where *n* is the number of training samples and *k* is the number of principal components used to construct the model. To classify each sample, a ratio of variances with *1/(n – k – 1)* degrees of freedom is calculated and compared to a tabulated *F* value.

$$F = \frac{s_i^{\,2}}{s_o^{\,2}} \cdot \frac{1}{(n-k-1)} \qquad \text{(Eq. 16)}$$

The probability level for sample acceptance is the same as previously described in the Mahalanobis distance calculation.

1.2.2.3.4.3 Bootstrap Error-Adjusted Single-sample Technique

The Bootstrap Error-Adjusted Single-sample Technique (BEAST) is a non-parametric pattern recognition procedure designed to operate in the high-speed parallel or vector mode. Lodder and Hieftje (78) have discussed this algorithm, derived from Efron's bootstrap calculation (79), in detail and have provided examples of its application.

The BEAST begins by treating each wavelength in a spectrum as a single point in multidimensional space ("hyperspace"). Each point is translated from the origin along each axis by an amount that corresponds to the magnitude of the signal observed at each wavelength. Samples having similar spectra map into clusters of points in similar regions of hyperspace. Larger cluster size corresponds to samples having greater intrinsic variability.

The BEAST develops an estimate of the total sample population using a small set of known (training) samples. A predetermined number of randomly selected sample sets (containing the same number of elements as the training set) is drawn from the training set, with replacement, to form a bootstrap distribution by Monte Carlo approximation. A point estimate of the center of this distribution, representing the estimate of the true population distribution for the sample set, is also calculated. Bootstrap distribution quantiles are readily converted into confidence intervals and are therefore useful in defining the boundaries of a training set in the hyperspace of spectral points. Assuming the parameter of interest is represented by the bootstrap-set center, selecting any two bootstrap-distribution percentiles gives the corresponding confidence limits for the center-parameter (e.g., selecting the 16th and 84th percentiles of the bootstrap distribution produces the central 68% confidence limits).

When a new sample is analyzed, its spectrum is projected into the same hyperspace as the known samples. A vector is then formed in hyperspace to connect the center of the population estimate to the new sample spectral point. A hypercylinder is formed about this vector to contain a number of estimated-population spectral points. The distances between the center of the hypercylinder and the points within it are sorted and the upper and lower confidence limits are scaled in accordance with a measure of the skew of the distribution. The distance from the center to the new sample spectrum is scaled by a skew-adjusted standard deviation (SD) calculated from the sorted distances

BEAST distances are used to identify sample constituents. Uncorrected BEAST distances (suitable for unskewed training sets) are calculated as follows:

$$\left(\sum_{j=1}^{d} \left(c_j - x_j \right)^2 \right)^{1/2} \Big/ \sigma \qquad \text{(Eq. 17)}$$

where c_j is the center of the bootstrap distribution, x_j is the test sample spectrum and σ is a BEAST standard deviation. When a sample spectrum projects to a point within three standard deviations of the center of a cluster of spectral points from a known substance or product, the sample is considered to be a sample of the known material. The known product is either a pure substance or a mixture of components. When the new sample contains different substances or components in concentrations that differ from the known product, the new sample spectral point is displaced from the known spectral cluster. The magnitude of this displacement increases as the difference between the new sample and the set of known samples increases. Furthermore, the direction of the displacement of the new sample point corresponds to the spectra of the constituents responsible for the displacement.

Although the BEAST is primarily utilized for qualitative analysis, this technique can also be used quantitatively (80,81). Using the estimated BEAST distances within a training group and their corresponding analyte response variables, a calibration model may be developed. When an unknown sample is tested, its BEAST distance is calculated and its analyte response is determined using the calibration model.

1.2.2.4 Pharmaceutical Applications of Near-Infrared Spectroscopy

Near-infrared spectroscopy has gained widespread acceptance in the pharmaceutical industry as a rapid and non-destructive analytical technique.

Applications of this technology can be found throughout many phases of pharmaceutical manufacturing, from identification and testing of incoming raw materials (54,82), to analytical control of unit process operations (83,84), and finally analysis of finished dosage forms (85-93). Recently, a general chapter regarding near-infrared spectrophotometry has been included in the United States Pharmacopeia (94). Additionally, the technique has been addressed in a FDA draft guidance for industry regarding analytical procedures and methods validation (95). Although near-IR is not specifically addressed in FDA's guidance document for PAT, it has been reported that near-infrared applications appeared in 41% of the literature citations in FDA's PAT Initiative Literature References (26).

Early pharmaceutical applications of near-IR focused on the determination of active ingredients in formulations after appropriate extraction (96,97). The majority of work has, however, involved the analysis of a variety of intact pharmaceutical dosage forms including powders (98-99), blends (99-101), granulations (102-104), tablets (81, 85, 87, 106) capsules (80, 88), creams (89), liquids (90,106), and parenterals (107-108). Comprehensive review articles regarding the historical development of near-IR applications have been published by Kirsch and Drennen (45), and by Morisseau and Rhodes (109). The following discussion highlights some of the major developments in the use of near-IR spectroscopy for pharmaceutical applications discussed in this dissertation.

1.2.2.4.1 Analysis of Coated Dosage Forms

Coatings are applied to solid dosage forms for a variety of reasons including aesthetics, taste-masking, stability enhancement, or to provide modified release of active drug substance (110). Application of a proper amount of coating to a dosage form is essential to provide desired physicochemical, pharmacological, or cosmetic effects. For example, insufficient levels of applied rate controlling polymer coating on a sustained release dosage form may result in faster than desired drug release, while excessive levels of applied coat may retard drug release to a greater than desired extent. Therefore, it is important to closely monitor the quantity of coating applied to solid dosage forms during processing.

For tablets, the amount of applied coating is typically determined by calculating the difference between the average weight of a coated tablet and the average weight of an uncoated core. Measurement of coated tablet thickness (111) has been suggested for monitoring the level of applied coating. This technique, however, is indirect and is based on measurement of average core and coated tablet weight. Therefore, it provides little information regarding individual tablet coating weight variation. For pellet processes, researchers and manufacturing personnel must rely on determinations of applied solids to predict coating process endpoints. This is usually performed by applying a specified quantity of coating solution onto a known quantity of core pellet substrate. This technique, which is primarily theoretical, assumes no loss of core material during processing with complete application of the applied coat. Therefore, it provides limited information regarding the actual quantity of coating material present on the core substrate at any point during processing.

Laboratory methods, such as microscopy, have the potential for providing a direct measurement of coating thickness, but often require laborious sample preparation, and are, therefore, not feasible for real-time analysis. Microscopy may also have associated with it a considerable degree of error due to inherent variability in thickness of the substrate or applied coating. Several thickness measurements per sample must be obtained to provide an accurate assessment of coating thickness. Direct assessment of the quantity of polymer applied to tablets has been achieved via a gel permeation chromatographic methods described by MacLaren and Hollenbeck (112) and Scattergood *et al.* (113). Such techniques also require labor-intensive sample preparation and analyses, and are not suitable for process analysis applications.

One of the first references regarding near-IR analysis of coated dosage forms involved the quantification of amiodarone content of coated tablets (105). In this application, the researchers indicated a need to scrape the coating from the tablets prior to analysis because of spectral interference with the drug substance. In 1995, Kirsch and Drennen (115) demonstrated that valuable information about core tablet properties of film coated tablets could be assessed using near-IR spectroscopy. Prediction of core tablet hardness, drug content, and time to 50% dissolution of ethylcellulose coated cimetidine tablets was effectively accomplished using principal component regression using near-IR spectra collected on both grating-based and acousto-optic tunable filter spectrometers.

Kirsch and Drennen (83) also published a near-IR method for monitoring the coating of tablets in a Wurster column. In this work, the Wurster column was retrofitted with a sample thief (115) to allow tablet samples to be withdrawn from the process

stream for obtaining near-IR spectra during coating. As coating proceeded, decreasing absorbance was observed in regions characteristic of the primary core tablet components while increasing absorbance was noted in regions characteristic of the applied coating. Principal component analysis of scatter-corrected or second derivative spectra was employed to predict the quantity of ethylcellulose or hypromellose applied. Over a coating range of 2% to 30%, SEE and SEP values for applied polymer solids were approximately 1%.

The use of near-IR spectroscopy to evaluate the quantity of active ingredient applied to a tablet via a film coating operation was investigated by Buchanan *et al.* (116). A partial least squares regression model was developed using scatter corrected near-IR reflectance data obtained using a NIRSystems Model 6500 spectrometer equipped with a Rapid Content Sampler. HPLC was employed as reference laboratory method for determining active drug content contained per tablet. SEP values in the range of 3% to 4% were reported for the model studied.

Another application of near-infrared analysis of coated tablets was reported by Andersson and coworkers (117), who quantified the amount of coating applied to a dual-active bilayer tablet. Each half tablet was composed of different granulations containing different active ingredients. Tablets were coated in a side-vented coating pan and removed from the process stream prior to near-IR analysis. A PLS model was developed utilizing spectra obtained from both tablet sides, pretreated with MSC, and ordered into one object. Characterization of the coating measurements was achieved by calibrating the spectra versus coating thickness obtained from optical microscopy. Using PCA, the

authors estimated the maximum depth in the coating material that returned chemical information to be approximately 0.1 mm to 0.2 mm.

1.2.2.4.2 Analysis of Pelletized Dosage Forms

The earliest reference to near-infrared analysis of pharmaceutical pellets was in a 1966 paper by Sinsheimer and Keuhnelian (96). This work involved the qualitative analysis of compressed pellets composed of either a mixture of amine salts and potassium chloride or amine salts alone. Spectra were collected in the 1050 to 2800 nm region and analyzed qualitatively using peak assignments. Although no calibrations were developed, several spectral features of these samples were noted for showing promise in the quantification of drugs in the solid state.

An on-line near-IR monitoring method for monitoring pellet product uniformity during encapsulation was described by Duff *et al.* (118). This study utilized a remote reflectance fiber optic probe mounted to the feed chute of a commercial encapsulation machine. Assay calibrations were developed using multiple linear regression and PLS analysis of second derivative spectra. Both models had correlation coefficients of about 0.98 and standard errors of calibration of better than 0.5% over an assay range of 98% - 100%.

In another study, Andersson *et al.* (119) described a near-IR method suitable for analysis of the film coating on pharmaceutical pellets during processing. In this study, core pellets were sieved to a diameter of 400-500 μm and subsequently coated with a solution of ethylcellulose and ethanol. During processing, the pellets increased in size by ~30% corresponding to a coating thickness of ~60-75 μm. Near-IR spectra were

collected using a sampling device and diffuse reflectance probe positioned inside the process vessel of an in-house constructed fluid bed processor. The sampling device utilized was similar to that described by Kirsch and Drennen (83,114,115) from which samples were withdrawn from the process stream, spectra were acquired, and the samples were returned for additional processing. A PLS regression model was employed to predict coating thickness using fluorescence microscopy and image analysis (120) as a reference method. Using as little as one PLS projection, R^2 values of 0.97 and standard errors of calibration and prediction of 2.2 μm and 2.3 μm, respectively, were achieved.

1.2.2.4.3 Analysis of Moving Solids

Physical sampling and the presentation of a sample to a fiber-optic probe are essential elements of any process analysis (121). Although a stationary sample presentation can be obtained by means of an in-line sub-sample (83,114), or by stopping or removing a sample from the process (83,116,122,123), such a sample-spectrometer interface may be difficult to develop and may also limit sampling rate. Analysis of moving samples are essential for various process analytical applications.

For a given sample, there will always be scattering variation due to heterogeneity with respect to sample characteristics such as powder packing, surface roughness, and distance from the probe, even if the sample is homogenous with respect to chemical composition. This is due to the fact that near-IR diffuse reflectance is the result of both absorption and scattering, where the scattering coefficient is typically an order of magnitude larger than the absorption coefficient (124,125). Measurement of a moving

sample can, therefore, become quite complicated since its signal is likely to have random variations as the sample moves.

Although near-IR sampling of moving solids is frequently carried out in industry, the number of publications describing moving sample/spectrometer interfaces has been somewhat limited. Several patents describing the development of moving sample-spectrometer interfaces have been granted. In one such patent, Kemeny *et al.* (126) described a system where material is moving under an optical window suitable for on-line near-IR applications. He noted that if particle size was small as compared to the illuminated surface, the concentration of stationary product could be determined within acceptable limits. However, if the average diameter was larger and its size distribution wider, the measurement was only precise if the sample was moving, i.e., if a sufficiently larger sample was analyzed. Two additional patents (127,128) describe methods for monitoring moving base materials such as paper, in which near infrared radiation is directed upon the material.

In a 2001 paper, Berntsson *et al.* (121) characterized the effect of sample movement on spectral response using FT-NIR spectroscopic analysis of model samples such as paper, plastic and fine and coarse powders. The authors found that controlled movement caused sample artifacts to appear in sample interferograms. They attributed the origin of these artifacts to variation in the detector signal level caused by sudden changes in the overall sample reflectance as the sample moves. In this study, it was shown that these artifacts did not affect the near-IR spectra range, and that spectra obtained from moving samples could not be distinguished from spectra obtained from stationary samples.

Most recently, Andersson *et al.* (129) characterized the effect of sample movement on spectral response during fiber optic probe diffuse reflectance near-IR spectroscopy sampling. In this study 400 – 500 μm pellets were used to model coarse powder while microcrystalline cellulose was used as a model fine powder. Controlled movement of the model samples during fiber optic probe sampling was accomplished through the construction of a 300 mm rotating disk apparatus. In the initial phase of study, the probe was placed 1 mm above the rotating disk at a fixed radius from the center of the disk and rotation speeds ranging from 3 – 61 rpm were investigated. In the second phase of study, additional measurements were obtained by inserting the probe into a glass vessel containing a powder sample, which was placed on the rotating disk. The third phase of this study involved analysis of ethylcellulose coated pellets, containing between 8% and 120% w/w of applied target coating solids, which were arranged in monolayers on the rotating disk using double-sided tape. For each test condition, measurements were performed at 1 and 10 scans per spectrum, and approximately 100 spectra were acquired at each rotational speed. Chemometric routines of MSC, PCA, PLS and SIMCA were employed in the analysis of the near-IR spectra.

Following chemometric analysis, two spectral artifacts were observed. First, a baseline offset occurred due to variations in the average distance between the probe and the samples, different packing, or the presence of cavities in the samples analyzed. Additional spectral artifacts were also observed that appeared as momentary transitions between spectra from different materials within the scanned spectrum. A correlation between the sample speed and the number of transitions was also observed. Such

artifacts were difficult to identify by visual inspection, but could be tracked by multivariate methods such as PCA and PLS.

The reasons for measuring a moving solid sample may, for example, be to obtain a large effective sample. Similarly, it may simply be impossible to interrupt the process to obtain a stationary sample. In this case, material inhomogeneities, such as differences in particle size, inevitably influenced the reflectance spectra. The presented data demonstrated that by analyzing moving samples, thereby increasing the effective sample size, such effects could be suppressed because the cumulative sample studied yielded reproducible average values even if the sample was locally inhomogeneous. However, local product variations could be hidden when the effective sample size was increased. Therefore, the number of samples acquired during in-line analysis of process streams should be carefully considered.

In this study, it was determined that, for monitoring moving solids and mimicking conditions typically encountered during in-line or on-line process analysis, at least 20 to 40 consecutive samples should be used to predict an average value with sufficient precision.

2 EXPERIMENTAL

2.1 Laboratory-Scale Rotogranulation

2.1.1 Materials

Diltiazem hydrochloride (Gyma, Milan, Italy), polyvinypyrrolidone K29/32 (ISP, Wayne, NJ), micronized talc (Alphafil 500, Luzenac America, Englewood, CO), and 25-30 mesh non-pareil seeds (Chr. Hanson, Milwaukee, WI) were donated by Mylan Pharmaceuticals, Inc. (Morgantown, WV).

2.1.2 Formulation

Triplicate batches of pellets containing 150mg/g (15%), 300mg/g (30%), and 550mg/g (55%) theoretical active drug content were prepared by layering a 40% w/w aqueous suspension of diltiazem HCl (88% w/w), PVP K29/32 (6% w/w), and micronized talc (6% w/w) onto 25 – 30 mesh (600 μm – 710 μm) non-pareil seeds. Quantitative descriptions of the formulations under investigation are presented in **Table 1**.

2.1.3 Drug Suspension Layering

Suspension layering was conducted using a Glatt GPCG-3 fluid bed processor (Glatt Air Techniques, Ramsey, NJ) equipped with a 12 inch rotor insert (Vector

Table 1. Diltiazem HCl pellet formulations.

Ingredient	Theoretical Quantity per Unit (mg/g)	Quantity per Batch (g)
<u>150 mg/g (15%)</u>		
Non-Pareil Seeds (25-30 mesh)	828.8	2700
Diltiazem HCl	150.0	525*
PVP K29/32	10.6	37*
Micronized Talc	10.6	37*
Purified Water**	---	(900)*
Total	1000	3299
<u>300 mg/g (30%)</u>		
Non-Pareil Seeds (25-30 mesh)	657.2	2100
Diltiazem HCl	300.0	1050*
PVP K29/32	21.4	75*
Micronized Talc	21.4	75*
Purified Water**	---	(1800)*
Total	1000.0	3300
<u>550 mg/g (55%)</u>		
Non-Pareil Seeds (25-30 mesh)	371.6	1099
Diltiazem HCl	550.0	1923*
PVP K29/32	39.2	137*
Micronized Talc	39.2	137*
Purified Water**	---	(3299)*
Total	1000.0	3296

* Quantity represents a 6% overage to provide 106% theoretical potency.
** Removed during processing.

Corporation, Cranberry, NJ). Formulations were designed to yield approximately 3300 grams of finished product, in order to achieve 100% rotor capacity at the process endpoint. Drug suspension was delivered via a Masterflex peristaltic pump (Cole-Parmer Instrument Co., Chicago, IL) to a tangential spray system equipped with a 1.2 mm nozzle tip. The spray gun was completely immersed in the rotating product throughout the layering process. During processing, product temperatures were maintained between 38°C and 42°C, and rotor speeds varied from 525 to 575 rpm. Angular velocity was ~29 ft/sec. Spray rates varied from 10 g/min to 25 g/min while atomizing air pressure was constant at 40 psi. Processing parameters are presented in **Table 2**. Of the listed parameters, inlet air temperature and process spray rate were most critical for maintaining appropriate temperature control to avoid spray drying or agglomeration. Process spray rates for the 150mg/g, 300mg/g and 550mg/g formulations are presented in **Figures 3, 4, and 5**, respectively, as a function of time.

Suspension spray rates were kept low at early process times to ensure rapid solvent evaporation following suspension contact with the pellet surface and prevent agglomeration. As the rotor and the product reached an equilibrium temperature and the particle size and quantity of the pellets increased during processing, it was possible to increase spray rates without forming agglomerates. Inlet air temperature and air flow were adjusted to maintain a product temperature of ~40ºC, which, during initial process optimization studies, produced few agglomerates (≥16 mesh) or fines (<30 mesh). Spray rates varied depending on the pellet strength being processed. Smaller diameter pellets, such as those employed in the 150mg/gram strength, required slightly slower spray rates

Table 2. Processing parameters for laboratory-scale drug suspension layering.

Process Parameter	Target
150 mg/g	
Inlet Air Temperature	55 ± 5° C
Product Temperature	40 ± 2° C
Exhaust Air Temperature	44 ± 3° C
Spray Rate	9 – 12 g/min
Air Flow	120 ± 10 cfm
Atomization Air Pressure	40 psi
Rotor Speed	550 ± 25 rpm
Non-pareil Charge	2700 g
Process Time	135 ± 8 min
300 mg/g	
Inlet Air Temperature	55 ± 5° C
Product Temperature	40 ± 2° C
Exhaust Air Temperature	46 ± 3° C
Spray Rate	9 – 20 g/min
Air Flow	110 ± 10 cfm
Atomization Air Pressure	40 psi
Rotor Speed	550 ± 25 rpm
Non-pareil Charge	2100 g
Process Time	210 ± 11 min
550 mg/g	
Inlet Air Temperature	60 ± 5° C
Product Temperature	40 ± 2° C
Exhaust Air Temperature	46 ± 3° C
Spray Rate	10 – 27 g/min
Air Flow	120 ± 10 cfm
Atomization Air Pressure	40 psi
Rotor Speed	550 ± 25 rpm
Non-pareil Charge	1099 g
Process Time	300 ± 10 min

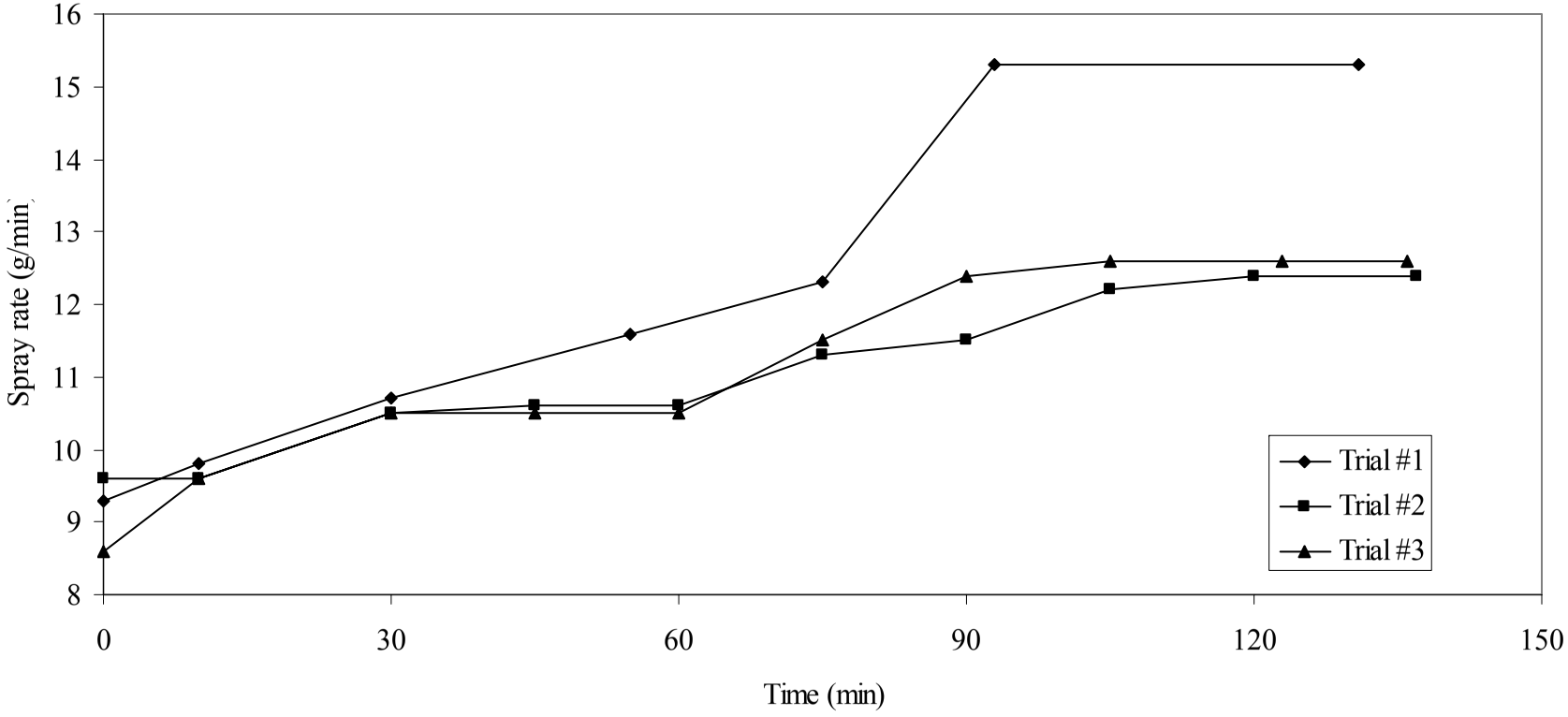

Figure 3. Process Spray Rates, 150 mg/gram Diltiazem HCl Pellets

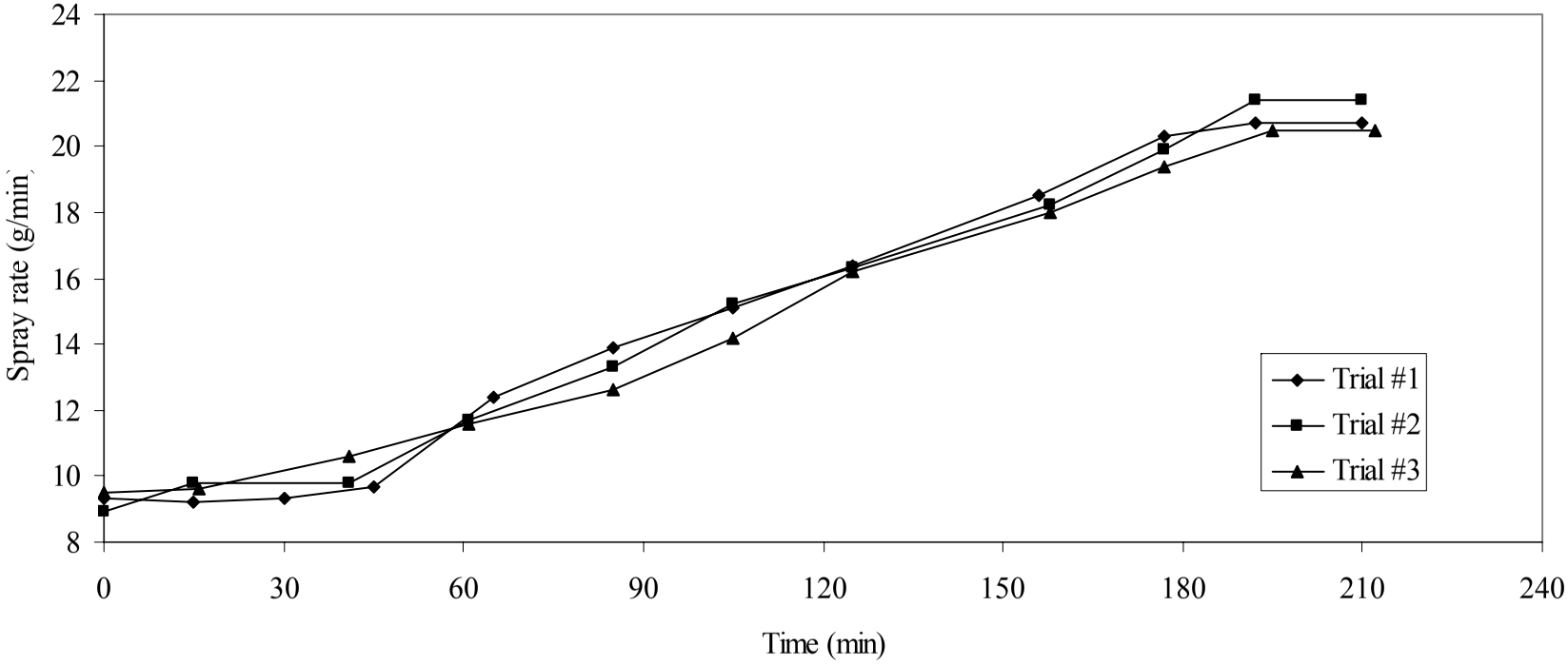

Figure 4. Process Spray Rates, 300mg/gram Diltiazem HCl Pellets

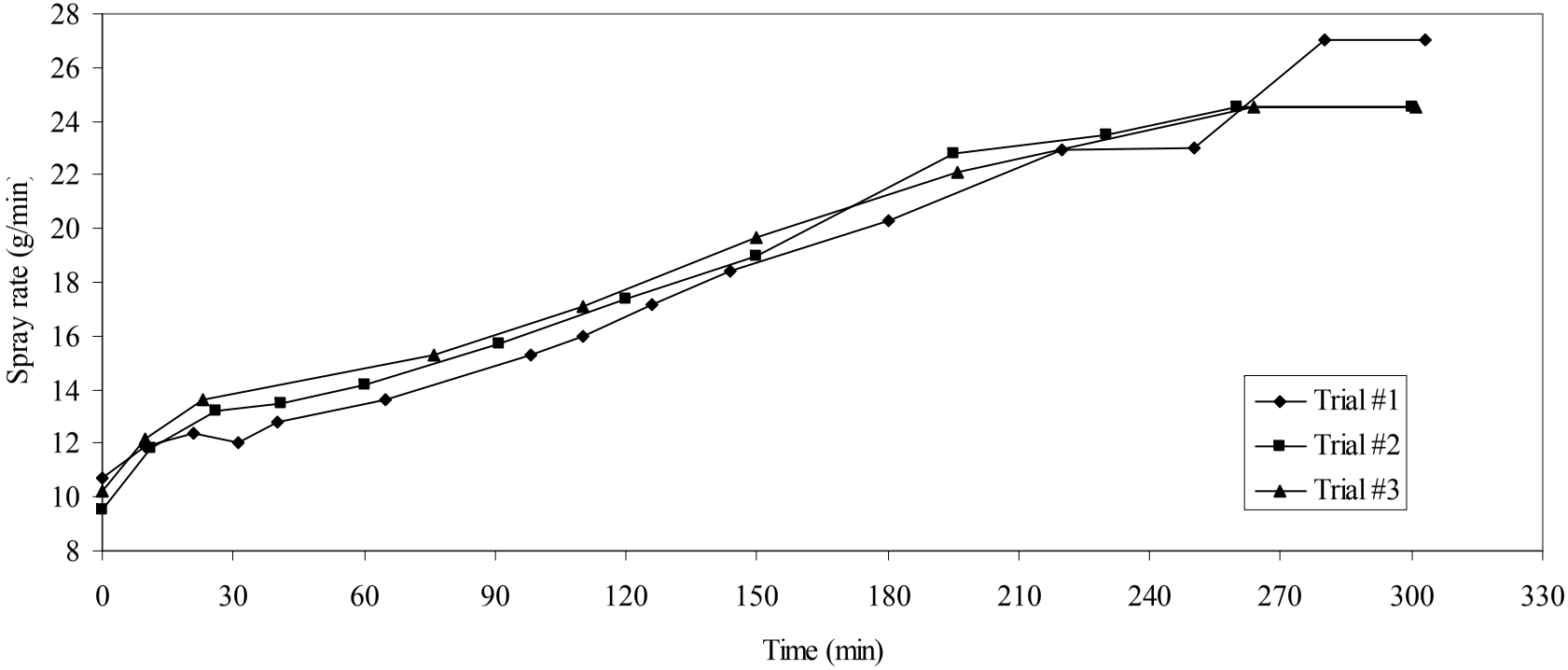

Figure 5. Process Spray Rates, 550mg/gram Diltiazem HCl Pellets

to prevent excessive agglomeration. Agglomerates were classified as groups of pellets such as doublets, triplets, or higher order multiplets.

A graphic presentation of the pellet particle size distributions, based on sieve analysis, is presented in **Figure 6.** Corresponding numerical sieve analysis data are summarized in **Appendix 1**. Trial #1 for the 150mg/g strength employed slightly higher spray rates than runs #2 and #3. The higher spray rates produced 5% agglomerates (≥16 mesh). Trials #2 and #3, which utilized slower spray rates, each had only 0.4% agglomerates.

For the 300mg/g and 550mg/g processes, it was possible to use much higher spray rates than those utilized in the 150mg/g batch. All trials for the 300mg/g strength demonstrated approximately 90% pellets retained on a 20 mesh screen with approximately 10% of the pellets retained on an 18 mesh screen. All pellets were classified as singlets. For the 550mg/gram strength, trials 1, 2, and 3 demonstrated 1.2%, 1.2%, and 4% agglomerates (≥16 mesh), respectively. In Trial 1, the larger number of pellets retained on the 18 screen was attributed to a significant quantity of non-pareil seeds that fell into the air plenum after the start of fluidization, and prior to the initiation of spraying. These beads were assayed and found to contain no diltiazem. The decreased quantity of non-pareil seeds available for the drug layering process subsequently resulted in the production of larger, super-potent pellets. The 4% agglomerates in trial #3 were attributed to several line clogs that occurred during layering, resulting in localized overwetting.

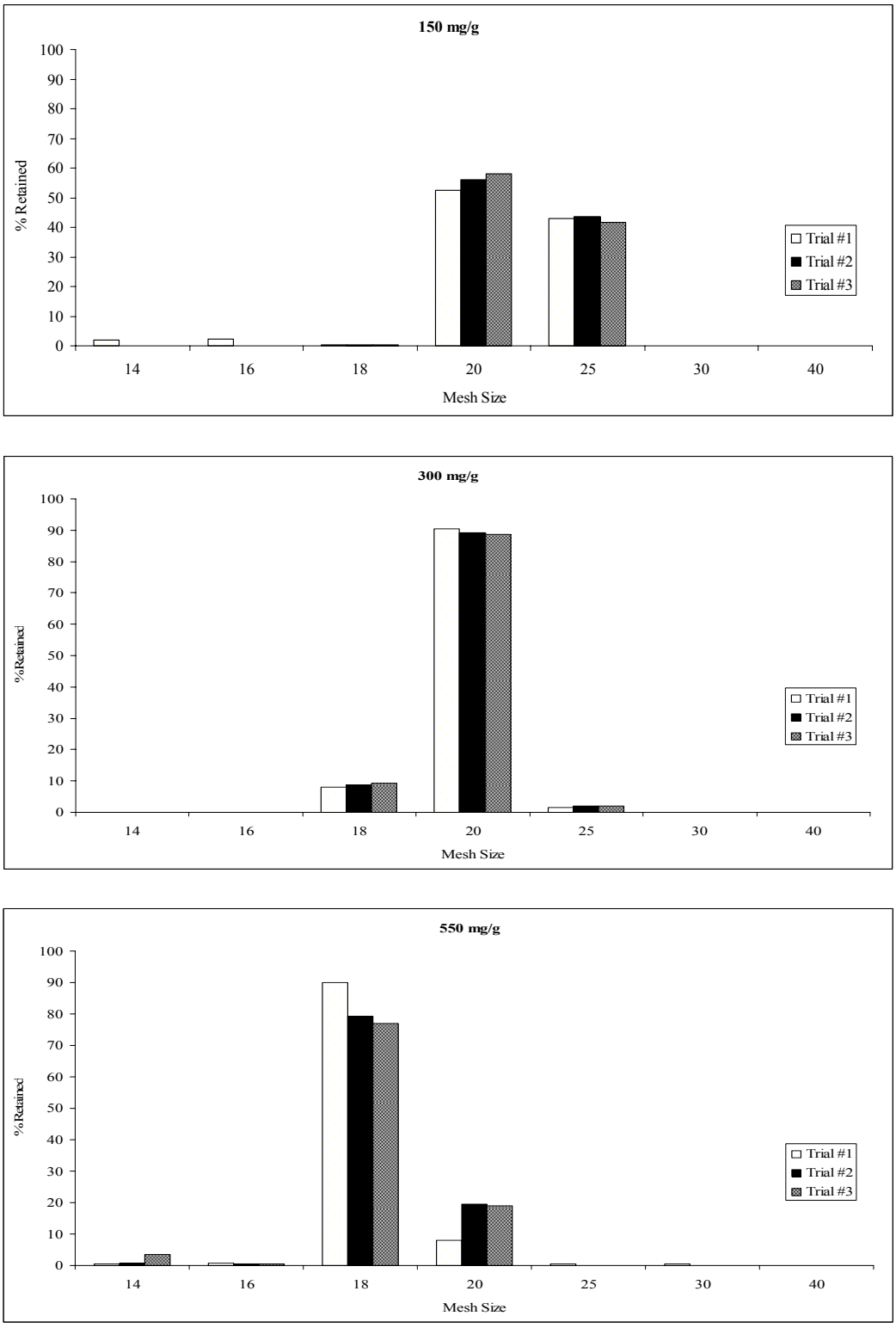

Figure 6. Diltiazem HCl Pellet Particle Size Distribution via Sieve Analysis

Potency was evaluated over a theoretical target potency range of 96% to 106% for all formulations. The theoretical quantity of applied suspension to achieve desired pellet potency was determined by:

$$\frac{Q * D * P}{35000 - (0.4 * D * P)} \qquad \text{(Eq. 18)}$$

where Q is the weight in grams of non-pareil seeds, D is the theoretical quantity of active drug substance per gram of pellets at 100% potency, and P is the desired potency in percent. Time points for sample selection were identified by monitoring the weight of suspension delivered during processing. A description of the sampling scheme is presented in **Table 3**. Within the studied range, theoretical potency increased by approximately 1% every 1.5, 3 or 4 minutes for the 150mg/gram, 300mg/gram, and 550mg/gram lots, respectively.

2.1.4 Near-IR Methodology

2.1.4.1 Instrumentation

Near-IR reflectance spectra were collected using a NIRSystems Model 6500 grating-based spectrometer (Foss NIRSystems, Silver Springs, MD). Spectra were collected in reflectance mode as an average of 20 scans over a wavelength range of 1100 to 2500 nm with a data interval of 2 nm. Because of significant spectral noise above 2200 nm due to the fiber optics, only the 1100 nm to 2200 nm region was used for spectral analysis.

Table 3. Sampling scheme – laboratory-scale drug suspension layering.

150mg/g Diltiazem HCl Pellets

Theoretical Potency (%)	Theoretical Potency (mg/g)	Quantity Sprayed (g)	Sample Time (min)
87	130.6	1183	105
90	135.1	1232	108
93	139.6	1280	111
96	144.1	1330	114
98	147.1	1363	117
100	150.1	1397	120
102	153.1	1431	123
104	156.1	1465	126
106	159.1	1499	130

300mg/g Diltiazem HCl Pellets

Theoretical Potency (%)	Theoretical Potency (mg/gram)	Quantity Sprayed (g)	Sample Time (min)
96	288.1	2577	180
98	294.1	2658	186
100	300.1	2741	192
102	306.1	2825	198
104	312.1	2911	204
106	318.1	2999	210

550mg/g Diltiazem HCl Pellets

Theoretical Potency (%)	Theoretical Potency (mg/g)	Quantity Sprayed (g)	Sample Time (min)
96	528.6	4189	260
98	539.6	4417	268
100	550.6	4660	276
102	561.6	4920	284
104	572.6	5199	292
106	583.6	5500	300

2.1.4.2 In-line Spectrometry

To facilitate in-line spectroscopic monitoring of the drug suspension layering process, the rotor unit was modified to allow the insertion of a 0.5 inch diameter near-IR fiber-optic probe (Smart-Probe®, Foss/NIRSystems, Silver Spring, MD) directly into the processing chamber. The probe had a 0.8 cm sapphire window, and consisted of two collinear fiber optic bundles. Each bundle was 2.5 m long, and was comprised of 210 optic fibers (each 200 μm diameter). One bundle transmitted light from the exit slit of the monochromator to the sample, while the other bundle returned the reflected light from the sample to a PbS detector. The fiber-optic-probe was located 180° from the tangential spray nozzle 2 inches above the rotor disk. This vertical proximity of the probe was equivalent to approximately ½ of the product bed height. The probe was adjusted such that its tip was even with the inside wall of the rotor processor, and in direct contact with the rotating particles. **Figure 7** presents a schematic drawing of the in-line sampling system for rotogranulation. Photographs of the sampling system are shown in **Figure 8.**

During manufacturing, near-IR spectra of the rotating particles were obtained at specified theoretical potency intervals by monitoring the weight of suspension delivered. The time required to obtain one spectrum of 20 averaged scans was 20 seconds. The number of pellets comprising a monolayer across the surface of the probe's window was approximately 77, 58, and 47, for the 150mg/g, 300mg/g, and 550mg/gram strengths, respectively. Therefore, in the time to obtain one spectrum, between ~950,000 (550mg/g) and ~1.5 million pellets (150mg/g) were scanned.

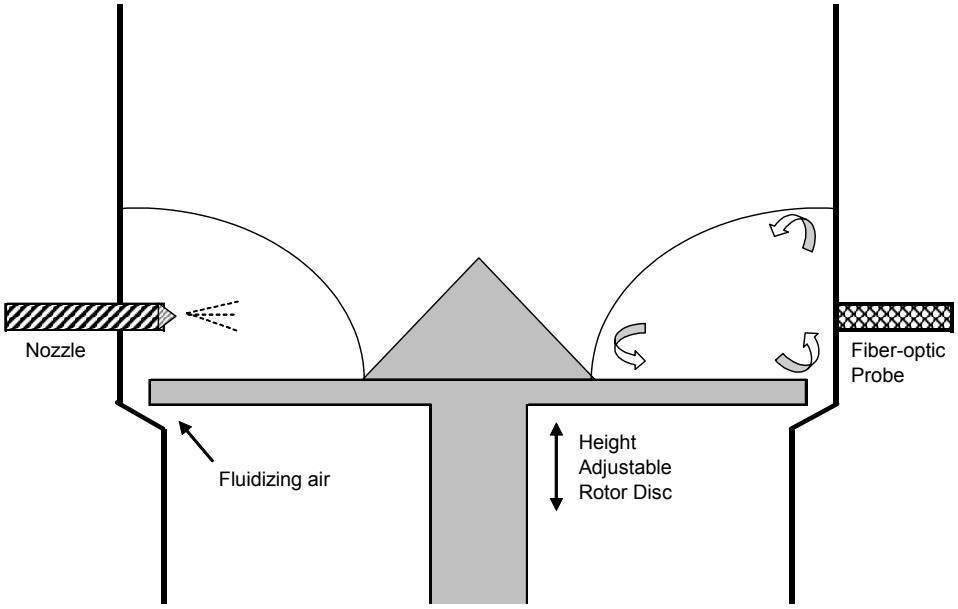

Figure 7. Fiber-optic Sampling System for Rotogranulation

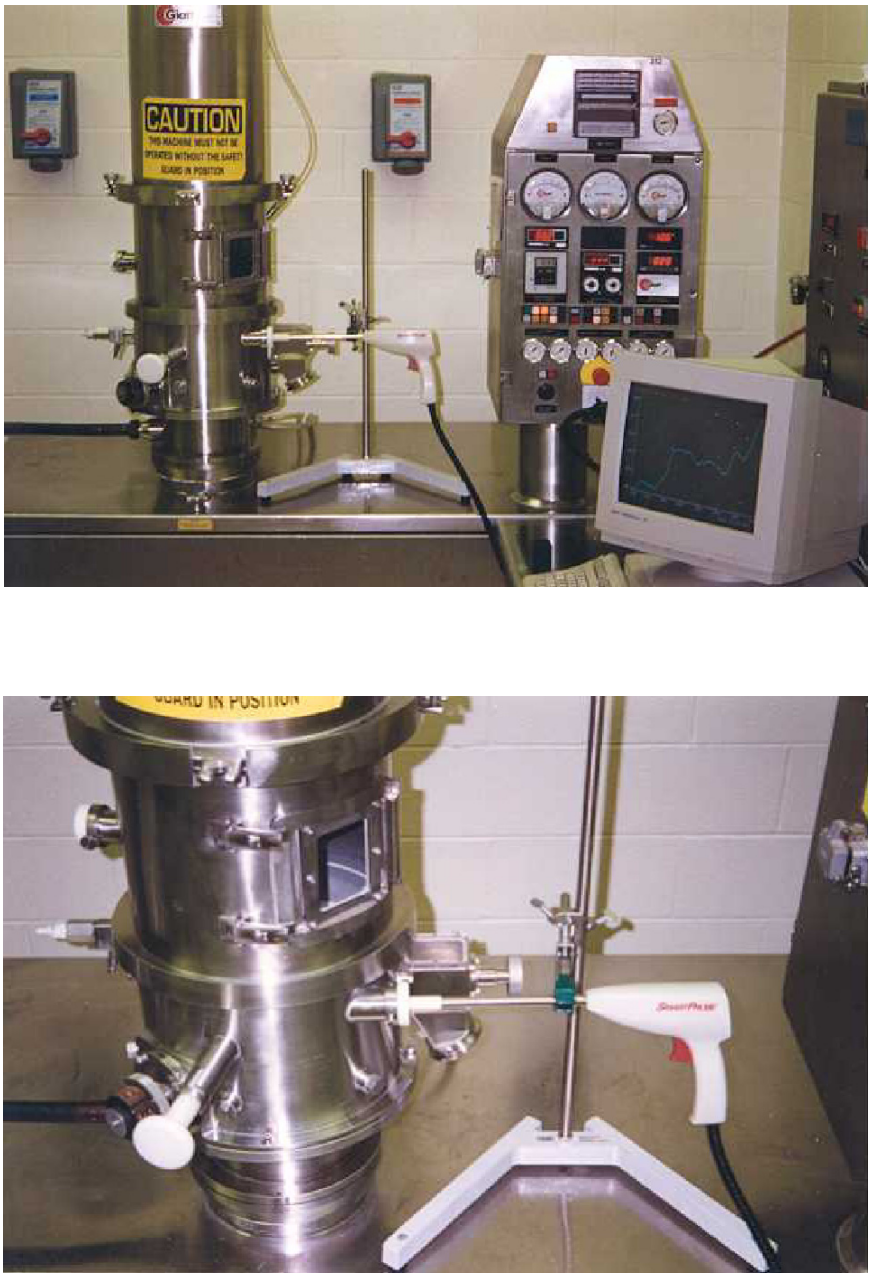

Figure 8. Fiber-Optic Sampling System for Rotogranulation

2.1.4.3 At-line Spectrometry

Although the fiber-optic probe obviated the need to remove samples from the processor, pellet samples were thieved from the processor immediately following each in-line scan. The samples, each weighing approximately 5 grams, were immediately screened through #16 and #30 mesh sieves to remove agglomerates and fines, and transferred to 3 dram glass scintillation vials.

Near-IR spectra were obtained in triplicate using a Rapid Content Analyzer® (RCA) sampling system (Foss NIRSystems, Silver Springs, MD). Near-IR radiation from a tungsten-halogen source was brought to the RCA sample compartment by means of a fiber-optic bundle (420 fibers, each 200 μm diameter). Reflected light from the sample was reflected back into the detector array of the RCA, which consisted of four PbS detectors and four Si detectors for collection of near-IR and visible spectra, respectively. Spectra were obtained by scanning through the base (1.8 cm diameter) of the glass vials. The number of pellets comprising a monolayer across a sample vial base was approximately 390, 290, and 240 for the 150mg/g, 300mg/g, and 550mg/g strengths, respectively. Each vial was inverted three times between scans. Replicate scans were averaged to obtain one spectrum for each sample time point. Total collection time per sample was approximately 90 seconds.

2.1.4.4 Spectral Preprocessing

Spectra were reference-corrected using a 99% Spectralon® disk (Labsphere, North Sutton, NH) and reflectance values were linearized with a log(1/R) transformation prior to analysis. NIRSystems NSAS® software (Version 3.25, Foss NIRSystems, Silver

Springs, MD) was used for spectral processing. Chemometric analysis was performed using proprietary programs written in SPEAKEASY IV EPSILON +® (Speakeasy Computing Corp., Chicago, IL) and NSAS® software. Multiplicative scatter correction (MSC) or second derivative (D2) transformation of the spectra was performed prior to calibration development and at-line or in-line prediction to remove unwanted spectral variation due to particle size, density, and sample positioning, temperature and humidity fluctuation.

2.1.5 Diltiazem HCl Reference Assay

Diltiazem HCl content of the pellet samples was determined using a validated HPLC method according to the USP 24 monograph for Diltiazem HCl Extended Release Beads (130). A stock solution of diltiazem HCl (1 mg/ml) was prepared in methanol. Subsequently, the stock solution was diluted with 50:50 phosphate buffer:acetonitrile to obtain standard concentrations of 5, 10, 20, 30, 40, and 50 μg/ml. The samples were analyzed using a Hewlett-Packard model liquid chromatograph (Model 1050, Palo Alto, CA) equipped with a diode array detector. A 4.6 mm x 150 mm column (Phenomenex, Torrance, CA) having 5 μm L7 (C-8) packing was used in the study. A 50:50 v/v mixture of 0.05M monobasic potassium phosphate pH 3.0 buffer containing 0.05% triethylamine and acetonitrile was employed as the mobile phase. The mobile phase was degassed by sparging with helium for 30 minutes and filtered through a 25 mm 0.45 μm hydrophilic PTFE membrane filter (Millex-LCR®, Millipore, Bedford, MA) prior to use. The flow rate was 1 ml/min, the detector wavelength was set at 240 nm, and the sample injection volume was 20 μl. A linear regression was performed between the area-under-

the-curve (AUC) and the drug concentration values. Replicate solutions were made for each concentration over a three day period. **Figure 9** displays the standard curve obtained. The R^2 value for the calibration was 0.9999. Triplicate injections of the 30 mcg/ml standard over a three day period demonstrated an RSD of 0.25%.

The diltiazem HCl content of prepared pellet samples was determined by transferring each pellet sample to a 100 ml volumetric flask and diluting with 60 ml methanol. The flasks were capped, placed on a mechanical shaker for 30 min, sonicated for 10 min, and then diluted to volume with methanol. From each flask, a 3 ml aliquot was obtained, diluted to 100 ml with mobile phase, and mixed. The resulting solution was passed through a 0.45 μm filter and transferred to HPLC vials for analysis.

2.1.6 Quantitative Prediction of Pellet Potency

Several calibration models were investigated for predicting the diltiazem HCl content of drug layered pellets. The simplest models assessed single or multiple wavelength calibration. More complex multivariate techniques such as PCR and PLSR were also investigated in this study. To assess the significance of spectral preprocessing on calibration development and performance, separate were developed for MSC and D2 spectra. Single and multiple wavelength calibrations, and PCR were performed using chemometric routines written in SPEAKEASY®. PLSR was performed using NSAS® software.

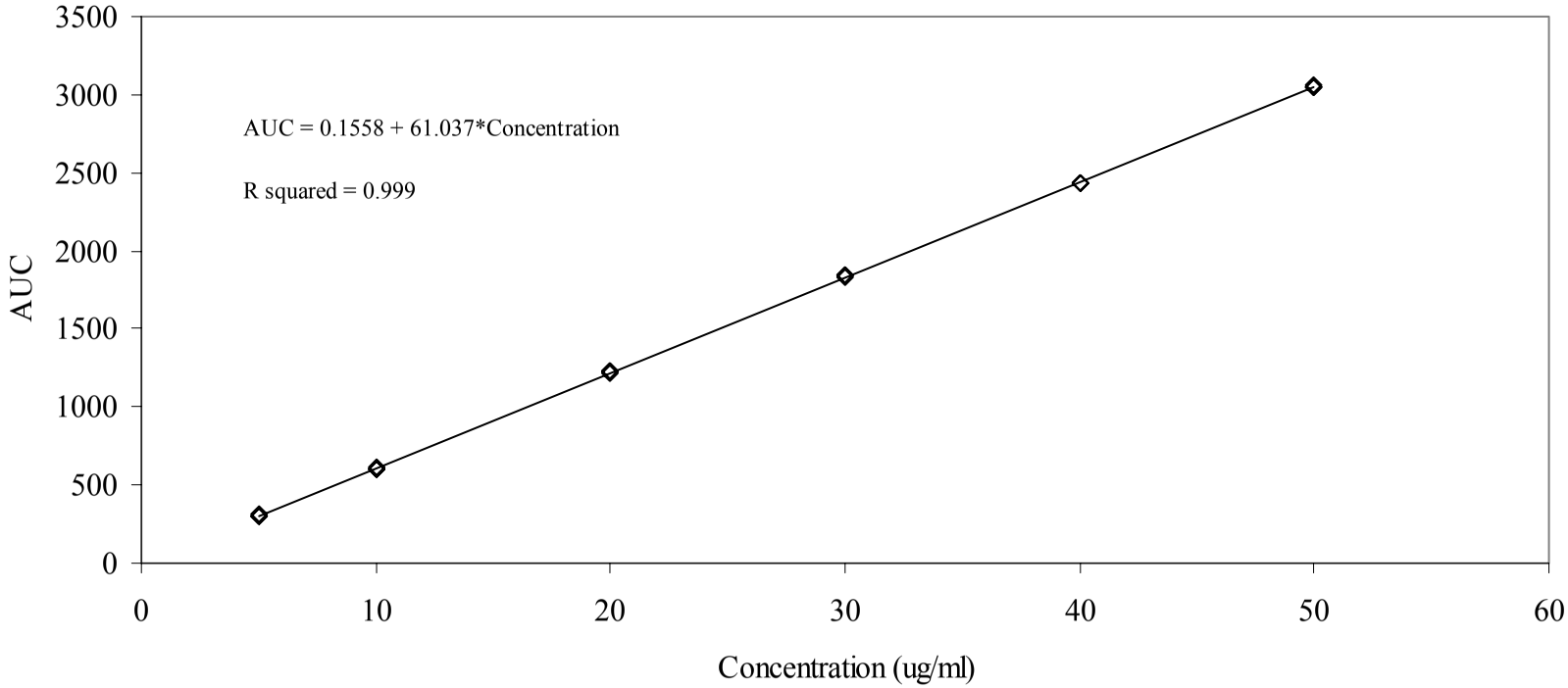

Figure 9. Standard Curve for Diltiazem HCl Assay by HPLC

2.2 Pilot-Scale Rotogranulation

2.2.1 Materials

Diltiazem hydrochloride (Gyma, Milan, Italy), polyvinypyrrolidone K29/32 (ISP, Wayne, NJ), micronized talc (Alphafil 500, Luzenac America, Englewood, CO), and 25-30 mesh non-pareil seeds (Chr. Hanson, Milwaukee, WI) were donated by Mylan Pharmaceuticals, Inc. (Morgantown, WV).

2.2.2 Formulation

Two 75 kg batches of pellets containing 550mg/g (55%) theoretical active drug content were prepared by layering a 40% w/w aqueous suspension of diltiazem HCl (88% w/w), PVP K29/32 (6% w/w), and micronized talc (6% w/w) onto 25-30 mesh non-pareil seeds. Quantitative descriptions of the formulations under investigation are presented in **Table 4**.

2.2.3 Drug Suspension Layering

Suspension layering was conducted using a Vector FL-Multi-60 fluid bed processor (Vector Corporation, Marion, IA) equipped with a 30 inch rotor insert (Vector Corporation, Marion, IA). Formulations were designed to yield approximately 75 kg of finished product to achieve 100% rotor capacity at the process endpoint. Drug suspension was delivered via a peristaltic pump (Model 520DI, Watson Marlow, Wilmington, MA) to a four-nozzle tangential spray system in which each spray gun was equipped with a 1.2 mm nozzle tip. The spray gun was completely immersed in the rotating product throughout the layering process. During processing, product

Table 4. Pilot-scale diltiazem HCl pellet formulation.

Ingredient	Theoretical Quantity per Unit (mg)	Quantity per Batch (kg)
550 mg/g (55%)		
Non-Pareil Seeds (25-30 mesh)	371.6	27.9
Diltiazem HCl	550.0	41.3
PVP K29/32	39.2	2.9
Micronized Talc	39.2	2.9
Purified Water*	---	(70.7)*
Total	1000.0	75.0

* Removed during processing.

temperatures were maintained between 38°C and 48°C, and rotor speeds varied from 75 to 90 rpm. Angular velocity was ~12 ft/sec. Spray rates varied from ~240 g/min to ~465 g/min while atomizing air pressure was constant at 50 psi. Processing parameters are presented in **Table 5**. Of the listed parameters, inlet air temperature and spray rate were most critical for maintaining proper product temperature and avoiding spray drying or agglomeration. Process spray rates, as a function of time, for the pilot-scale formulations are presented in **Figure 10.**

Process spray rates were initially low to prevent agglomeration of the pellets during early process stages. As processing continued and the product and the fluid bed processor reached equilibrium temperature, spray rates were increased as necessary to maintain a target bed temperature of ~48°C. A graphic representation of the pellet particle size distributions, based on sieve analysis, is presented in **Figure 11**. Corresponding sieve analysis data are summarized in **Appendix 2**.

Both pilot-scale batches had approximately 80% of the pellets retained on a #20 mesh screen and approximately 15% of the pellets retained on a #18 mesh screen. All pellets retained on these screen sizes were classified as singlets. Trial #1 had approximately 2.4% agglomerates (>18 mesh) and Trial #2 had approximately 4.6% agglomerates. The slightly higher quantity of agglomerates observed for Trail #2 as compared to Trail #1 and was attributed to a slightly higher spray rate at early time points.

Table 5. Processing parameters for pilot-scale drug suspension layering.

550 mg/g	
Inlet Air Temperature	67 ± 7° C
Product Temperature	48 ± 12° C
Exhaust Air Temperature	37 ± 6° C
Number of Spray Guns	4
Spray Rate	244 – 464 g/min
Nozzle Size	1.2 mm
Air Flow	700 ± 200 cfm
Atomization Air Pressure	50 psi
Rotor Speed	90 - 105 rpm
Non-pareil Charge	27.9 kg
Process Time	5 hours

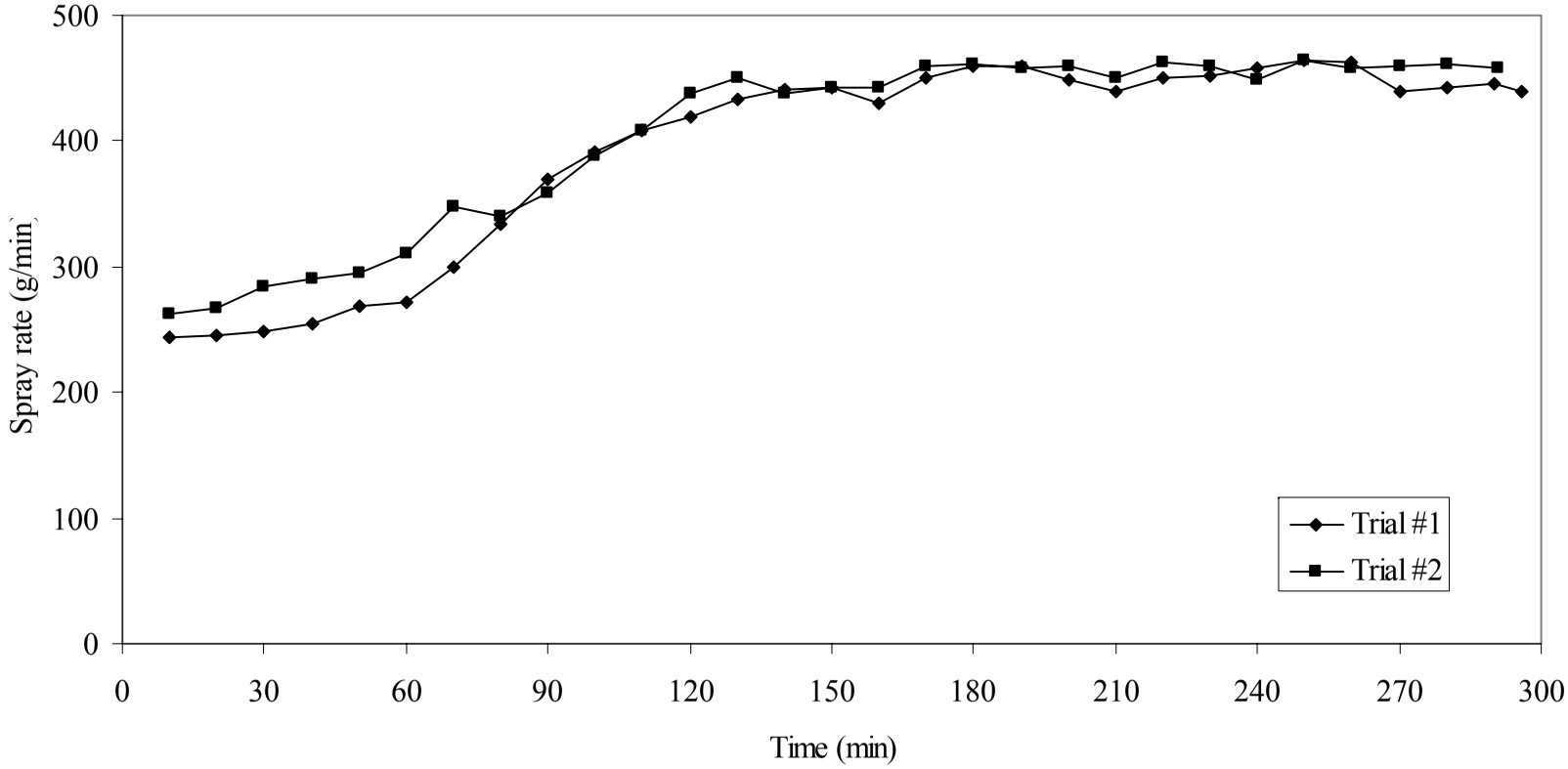

Figure 10. Pilot-scale Process Spray Rates, 550 mg/g Diltiazem HCl Pellets

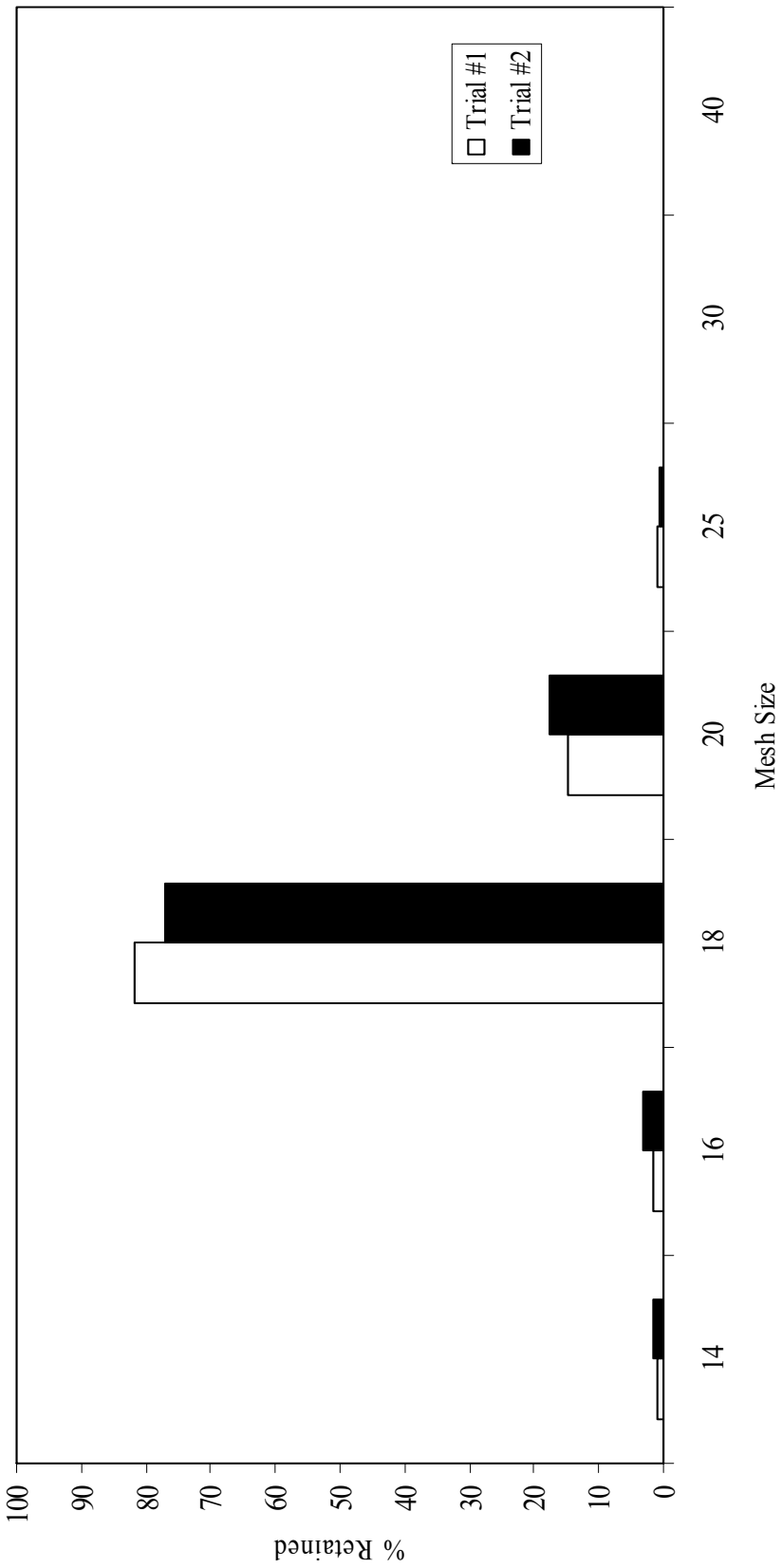

Figure 11. Pilot-scale 550 mg/g Diltiazem HCl Pellet Particle Size Distribution via Sieve Analysis

Potency was evaluated over a theoretical target potency range of 90% to 100% for both formulations. The theoretical quantity of applied suspension to achieve desired pellet potency was determined by:

$$\frac{Q * D * P}{35000 - (0.4 * D * P)} \qquad \text{(Eq. 19)}$$

where Q is the weight in kg of non-pareil seeds, D is the theoretical quantity of active drug substance per gram of pellets at 100% potency, and P is the desired potency in percent. Time points for sample selection were identified by monitoring the weight of suspension delivered during processing. A description of the sampling scheme is presented in **Table 6**. Within the studied range, theoretical potency increased by approximately 1% every 10 minutes.

2.2.4 Near-IR Methodology

2.2.4.1 Instrumentation

Near-IR reflectance spectra were collected using a NIRSystems Model 6500 grating-based spectrometer (Foss NIRSystems, Silver Springs, MD). Spectra were collected in reflectance mode as an average of 20 scans over a wavelength range of 1100 to 2500 nm with a data interval of 2 nm. Because of significant spectral noise above 2200 nm due to the fiber optics, only the 1100 nm to 2200 nm region was used for spectral analysis.

Table 6. Sampling scheme – pilot-scale drug suspension layering.

Theoretical Potency (%)	Theoretical Potency (mg/g)	Quantity Sprayed (kg)
90	495	72.3
91	551	75.7
92	506	79.3
93	512	83.1
94	517	87.1
95	523	91.4
96	528	96.0
97	534	101.0
98	539	106.2
99	545	111.9
100	550	117.8

2.2.4.2 At-line Spectrometry

Although the fiber-optic probe obviated the need to remove samples from the processor, pellet samples were thieved from the processor immediately following each in-line scan. The samples, each weighing approximately 5 grams, were immediately screened through #18 and #30 mesh sieves to remove agglomerates and fines and transferred to 3 dram glass scintillation vials.

Near-IR spectra were obtained in triplicate using a Rapid Content Analyzer® (RCA) sampling system (Foss NIRSystems, Silver Springs, MD). Near-IR radiation from a tungsten-halogen source was brought to the RCA sample compartment by means of a fiber-optic bundle (420 fibers, each 200 μm diameter). Reflected light from the sample was reflected back into the detector array of the RCA, which consisted of four PbS detectors and four Si detectors for collection of near-IR and visible spectra, respectively. Spectra were obtained by scanning through the base (1.8 cm diameter) of the glass vials. Approximately 240 pellets comprised the monolayer across sample vial base. Each vial was inverted 3 times between scans. Replicate scans were averaged to obtain one spectrum for each sample time point. Total collection time per sample was approximately 90 seconds.

2.2.4.3 Spectral Preprocessing

Spectra were reference-corrected using a 99% Spectralon® disk (Labsphere, North Sutton, NH) and reflectance values were linearized with a log(1/R) transformation prior to analysis. NIRSystems NSAS® software was used for spectral processing and all chemometric analysis was performed using proprietary programs written in

SPEAKEASY IV EPSILON +® (Speakeasy Computing Corp., Chicago, IL). Multiplicative scatter correction (MSC) or second derivative (D2) transformation of the spectra was performed prior to calibration development and at-line or in-line prediction to remove unwanted spectral variation due to particle size, density, and sample positioning, temperature and humidity fluctuation

2.2.5 Quantitative Prediction of Pellet Potency

Single wavelength, PCR and PLSR calibration models were investigated for predicting the diltiazem HCl content of drug layered pellets. To assess the significance of spectral preprocessing on calibration development and performance, separate calibrations were developed for MSC and D2 spectra. Single wavelength and PCR analyses were performed using chemometric routines written in SPEAKEASY®. PLSR was performed using NSAS® software.

2.3 Laboratory-Scale Wurster Coating

2.3.1 Materials

Eudragit® RS30D (Rohm-Pharma, Darmstadt, Germany), triethyl citrate, NF (Citroflex®2 NF, Morflex Inc., Greensboro, NC) and micronized talc (Alphafil 500®, Luzenac America, Englewood, CO) were donated by Mylan Pharmaceuticals, Inc. (Morgantown, WV).

2.3.2 Formulation

The diltiazem HCl pellets prepared in the rotogranulation studies were coated with a 20% w/w suspension consisting of Eudragit® RS30D, triethyl citrate (18% w/w of polymer solids), and micronized talc (30% w/w of polymer solids). Triplicate coating batches were processed for each of the three different potency beads. A quantitative description of the coating system under evaluation is presented in **Table 7**.

All coating suspensions were prepared according to the following procedure. The triethyl citrate (TEC) was dispersed in the water and mixed for 30 min using a laboratory mixer (Model G3UO5R, Lightnin, Rochester, NY) and 8 mm diameter axial flow impeller (Model A310, Lightnin, Rochester, NY). The micronized talc was slowly added to the TEC/water dispersion then mixed for an additional 30 min. The Eudragit® RS30D was passed through a 40 mesh sieve to remove agglomerates then slowly stirred into the TEC/talc suspension. The final suspension was mixed a minimum of 60 minutes prior to application, as per the manufacturer's recommendation, to ensure proper plasticization of the mixture.

2.3.3 Sustained-release Coating

Coating was conducted using a Glatt GPCG-3 fluid bed processor (Glatt Air Techniques, Ramsey, NJ) equipped with a 6 inch Wurster insert. Drug suspension was delivered via a Masterflex peristaltic pump (Cole-Parmer Instrument Co., Chicago, IL) to a spray system equipped with a 0.8 mm nozzle tip. During processing, spray rates varied from 10 g/min to 15 g/min, and atomization air pressure was kept constant at 30 psi. Airflow was varied between 800 cfm and 850 cfm and the partition height was adjusted

Table 7. Eudragit® RS30D coating system formulation.

Ingredient	Solids Quantity per Batch* (grams)	Quantity per Batch* (grams)
Eudragit RS30D	280	933.3
Triethyl Citrate, NF	50.4	50.4
Micronized Talc	84.0	84.0
Purified Water**	---	(1004.3)**
Total	414.4	2072

* Quantity applied to 1750 grams of core beads to achieve 16% polymer coat.
** Removed during processing.

as needed to maintain adequate movement of the particulate bed. Inlet air temperature was varied between 40ºC and 46ºC to maintain product temperatures between 28ºC and 30ºC. Summaries of the coating process parameters and spray rates are presented in **Table 8**. Coating application rates for Eudragit® RS30D applied to 300mg/g diltiazem HCl beads are presented in **Figure 12** as a function of time**.** Spray rates for the 150mg/g and 550mg/g pellets were similar to those utilized in the 300mg/g trials.

Coating was evaluated over the range of 5% to 16% applied polymer solids. Sample points were identified by monitoring the weight of coating suspension delivered during processing. A description of the theoretical sampling scheme is presented in **Table 9**. Each minute the quantity of applied polymer increased by 0.11% which corresponded to a 1% increase in coating level approximately every 9 minutes.

2.3.4 Near-IR Methodology

2.3.4.1 Instrumentation

Near-IR reflectance spectra were collected using a NIRSystems Model 6500 grating-based spectrometer (Foss NIRSystems, Silver Springs, MD). Spectra were collected in reflectance mode as an average of 20 scans over a wavelength range of 1100 to 2500 nm, with a data interval of 2 nm. Since the Model 6500 spectrometer employs a fiber optic bundle, which has significant absorbance above 2200 nm, only the 1100 nm to 2200 nm region was used for spectral analysis due to a lower instrumental signal-to-noise (S/N) ratio within this region.

Table 8. Processing parameters for laboratory-scale Wurster coating.

Inlet Air Temperature	40 - 46°C
Product Temperature	28 – 30°C
Exhaust Air Temperature	29 – 30°C
Spray Rate	10 – 15 g/min
Air Flow	800 – 850 cfm
Atomization Air Pressure	30 psi
Diltiazem HCl Core Bead Charge	1750 g
Process Time	160 ± 10 min

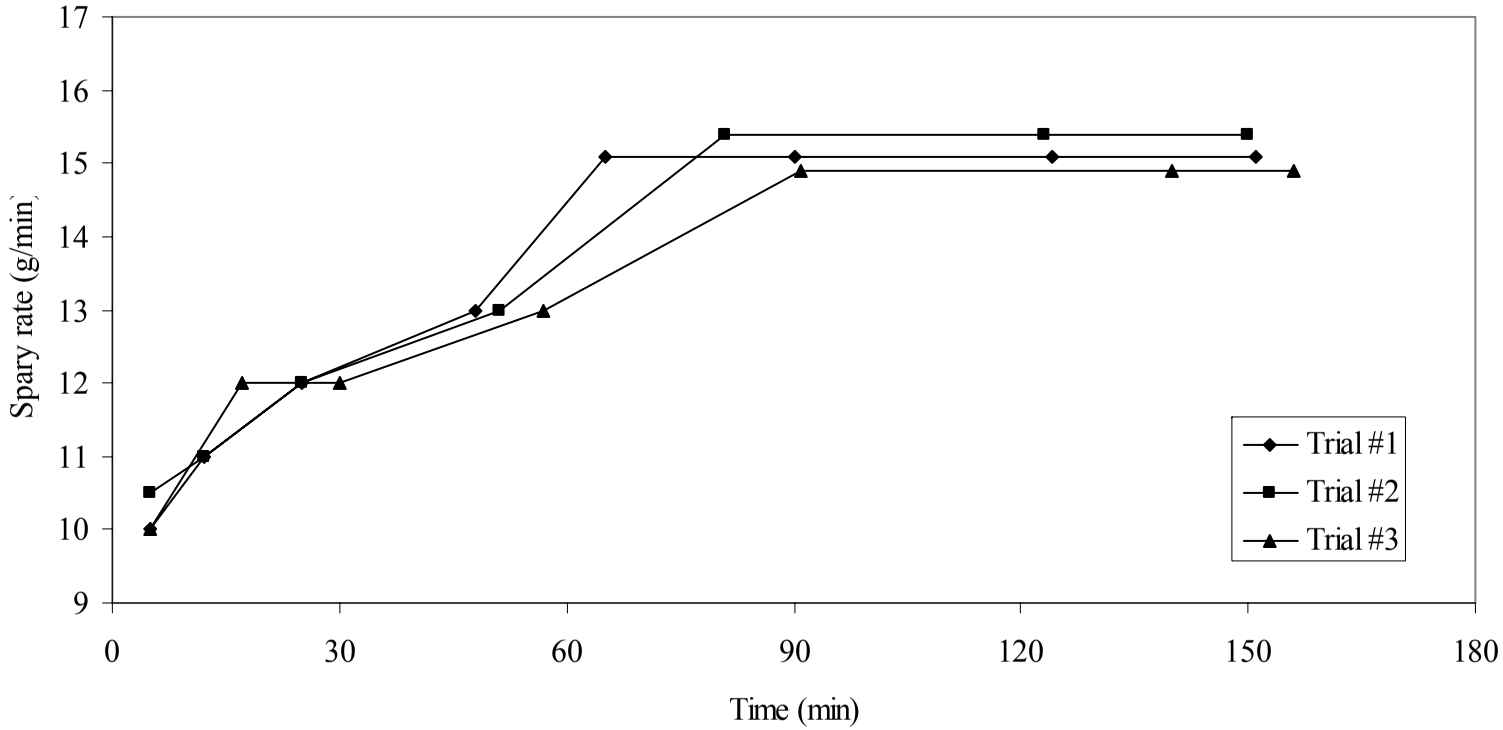

Figure 12. Eudragit RS30D Spray Rates for 300mg/g Diltiazem HCl Pellets

Table 9. Sampling scheme – Laboratory-scale Wurster coating.

Theoretical Applied Polymer Solids (%)	Theoretical Applied Polymer Solids* (g)	Suspension Applied* (g)	Sample Time (min)
5	87.5	648	65
6	105	777	74
7	122.5	907	82
8	140	1036	91
9	157.5	1166	100
10	175	1295	108
11	192.5	1425	117
12	210	1554	125
13	227.5	1684	134
14	245	1813	143
15	262.5	1943	151
16	280	2072	160

* Per 1750 grams of diltiazem HCl core pellets.

2.3.4.2 In-line Spectrometry

In-line spectroscopic monitoring of the coating process involved the use of a 1 inch diameter near-IR fiber-optic probe (Direct Reflectance Probe, Foss NIRSystem, Silver Spring, MD). The probe had a 10 mm sapphire window, and consisted of two collinear fiber optic bundles. Each bundle was 1 m long, and was comprised of 420 source-to-sample fibers and 720 sample-to-detector fibers (each 200 μm diameter). One bundle transmitted light from the exit slit of the monochromator to the sample, while the other bundle returned the reflected light from the sample to a PbS detector.

Initial studies attempted to scan directly through the polycarbonate sight glass in the base of the Wurster column. However, the lexan exhibited very strong near-IR absorbance, which dramatically reduced the signal from the pellet samples. To overcome this interference, a 1 inch diameter hole was drilled in the sight glass and a sapphire window was inserted such that the sapphire was flush with the surrounding lexan material and in contact with the pellets. The sapphire and the adhesive used to secure it in place were transparent in the near-infrared region and did not interfere with spectral analysis. **Figure 13** shows the near-IR spectra of 300mg/g diltiazem pellet samples coated with 5%, 10% and 16% Eudragit RS30D obtained by scanning through either the lexan sight glass or the sapphire window. Spectra obtained through the sapphire window were representative of the coated product, whereas those obtained by scanning through the original sight glass resembled the strong lexan signal. Further evidence of the detrimental effects of lexan on the near-IR calibration is apparent in **Figure 14**, where it is obvious that there is no predictive ability for near-IR estimation of percent applied polymer solids (% w/w).

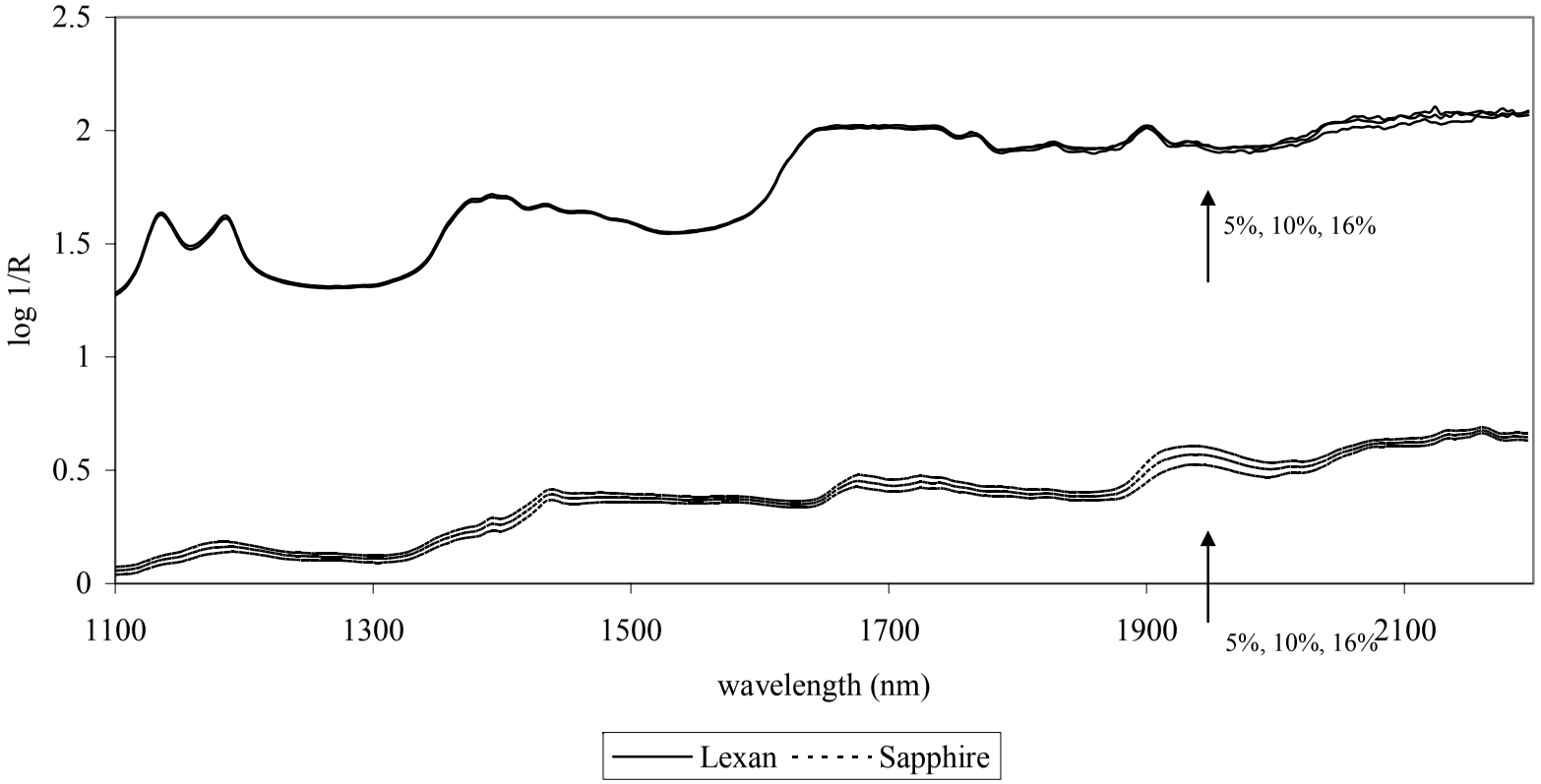

Figure 13. Effect of Lexan or Sapphire on 30% Diltiazem HCl Pellets Coated with 5%, 10%, & 16% Eudragit RS30D

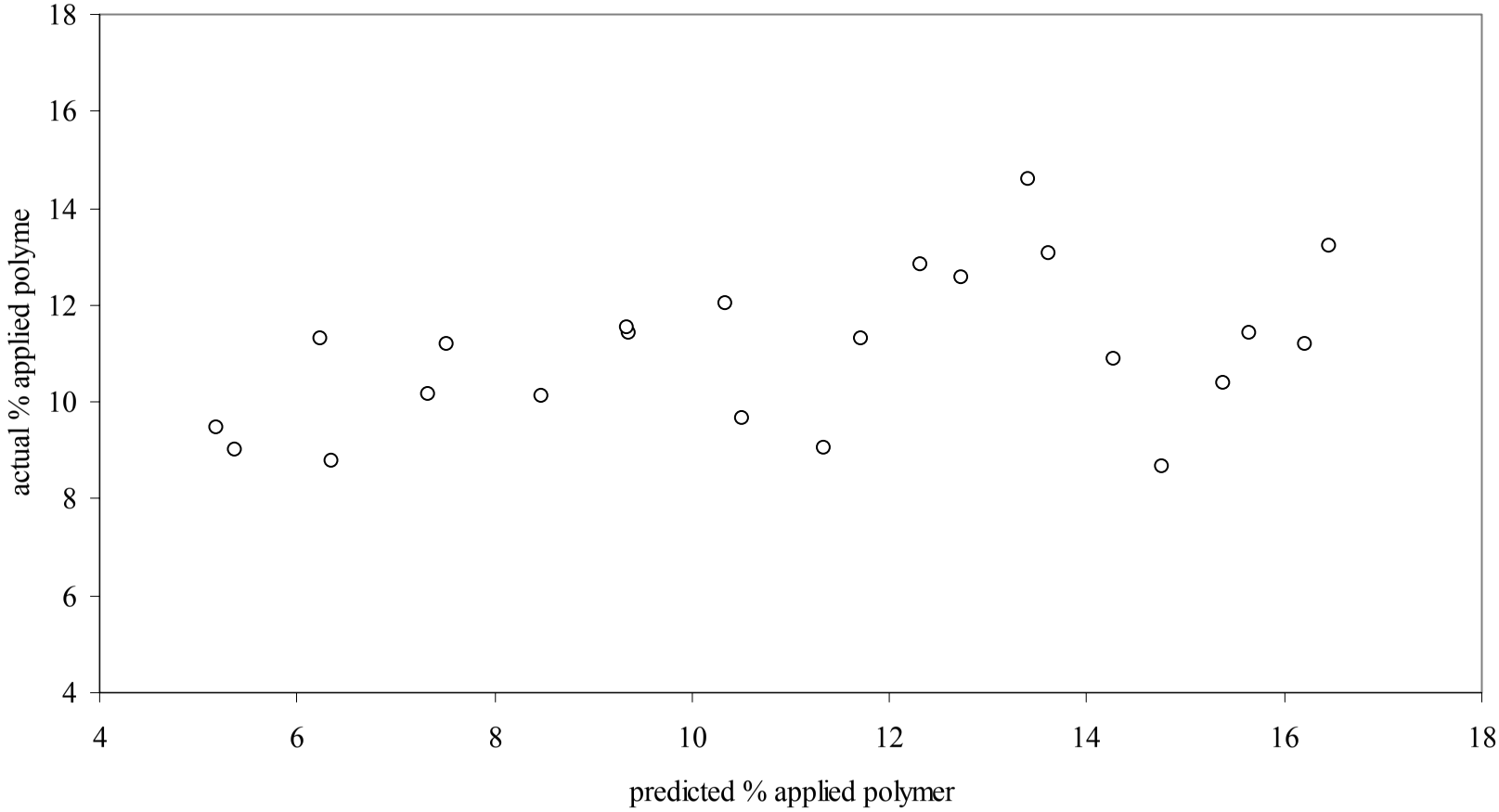

Figure 14. In-line Calibration for Applied Polymer Solids -- Scanning through Lexan

Near-infrared spectra were obtained by using the fiber-optic probe to scan the moving pellets as they passed the sapphire window during processing. Spectra were obtained at specified applications of polymer solids by monitoring the weight of coating suspension delivered. The time required to obtain one spectrum was 20 sec. The time required to obtain one spectrum of 20 averaged scans was 20 seconds. The number of pellets comprising a monolayer across the surface of the probe's window was approximately 120, 90, and 75, for the 150mg/g, 300mg/g, and 550mg/g strengths, respectively. During processing, it was observed that the particle bed moved at a rate of ~3 in/sec, therefore, in the time to obtain spectrum, between ~11,000 (550mg/g) and ~18,000 pellets (150mg/g) passed the sapphire window. **Figure 15** illustrates a schematic of the in-line sampling system for Wurster coating. Photographs of the sampling system are displayed in **Figure 16**.

2.3.4.3 At-line Spectrometry

Immediately following each scan, a 5 g sample of pellets was extracted from the Wurster processor using a thief, screened through 16 and 30 mesh screens to remove agglomerates and fines, then transferred to 3 dram glass vials. An additional near-IR evaluation of the pellet samples was performed at-line prior to reference analysis for polymer content.

Near-IR spectra were obtained in triplicate using a Rapid Content Analyzer® (RCA) sampling system (Foss NIRSystems, Silver Springs, MD). Near-IR radiation from a tungsten-halogen source was brought to the RCA sample compartment by means

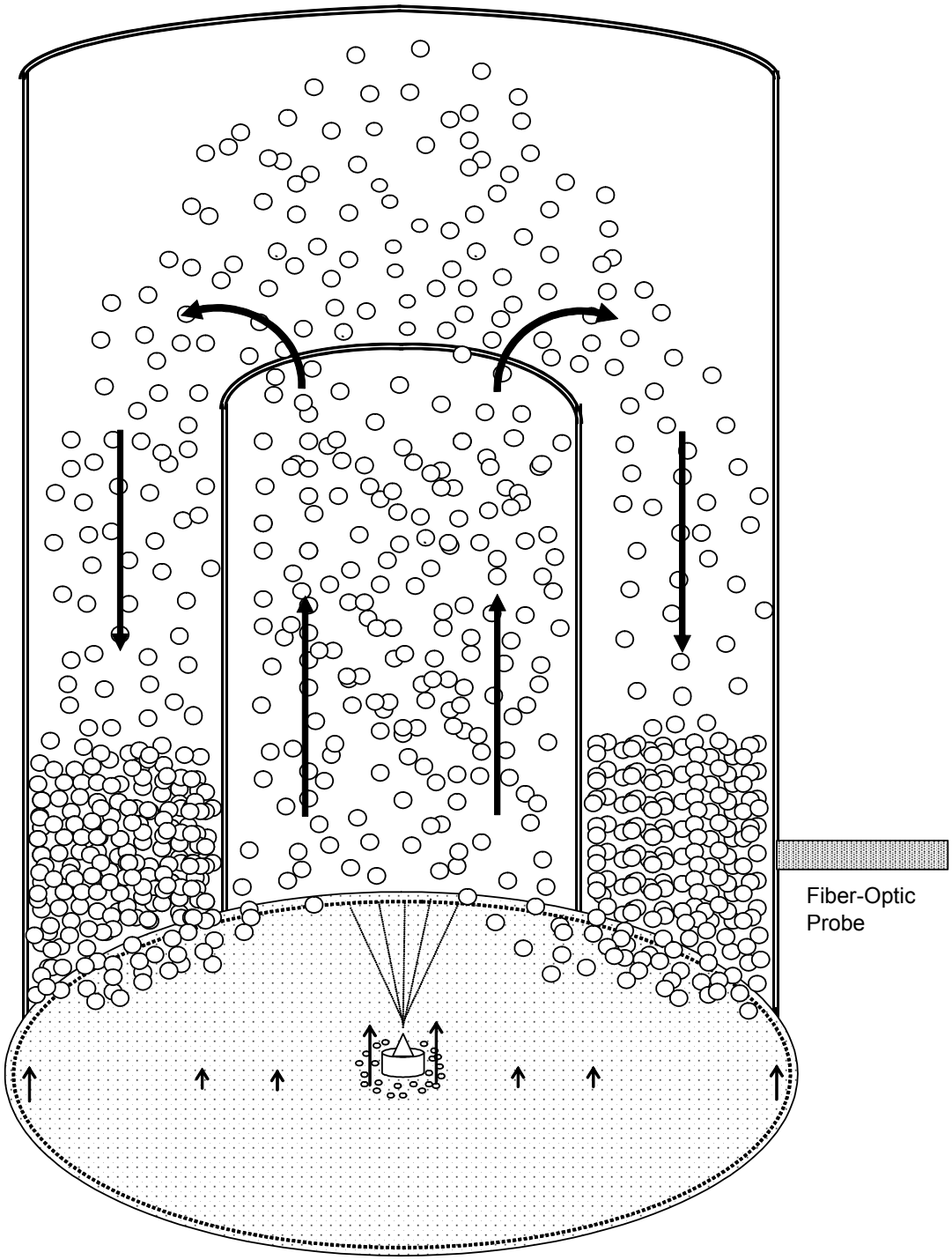

Figure 15. Fiber-Optic Sampling System for Wurster Coating

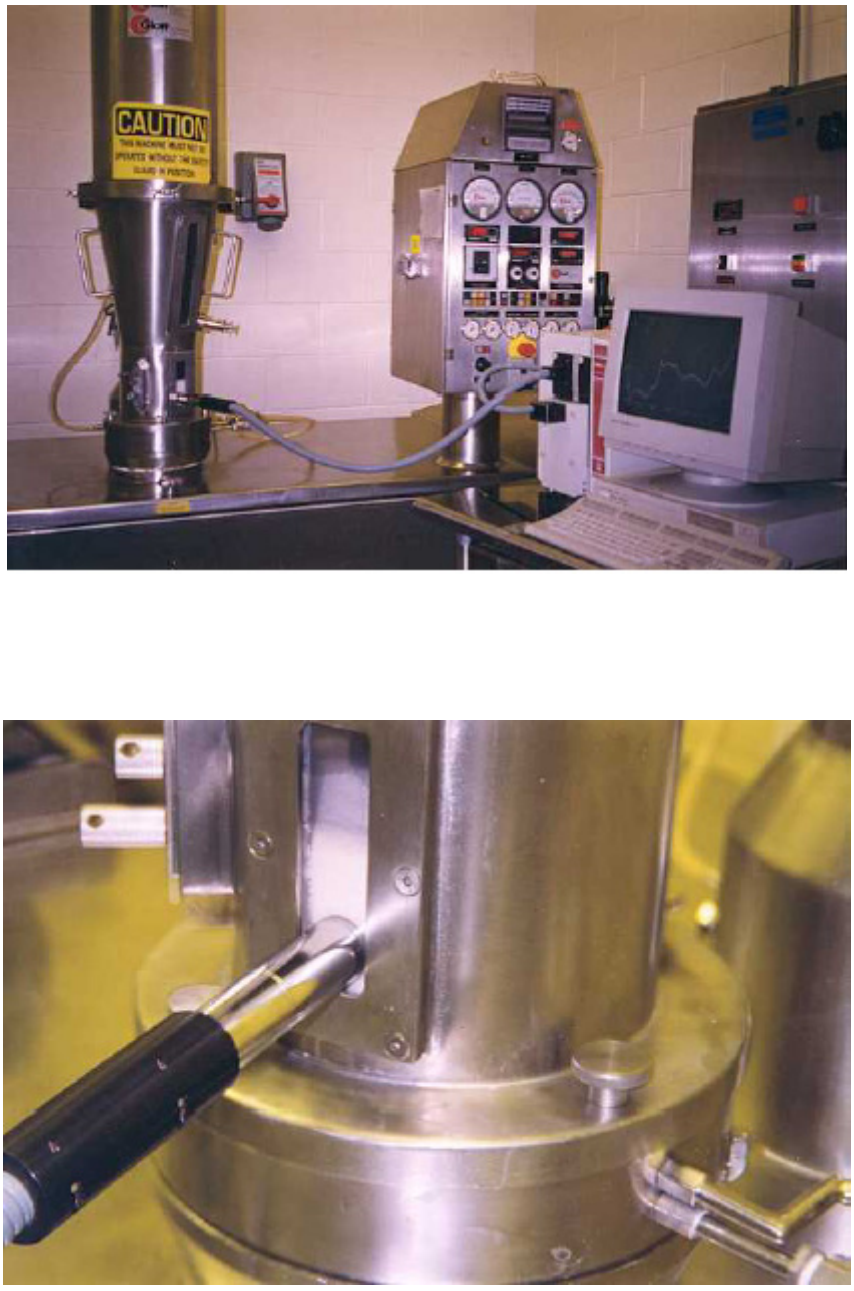

Figure 16. Fiber-optic Sampling System for Wurster Coating

of a fiber-optic bundle (420 fibers, each 200 μm diameter). Reflected light from the sample was reflected back into the detector array of the RCA, which consisted of four PbS detectors and four Si detectors for collection of near-IR and visible spectra, respectively. Spectra were obtained by scanning through the base (1.8 cm diameter) of the glass vials.. The number of pellets comprising a monolayer across a sample vial base was approximately 390, 290, and 240 for the 150mg/g, 300mg/g, and 550mg/g strengths, respectively. Each vial was inverted three times between scans. Replicate scans were averaged to obtain one spectrum for each sample time point. Total collection time per sample was approximately 90 sec.

2.3.4.4 Spectral Preprocessing

Spectra were reference corrected using a 99% Spectralon® disk (Labsphere, North Sutton, NH) and reflectance values were linearized with a log(1/R) transformation prior to analysis. NIRSystems NSAS® software was used for spectral preprocessing and all other chemometric analysis was performed using proprietary programs written in SPEAKEASY IV EPSILON +® (Speakeasy Computing Corp., Chicago, IL). To assess the significance of spectral preprocessing on calibration development and performance, separate calibrations were developed for MSC and D2 spectra.

2.3.5 Eudragit® RS30D Assay

The quantity of Eudragit RS30D (ERS) polymer solids applied to diltiazem HCl pellets was determined using a modified version of a colorimetric ion-pair complexation method described by Melia *et al.* (131). Eudragit RS30D solids were isolated from a

stock 30% w/w commercial aqueous latex dispersion by casting polymer films in polystyrene weigh boats and placing the samples in a 105 ºC laboratory oven for 48 h to remove water. The prepared films were stored in a desiccator over phosphorous pentoxide for 24 hours prior to analysis.

Standard solutions of dried ERS in chloroform were prepared over a concentration range of 0.25 mg/ml to 5 mg/ml. A 0.5 ml aliquot of stock solution was transferred to a 10 ml glass test tube and diluted with 4 ml chloroform and 5 ml 0.0016 M tropaeolin 000 in 0.1 M sodium chloride. The test tube was capped and mixed on a platform vortex mixer for two minutes. Chemical structures of ammonio methacrylate copolymer, the primary component of ERS, and tropaeolin 000 are presented in **Figure 17**. Upon mixing, the quaternary ammonium groups of the ERS complexed with the sulfonic acid functionalities of the anionic tropaeolin 000 dye and formed neutral species that partitioned into the organic layer. The mixture was then centrifuged for 10 minutes at 2500 rpm and the organic layer was analyzed by visible spectrometry through 1 cm quartz cuvettes. The absorption maximum of 485 nm was identical to that of the dye in the aqueous layer. Absorbance at 485 nm was linearly related to the polymer concentration of the sample. Absorbance at 485 nm in the chloroform layer was found to be linearly related to polymer concentration over the range of 0.2 to 1.4 absorbance units with an R^2 of 0.9997.

To determine the ERS content of coated diltiazem HCl pellets, 500 mg of sample pellets were transferred to 20 ml glass scintillation vials and vortexed for 15 min to dissolve the polymer. Based on a theoretical range of applied polymer solids of 5% to 16%, the test solutions had theoretical ERS concentrations of 1.25 mg/ml to 80 mg/ml.

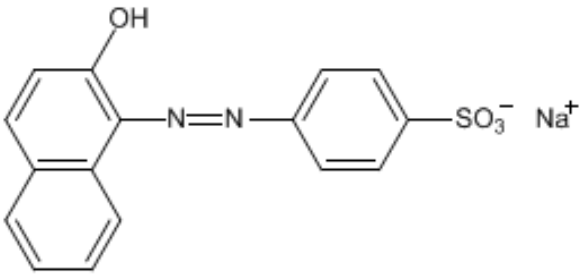

Tropaeolin OOO

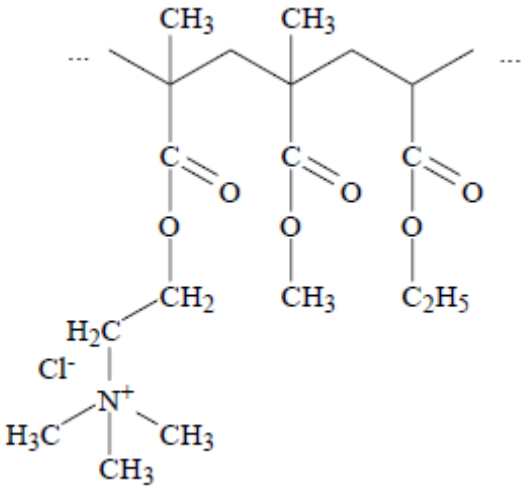

Ammonio Methacrylate Copolymer
the ratio of ethyl propenoate groups to methyl 2methylpropenoate groups to 2-(trimethylammonio)ethyl 2-methylpropenoate groups is about 1:2:0.1

Figure 17. Chemical Structures of Tropaeolin OOO and Ammonio Methacrylate Copolymer

These were within the working range of the standard curve. Subsequent dilution steps mimicked those used in preparation of the standard curve, however, following centrifugation it was observed that the entire quantity of tropaeolin 000 dye had partitioned into the organic layer. Upon investigation, it was noted that the pH of the aqueous orange dye solution was approximately 6.5. At this pH, the tertiary amine group of the basic diltiazem HCl drug substance, with a pKa of 7.7, would be ionized. This cationic species would then compete with the positively charged quaternary ammonium groups on the ERS polymer for anionic binding sites on the tropaeolin 000 dye. This was confirmed by testing additional samples spiked with varied levels of diltiazem HCl. The non-pareil seed, povidone, and talc components of the core pellets were determined to be non-interfering species.

To minimize ionization of the diltiazem HCl drug substance, the initial procedure was modified such that the stock 0.0016 M tropaeolin 000 in 0.1 M sodium chloride solution was adjusted to pH 13 with 0.1 N sodium hydroxide. At this pH, the color of the aqueous dye layer changed from orange to red. However, the chloroform solution remained orange and there was no detectable shift in wavelength or intensity. This pH adjustment was performed for all subsequent standard and test preparations. A linear regression was performed between the absorbance at 485 nm and Eudragit RS30D concentration values. Replicate solutions were made for each concentration over a three day period. **Figure 18** displays the standard curve obtained. The R^2 value for the calibration was 0.9998. Analysis of a 2.5 mg/ml standard over a three day period demonstrated an RSD of 0.32%, while analysis of freshly prepared standards over a three day period demonstrated an RSD of 0.41%.

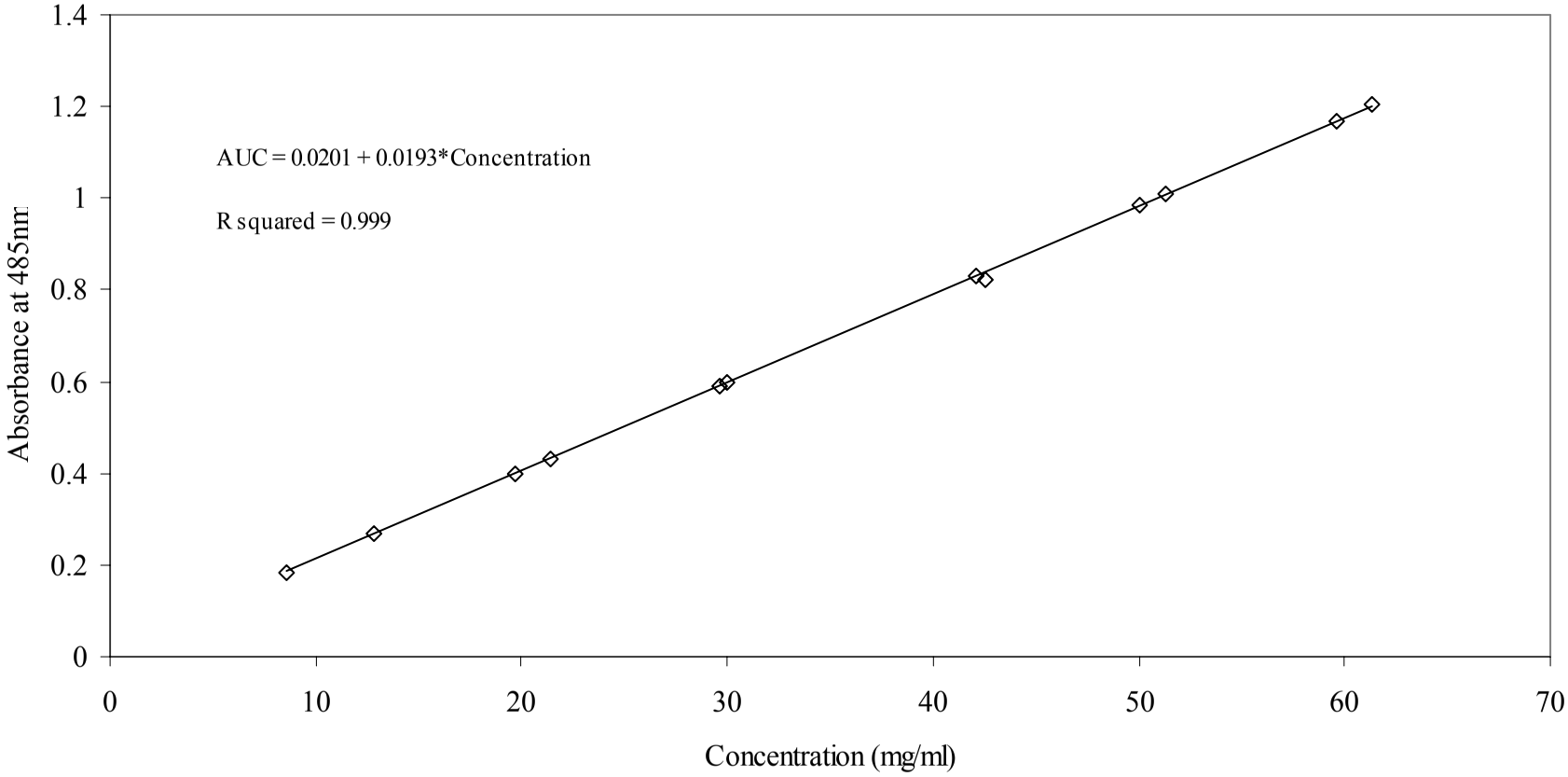

Figure 18. Standard Curve for Eudragit RS30D Assay

2.3.6 Quantitative Prediction of Eudragit RS30D Coating Level

Several calibration techniques were investigated for predicting the quantity of Eudragit RS30D applied to diltiazem HCl core pellets. Single and multiple wavelength calibrations as well as PCR and PLSR models were developed for both MSC and D2 spectra with the concentration of Eudragit RS30D as the dependent variable and spectral absorbance values, principal components or PLS factors as independent variables. Single and multiple wavelength calibration, and PCR were performed using programs written in SPEAKEASY®. PLSR was performed using commercial NSAS® software.

2.3.7 Qualitative Prediction of Eudragit RS30D Coating Endpoint

The ability of two pattern recognition algorithms to qualitatively predict coating process endpoints was assessed in this phase of study. The techniques under investigation included a Mahalanobis Distance (MD) calculation and a Bootstrap Error-Adjusted Single-sample Technique (BEAST). These methods classify samples according to their similarity relative to a training set. After training the computer to recognize the spectral qualities of acceptable material, the pattern recognition algorithms were employed to identify and classify unknown test samples. All qualitative analyses were performed using programs written in SPEAKEASY®.

In this study, near-IR spectra from six pellet samples containing a known quantity of polymer solids were used to develop spectral training sets. The quantity of applied coat solids was confirmed using the ERS assay previously described. During subsequent coating trials, samples were collected at various time points corresponding to different levels of applied coating and their spectral similarity to the training set was assessed via

the described pattern recognition techniques. For these analyses, samples within 3 SDs of the center of the training set cluster were considered to contain the desired level of Eudragit RS30D while samples with distances greater than 3 SDs were classified as outliers.

3 RESULTS and DISCUSSION

3.1 Quantitative Prediction of Pellet Potency

Because most pharmaceutical active ingredients and excipients absorb near-IR radiation, studies utilizing near-IR provide information regarding all system components. **Figure 19** displays the near-IR spectra of diltiazem HCl, nonpareil seeds, and 150 mg/g drug layered pellets corresponding to 86% to 106% theoretical potency based on applied suspension solids. As layering proceeds, decreasing absorbance is observed in regions characteristic of the sucrose and starch-based non-pareil seeds (1400 nm – 1600 nm and 2000 nm – 2150 nm), while increasing absorbance is noted in regions characteristic of diltiazem HCl (1680 nm – 1900 nm and 1200 nm – 1350 nm).

Chemical structures of sucrose and diltiazem HCl, the primary components of the drug-layered pellets, are presented in **Figure 20**. In the regions characteristics of the non-pareil seed, the decreasing absorbance in the 1400 nm to 1600 nm region lies within the first overtone region and is attributed to O-H stretching, while the 2000 nm to 2150 nm region represents a combination band arising from O-H stretching. In regions characteristic of diltiazem HCl, increasing absorbance in the 1680 – 1900 nm and the 1200 nm – 1350 nm region, are primarily the result of C-H stretching and S-H stretching in the first and second overtones, respectively.

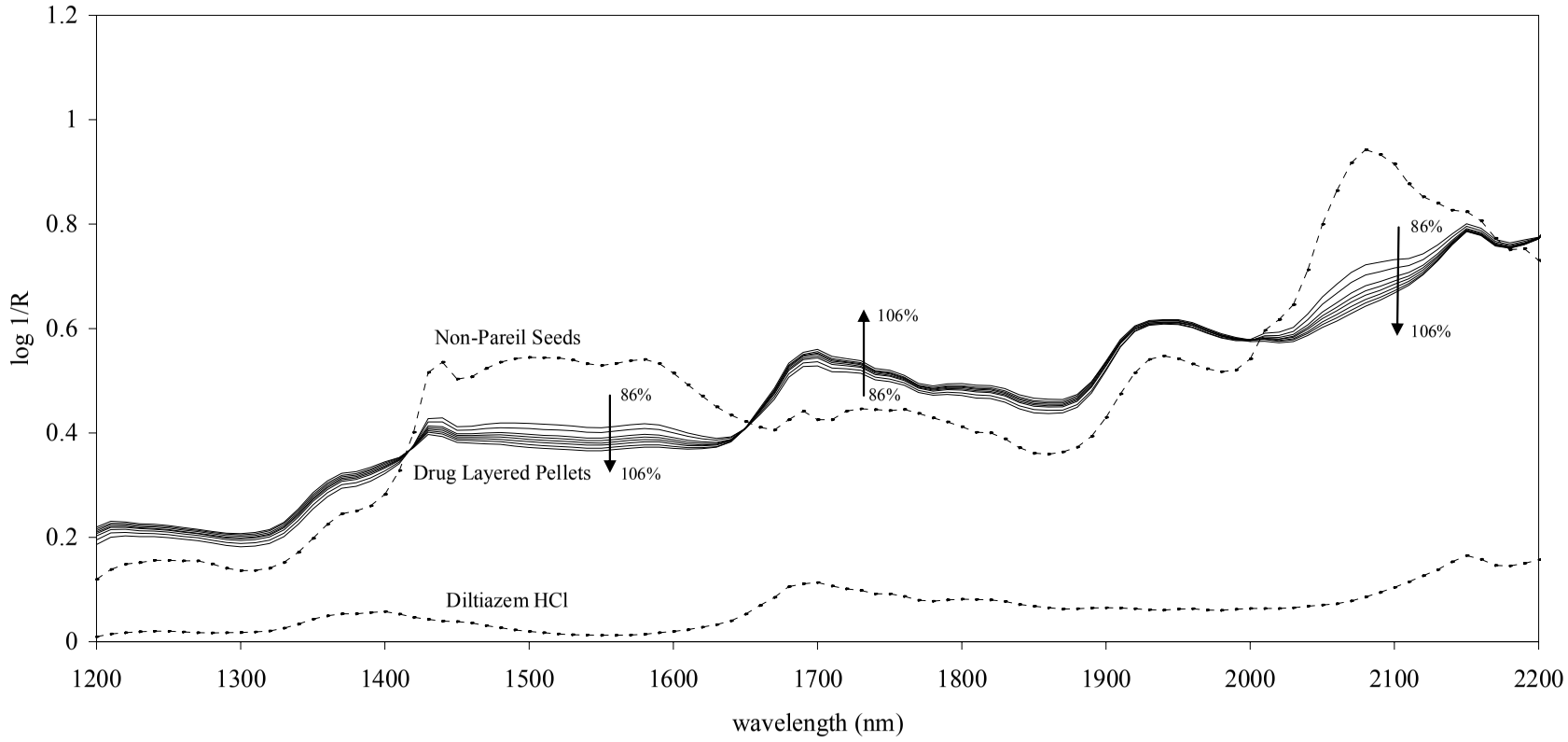

Figure 19: Near-IR Spectra of Diltiazem HCl Pellets, 150mg/g -- 86% to 106% Potency

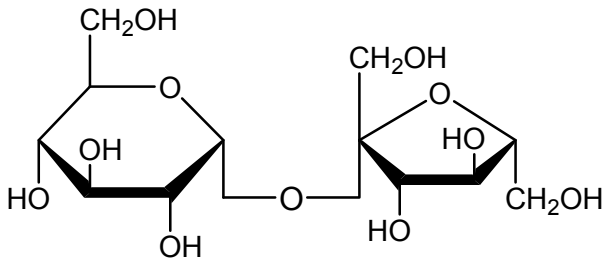

Sucrose

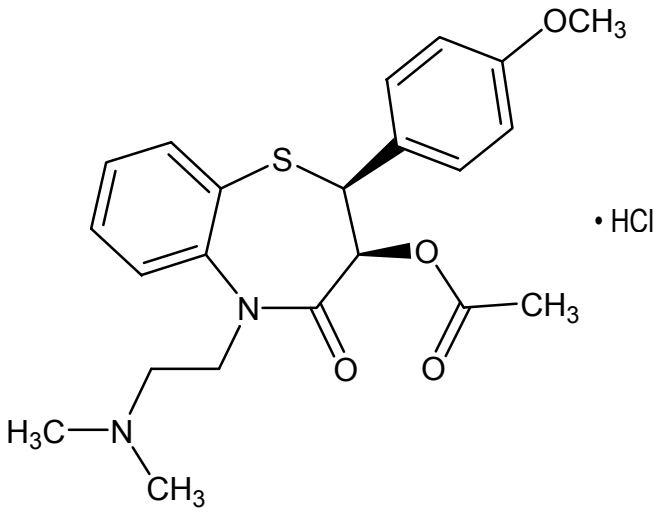

Diltiazem HCl

Figure 20. Primary Drug-layered Pellet Components

3.1.1 In-line Analysis of Pellet Potency

Single wavelength, multiple wavelength, and principal component calibrations were developed using both scatter corrected and second derivative spectra. A PLS calibration model was also developed using second derivative spectra. The choice of spectral preprocessing, MSC or D2, was based on the programs used to perform chemometric analysis. Single wavelength, multiple wavelength, and PCR analyses were performed on both MSC and D2 using SPEAKEASY® chemometric routines. PLSR was, however, performed using NSAS® software which offered only derivative-based spectral preprocessing. Because spectra were collected during processing, calibration model development was limited to one spectral scan per batch at each time point. Five batches were processed for each pellet strength. Each batch was processed on a unique day with a complete set-up and tear-down of the fluid bed processor occurring between lots. Calibrations were developed using 18 samples within the 96% to 106% theoretical potency range from three of the five batches for each formulation. Two additional batches from each formulation were processed to assess the predictive power of the developed calibrations.

3.1.1.1 Single and Multiple Wavelength Regression

For the single and multiple wavelength models, the most robust calibrations were developed using wavelengths from spectral regions characteristic of non-pareil seeds or diltiazem HCl drug substance. A single wavelength calibration was developed using absorbance values at 1672 nm which was highly correlated with diltiazem HCl. A two-wavelength model was developed using 1680 nm and 2040 nm, which correlated with

diltiazem HCl and non-pareil seeds, respectively. A SPEAKEZ® program provided preliminary identification of suitable wavelengths for calibration based on least-squares regression statistics R^2 and SEC. Wavelengths to be used for calibration were then selected based on their correlation to significant absorbance bands for diltiazem or non-pareil seeds.

For the 150mg/g strength, pellet potency increased by approximately 1% every 90 seconds. Single- and multiple-wavelength models for this strength had R^2 values of 0.93 and 0.92, respectively. SEC and SEP were 0.97% and 1.33%, respectively, for the single-wavelength model, and 0.89% and 1.25%, respectively, for the multiple wavelength calibration. For the 550mg/g strength, pellet potency increased by approximately 1% every four minutes. For this strength, both the single- and multiple-wavelength models provided R^2 values of 0.99. SEC and SEP were 0.30% and 1.72%, respectively, for the single-wavelength model, and 0.57% and 1.61%, respectively, for the multiple wavelength calibration.

3.1.1.2 Principal Component Regression

Principal component regression was used following an MSC or D2 treatment of the NIR data. Initially, spectra were transformed into principal component axis space. **Table 10** summarizes the sequences of principal components and their percentages of contribution to the total variations of spectral data for each pellet strength. The roots provide information about the magnitudes of variances along with principal component axes. The first principal component accounts for the largest amount of the total variations which, for MSC spectra, ranges from about 48% for 150mg/g pellets to about

Table 10. Principal components of in-line diltiazem HCl drug-layered pellets.

MSC				Second Derivative			
150 mg/g				150 mg/g			
Root No.	Roots	Proportional Variance	Cumulative Variance	Root No.	Roots	Proportional Variance	Cumulative Variance
1	130.65	0.4751	0.4751	1	78.62	0.2859	0.2859
2	88.79	0.3229	0.7980	2	33.83	0.1230	0.4089
3	34.09	0.1240	0.9219	3	23.10	0.0840	0.4929
4	8.67	0.0315	0.9535	4	19.46	0.0708	0.5636
5	6.34	0.0231	0.9765	5	14.68	0.0534	0.6170
6	3.65	0.0133	0.9898	6	13.64	0.0496	0.6666
7	1.03	0.0038	0.9936	7	12.45	0.0453	0.7119
300 mg/g				300 mg/g			
Root No.	Roots	Proportional Variance	Cumulative Variance	Root No.	Roots	Proportional Variance	Cumulative Variance
1	196.36	0.7140	0.7140	1	152.20	0.5535	0.5535
2	47.08	0.1712	0.8852	2	36.79	0.1338	0.6872
3	18.33	0.0667	0.9519	3	18.75	0.0682	0.7554
4	8.68	0.0316	0.9835	4	8.28	0.0301	0.7855
5	1.97	0.0072	0.9906	5	8.07	0.0294	0.8149
550 mg/g				550 mg/g			
Root No.	Roots	Proportional Variance	Cumulative Variance	Root No.	Roots	Proportional Variance	Cumulative Variance
1	255.67	0.9297	0.9297	1	153.56	0.5584	0.5584
2	11.70	0.0426	0.9723	2	15.59	0.0567	0.6151
3	4.88	0.0177	0.9900	3	13.13	0.0477	0.6628
				4	11.39	0.0414	0.7042
				5	10.32	0.0375	0.7418

93% for the 550mg/g strength. For D2 spectra, a greater number of PCs were required to explain the total spectral variation. The correlation of the first two PCs to the non-pareil seed and diltiazem HCl components of 150 mg/g and 550 mg/g drug layered pellets can be observed in **Figures 21 and 22**, respectively, which present the loadings spectrums of these components for MSC spectra. Although not readily apparent in the graphs, the correlation of these PCs to certain spectral regions characteristic of the primary pellets components was confirmed by comparing second derivative spectra of these ingredients to the loading spectra. Interestingly, a higher degree of noise is observed in 150mg/g pellets, relative to the 550mg/g strength, which has a much smoother loadings spectrum. The factors contributing to the increased noise in the 150 mg/g spectra are may be related to increased scatter from a smaller pellet particle size distribution, and a greater rate of change in potency occurring over the collection interval.

The principal components used for regression were limited to those that contributed significantly to the model (t-statistic >3.0). Regression results are summarized in **Table 11**. For both MSC and D2 spectra, two PCs were significant for all pellet strengths, which allowed potency to be predicted within ~1.5% of actual values. The inclusion of additional PCs was also investigated during calibration development. Although such models provided lower SEC values, they demonstrated higher SEP values, indicating potential overfitting of the data. Ideally, robust calibrations should be based on PCs which provide SEC and SEP values that are similar and as low as possible. The multivariate calibrations presented here have been optimized in such a manner.

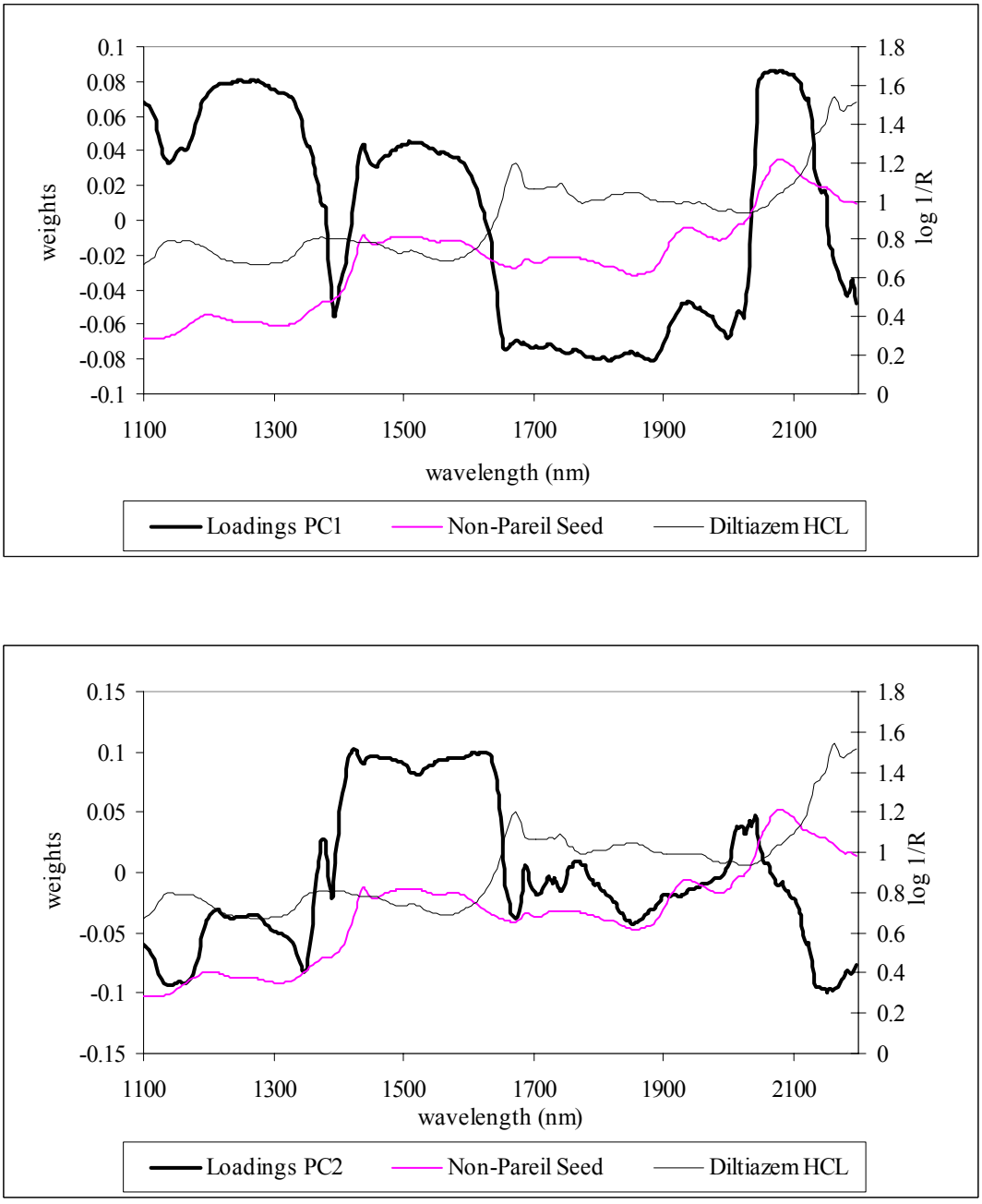

Figure 21. Loadings Spectrum of in-line 150mg/g Diltiazem HCl Pellets PC-1 (top) and PC-2 (bottom)

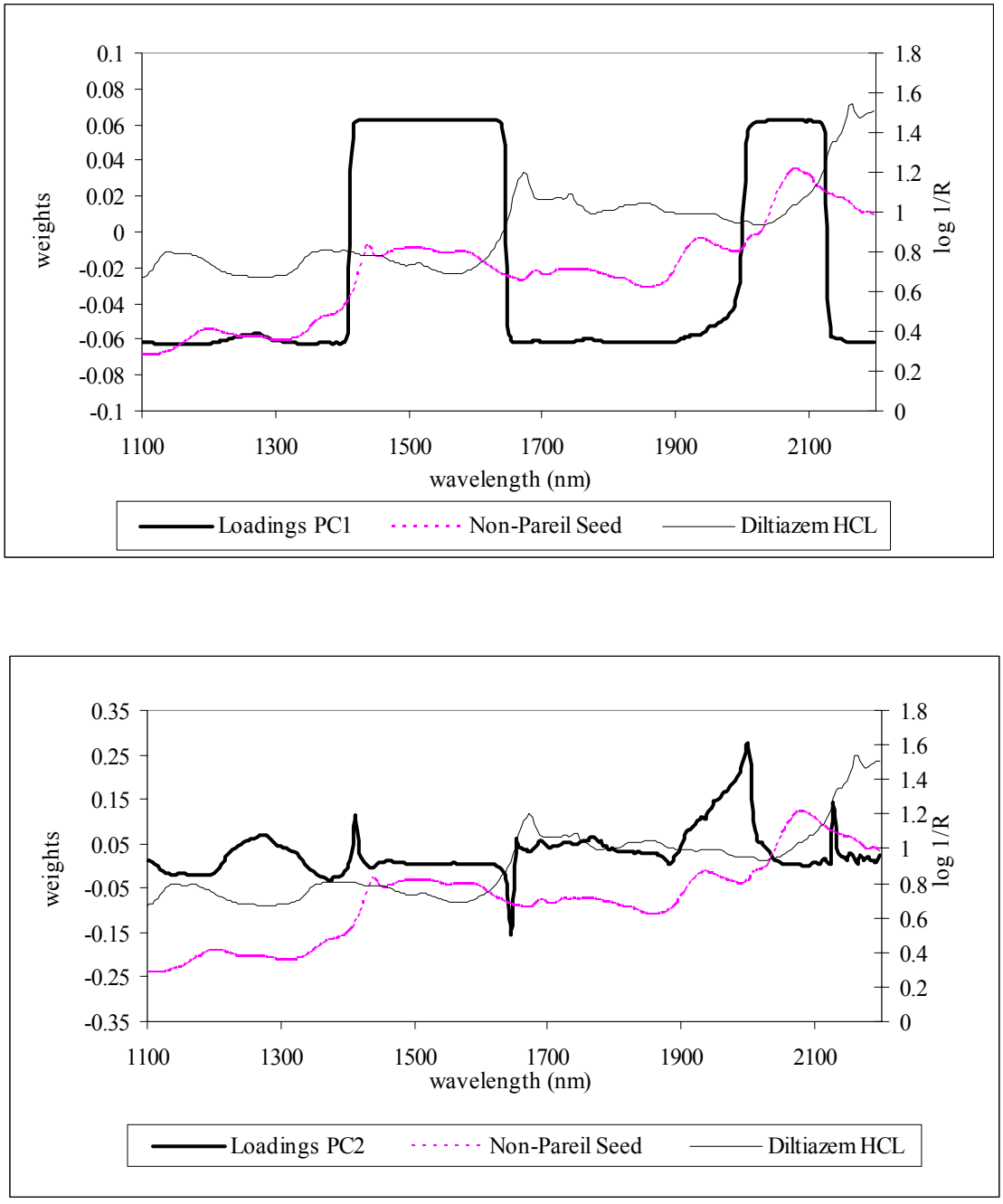

Figure 22. Loadings Spectrum of in-line 550mg/g Diltiazem HCl Pellets PC-1 (top) and PC-2 (bottom)

Table 11. Principal component regression results for in-line diltiazem HCl drug-layered pellets.

MSC						2nd Derivative					
150mg/g						**150mg/g**					
PCs Used	T-Statistic		R^2	SEC	SEP	PCs Used	T-Statistic		R^2	SEC	SEP
1	PC-1	-3.48	0.43	2.87%	2.68%	1	PC-1	-5.38	0.65	2.54%	2.27%
2	PC-1	-5.78	0.83	1.66%	1.49%	2	PC-1	-8.86	0.90	1.32%	1.09%
	PC-2	-5.39					PC-2	-5.32			
300mg/g						**300mg/g**					
PCs Used	T-Statistic		R^2	SEC	SEP	PCs Used	T-Statistic		R^2	SEC	SEP
1	PC-1	-6.40	0.81	1.66%	1.35%	1	PC-1	-7.09	0.83	1.52%	1.27%
2	PC-1	-15.3	0.88	1.42%	1.01%	2	PC-1	-25.4	0.88	1.27%	0.96%
	PC-2	-12.4					PC-2	-14.3			
550mg/g						**550mg/g**					
PCs Used	T-Statistic		R^2	SEC	SEP	PCs Used	T-Statistic		R^2	SEC	SEP
1	PC-1	-16.95	0.93	1.05%	1.12%	1	PC-1	-15.87	0.93	1.08%	1.13%
2	PC-1	-20.3	0.94	1.02%	0.93%	2	PC-1	-24.3	0.95	0.99%	1.02%
	PC-2	-4.03					PC-2	-6.7			

3.1.1.3 Partial Least Squares Regression

Partial least squares regression was performed on D2 spectra using a commercial software package, NSAS® Version 3.25, that was provided with the NIRSystems Model 6500 spectrometer. As previously described, PLSR is useful with small populations of samples that contain experimental noise in the near-IR and/or the chemical data. PLS is similar to PCA, in that the regression factors for both are linear combinations of wavelengths established from combinations of near-IR spectra. In PCA, principal axis transformation is performed independently of the calibration regression, and accounts for the maximum variation in the near-IR data. Under PLS, the principal axis transformation and the development of the calibration regression are concurrent, where the factors describe the types of spectral variation that are important for modeling the variables in the chemical data. A validation process is employed to assess the amount of error due to variation between the samples in the population and to identify the appropriate number of factors to provide a robust calibration without overfitting the model.

The cross validation approach employed by the NSAS® software splits the population into N segments (usually four) then validates the segment as an unknown against the remaining sections. The selection process designates as a segment, sample 1, sample 5, sample 9, etc. as the regression moves through the entire population until all the samples in the population are fully validated. The procedure calculates the mean square error or cross validation (MSECV) for the population and attempts to determine the number of factors that will characterize the sample set without overfitting it. The user is provided the option of comparing a separate test population against the calibration population to validate the model. For each model, the software determines and reports

the minimum MSECV, the ratio of the current MSECV value to the minimum value in the set, the correlation coefficient, and the standard error. It then recommends an appropriate number of factors based on the ratio of the current MSECV to the minimum MSECV in which it recognizes the optimal number of factors as those that provide a ratio of about 1.25 (132). A "prediction" function allows the user to apply a stored calibration equation to a spectral data file for prediction of constituent percentages.

The preceding discussion is provided to explain the approach taken in NSAS® for PLS calibration model development. The preceding explanation of the NSAS® method for PLS calibration, and the use of this software in the current study is, by no means, advocating the use of a "black-box" approach to near-IR calibration and analysis. At the time this work was performed, our laboratory was primarily focused on the development of PCA regression models for near-IR data. Since PLS was available in the commercial NSAS® software package that accompanied the spectrometer used to collect spectral data from drug layering and pellet coating experiments, a logical extension of this work was to assess the performance of the NSAS® PLS model in predicting pellet potency and applied polymer solids and compare its performance to PCA methods. When using any type of commercial software, the relevance of suggested regression factors with respect to the analyte characteristics under evaluation, should be well understood, and their effect on model performance and robustness critically assessed.

Partial least squares regression results of D2 spectra for all pellet strengths are summarized in **Table 12**. The results were similar to those obtained using PCR, with SEPs less than 1.5% observed for most models. Similar to PCR, the SEC and SEP observed using PLS regression improved as pellet strength increased. This was attributed to a slower rate of potency change over the spectral acquisition interval, and potentially less particle size related scatter associated with the higher strengths. Interestingly, the NSAS® software use of the ratio of current MSECV value to the minimum value in the calibration was effective at identifying an ideal number of factors to prevent overfitting. Although SEC could be improved by adding PLS factors to the model, SEP was observed to decrease when too many factors were included in the calibration. As previously reported, a similar phenomenon was observed for PCR regressions when non-statistically significant PCs were included in the calibration.

3.1.1.4 Summary of In-line Regression Model Performance

A summary of the performance of optimized single wavelength, multiple wavelength, PCR and PLS models for in-line analysis of all pellet strengths is presented in **Table 13**. Similar calibration results were obtained for 150 mg/g, 300mg/g, and 550mg/g drug layered pellets. Standard error of the laboratory (SEL) (133) for the HPLC reference method, calculated according to the following equation, was determined to be approximately 0.46%, which was well within the USP chromatographic system suitability limit of 2% (134).

Table 12. Partial least squares regression results for in-line analysis of diltiazem HCl drug-layered pellets.

		150 mg/g		
Factor	MSECV	R	SEC	SEP
1	2.862	0.87	2.67 %	2.71%
<2>	1.053	0.95	1.24 %	1.52%
3	1.634	0.97	1.11 %	1.63%
4	1.881	0.98	0.88 %	NT
5	1.347	0.99	0.61 %	NT
		300 mg/g		
Factor	MSECV	R	SEC	SEP
1	2.504	0.89	1.72 %	2.01%
2	1.223	0.95	1.04 %	1.12%
3	0.982	0.97	0.84 %	1.05%
<4>	0.828	0.99	0.58 %	0.96%
5	0.727	0.99	0.43 %	1.12%
		550 mg/g		
Factor	MSECV	R	SEC	SEP
<1>	0.815	0.97	1.04 %	0.71%
2	0.851	0.98	0.87 %	0.95%
3	1.151	0.98	0.74 %	NT
4	1.445	0.99	0.60 %	NT
5	1.600	0.99	0.50 %	NT

< > - factors recommended by NSAS®
NT - not tested.

Table 13. Summary of regression results for in-line assessment of pellet potency.

Regression Model	PCs	R^2	Potency (%) SEC	Potency (%) SEP
150mg/g Diltiazem HCl Pellets				
PCR – MSC	2	0.83	1.66	1.49
PCR – D2	2	0.90	1.32	1.09
PLS – D2	2	0.95	1.24	1.52
Multiple Wavelength	--	0.92	0.89	1.25
Single Wavelength	--	0.93	0.97	1.33
300mg/g Diltiazem HCl Pellets				
PCR – MSC	2	0.88	1.42	1.01
PCR – D2	2	0.88	1.27	0.96
PLS – D2	4	0.99	0.58	0.96
Multiple Wavelength	--	0.99	0.51	0.36
Single Wavelength	--	0.99	0.82	0.31
550mg/g Diltiazem HCl Pellets				
PCR – MSC	2	0.94	1.02	0.93
PCR – D2	2	0.95	0.99	1.02
PLS – D2	1	0.97	1.04	0.71
Multiple Wavelength	--	0.99	0.57	1.61
Single Wavelength	--	0.99	0.30	1.72

$$SEL = \sqrt{\left(\frac{\sum_{i=1}^{m} (Op_1 - Op_2)^2}{m} \right)} \qquad \text{(Eq. 20)}$$

In this equation, Op_1 and Op_2 are reference potency values measured on separate days, and m is the number of samples analyzed.

All multivariate calibration models, with the exception of the 150mg/g MSC/PCR model, demonstrated R^2 values of 0.88 or greater and standard errors of calibration no greater than 1.4%. Interestingly, even the simplistic single and multiple wavelength models demonstrated their ability to predict pellet potency within 2% of HPLC values. Such results indicate that it may be possible to employ inexpensive single filter instruments for on-line monitoring of drug layering operations. However, there are numerous advantages to full-spectrum methods, including: the ability to reduce noise by averaging data over both wavelengths and spectra; noise reduction by rejecting the higher factors, into which the noise is preferentially placed; the advantages inherent in the use of orthogonal variables; and the avoidance of the time-consuming step of performing the wavelength selection process. On the other hand, when a condition of differential non-linearity exists in the data, traditional wavelength selection (i.e., MLR) might be capable of creating more accurate models than full wavelength methods, since, almost be definition, this approach will find the wavelength(s) where the effect of non-linearity are minimal, which full-spectrum methods (PCS and PLS) may not do (134).

Of the three drug levels investigated, the 150mg/g pellets demonstrated the most rapid rate of potency change within the studied range**.** Pellet potency increased by approximately 1% every 90 seconds. **Figure 23** shows a plot of both the calibration and prediction results obtained by principal component regression of second derivative spectra for 150mg/g pellets. Despite the rapidly changing drug content of the pellets, potency could be accurately predicted using in-line near-IR analysis. The calibration model provided an R^2 value of 0.90 and a SEC of 1.32%. Although SEP and SEC values below 2% would be acceptable for most rotogranulation operations, the calibration performance of the 150mg/g strength could possibly be improved by slowing down the application rate or decreasing the solids content of the drug layering suspension.

3.1.2 At-line Analysis of Pellet Potency

Frequently, the physical modification of processing equipment to allow in-line process monitoring is not feasible. In such instances, at-line process monitoring may be a viable alternative. In this study, an at-line near-IR analysis of pellet samples was conducted prior to HPLC potency analysis. At-line spectra of unit-dose samples were obtained in triplicate by scanning through the base of the glass sample vials using a NIRSystems Rapid Content Analyzer and model 6500 spectrometer.

Figure 24 compares second derivative spectra of 300mg/g diltiazem HCl pellets collected in-line using the fiber-optic probe, or at-line using the rapid content analyzer. The spectral features of both samples are similar. Such spectral similarity may be attributed to the fact that both in-line and at-line samples are representative of the batch at specified sample time points, and that both instruments utilize similar optical

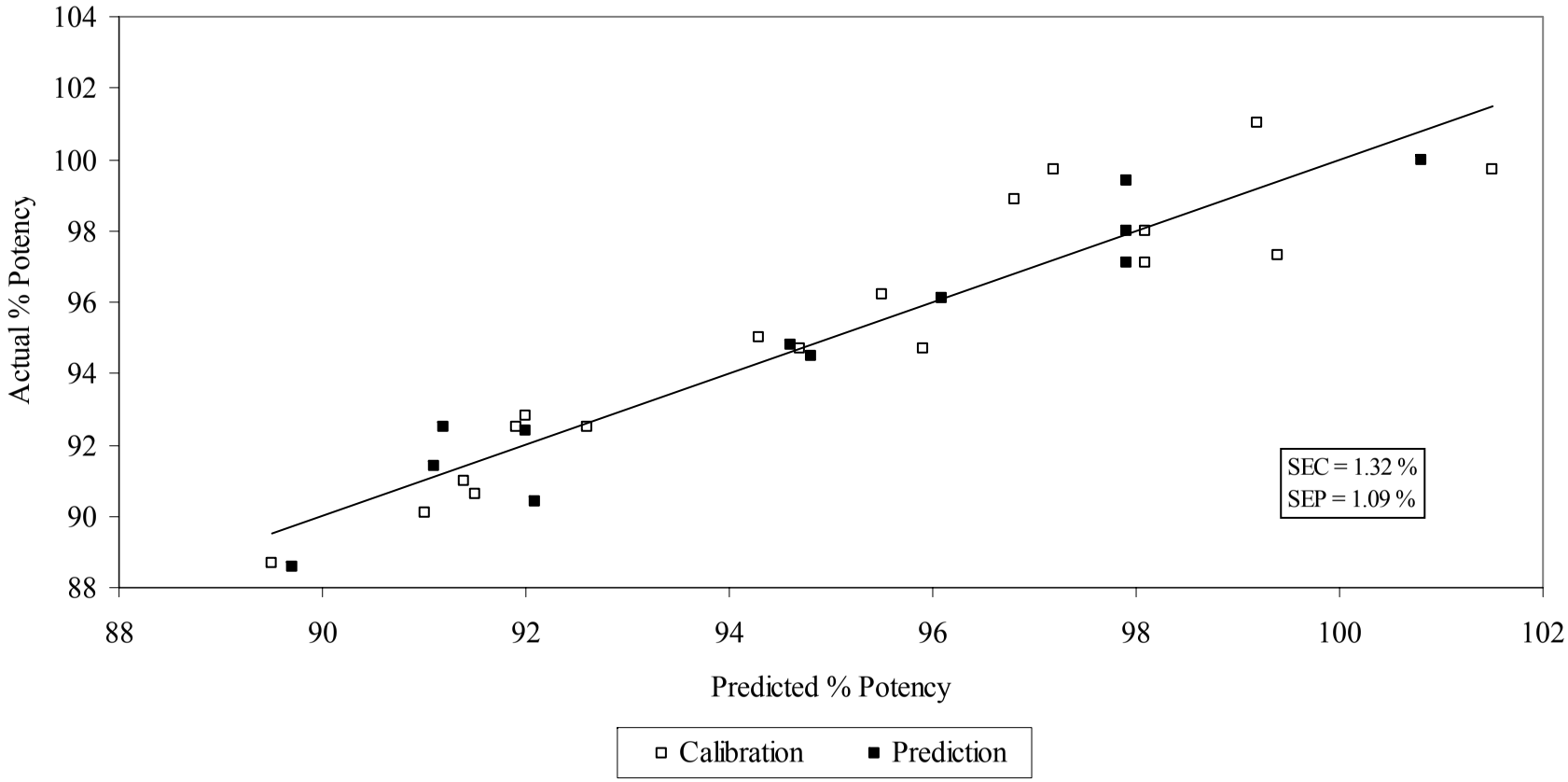

Figure 23. Potency Calibration and Prediction -- Diltiazem HCl 150mg/g Pellets In-line Analysis

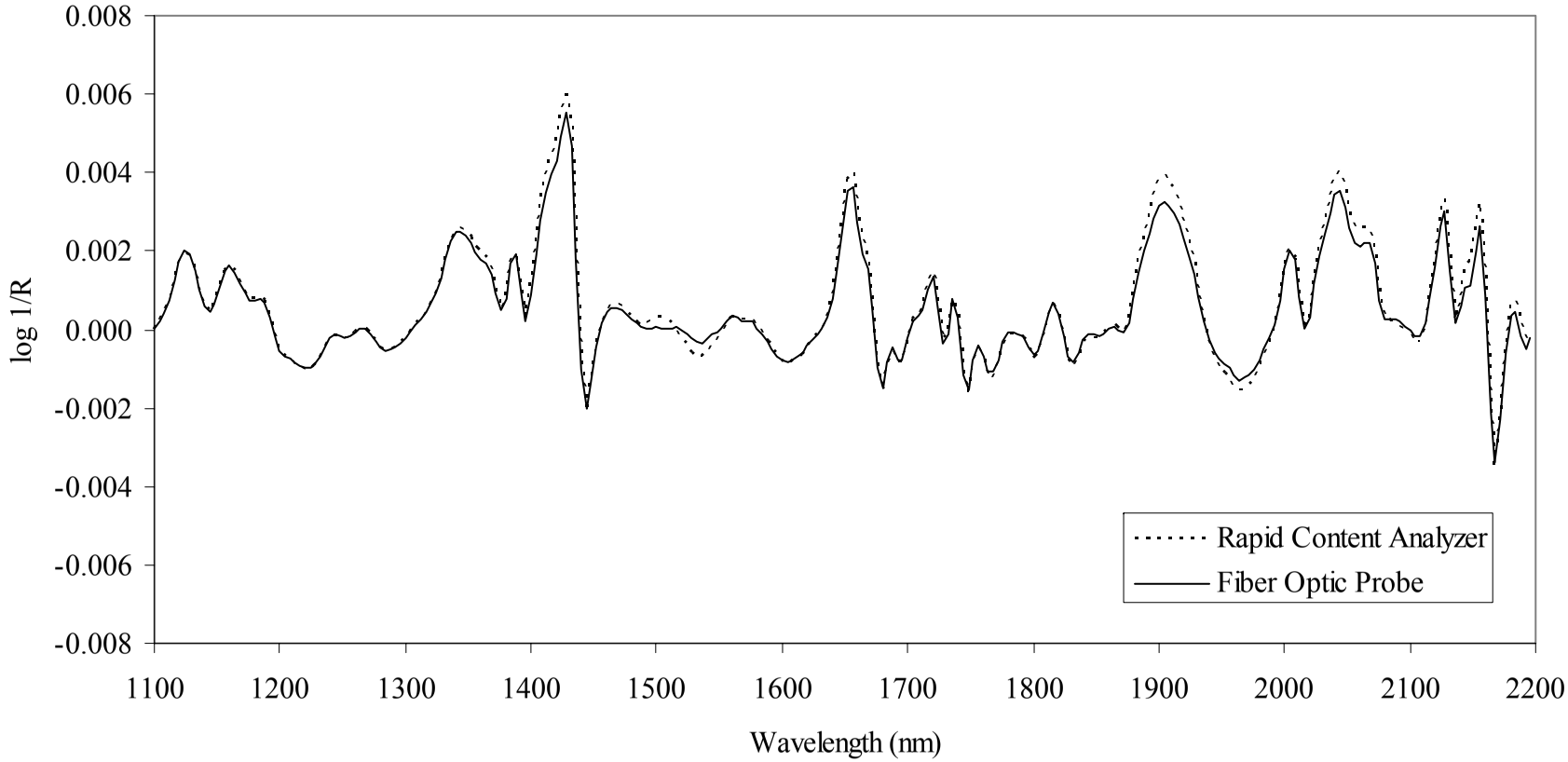

Figure 24. 2nd Derivative Spectra for 300mg/g pellets - RCA vs. Probe Sampling

design characteristics, a common monochromator system, and similar fiber optic bundles and detector materials.

3.1.2.1 Single and Multiple Wavelength Regression

Similar to the in-line studies, the single and multiple wavelength models that provided the most robust calibrations were developed using wavelengths from spectral regions characteristic of non-pareil seeds or diltiazem HCl drug substance. A single wavelength calibration was developed using absorbance values at 1672 nm which was highly correlated with diltiazem HCl. A two-wavelength model was developed using 1680 nm and 2040 nm, which correlated with diltiazem HCl and non-pareil seeds, respectively. For the 150mg/g strength, single- and multiple-wavelength models had R^2 values of 0.99 and 0.98, respectively. SEC and SEP were 0.76% and 0.84%, respectively, for the single-wavelength model, and 0.54% and 0.56%, respectively, for the multiple wavelength calibration. For the 550mg/g strength, both the single- and multiple-wavelength models provided R^2 values of 0.99. SEC and SEP were 0.49% and 0.56%, respectively, for the single-wavelength model, and 0.48% and 0.53%, respectively, for the multiple wavelength calibration. The improved performance of these techniques, relative to the in-line results, is likely due to the static nature of the samples, normalized particle size due to sieving prior to analysis, triplicate scans of the samples to provide a more representative spectrum of each sample, and a larger number of samples in the calibration set.

3.1.2.2 Principal Component Regression

Principal component regression was used following an MSC or D2 treatment of the NIR data. Initially, spectra were transformed into principal component axis space. **Table 14** summarizes, for each pellet strength, the sequences of principal components and their percentages of contribution to the total variations of spectral data. Similar to in-line sampling, the first principal component accounts for the largest amount of the total variations which, for MSC spectra, ranges from about 68% for 150mg/g pellets to about 91% for the 550mg/g strength. For D2 spectra, a greater number of PCs were required to explain the spectral variation. In these spectra, the amount of total variation explained by the first PC ranges from about 60% for 150mg/g pellets to about 78% for the 550mg/g strength.

The correlation of the first two PCs to the non-pareil seed and diltiazem HCl components of 150 mg/g and 550 mg/g drug layered pellets can be observed in **Figures 25 and 26**, respectively, which present the loadings spectrums of these components for MSC spectra. The loadings for 150 mg/g and the 550 mg/g at-line samples are very similar to those obtained from the vial samples; however, a smoother loading spectra was observed for the at-line samples relative to spectra collected in-line.

The principal components used for regression were limited to those that contributed significantly to the model (t-statistic >3.0). Regression results are summarized in **Table 15**. For the 150 mg/g and 300mg/g strengths, two PCs were significant (t-statistic > 3.0) and used in the calibration model development. For the 550 mg/g strength, one PC significant PC was used in the model. These models demonstrated that potency could be predicted within ~1% of actual values. In addition, for all models,

Table 14. Principal components of at-line diltiazem HCl drug-layered pellet samples.

MSC				Second Derivative			
150 mg/g				150 mg/g			
Root No.	Roots	Proportional Variance	Cumulative Variance	Root No.	Roots	Proportional Variance	Cumulative Variance
1	186.48	0.6781	0.6781	1	163.65	0.5951	0.5951
2	57.409	0.2088	0.8869	2	47.83	0.1739	0.7690
3	19.92	0.0724	0.9503	3	14.14	0.0514	0.8204
4	6.00	0.0218	0.0911	4	7.25	0.0263	0.8468
5	2.87	0.0105	0.9912	5	5.89	0.0214	0.8682
300 mg/g				300 mg/g			
Root No.	Roots	Proportional Variance	Cumulative Variance	Root No.	Roots	Proportional Variance	Cumulative Variance
1	206.46	0.7508	0.7508	1	178.11	0.6478	0.6478
2	30.98	0.1127	0.8634	2	27.43	0.0994	0.7471
3	25.90	0.0931	0.9564	3	1749	0.0636	0.8107
4	8.48	0.0309	0.9874	4	8.23	0.0299	0.8407
5	2.02	0.0074	0.9948	5	5.99	0.0218	0.8625
550 mg/g				550 mg/g			
Root No.	Roots	Proportional Variance	Cumulative Variance	Root No.	Roots	Proportional Variance	Cumulative Variance
1	250.54	0.9111	0.9111	1	216.16	0.7860	0.7860
2	19.83	0.0721	0.9832	2	15.45	0.0563	0.8422
3	3.43	0.0125	0.9957	3	12.98	0.0472	0.8894
				4	7.04	0.0256	0.9159
				5	4.06	0.0148	0.9298

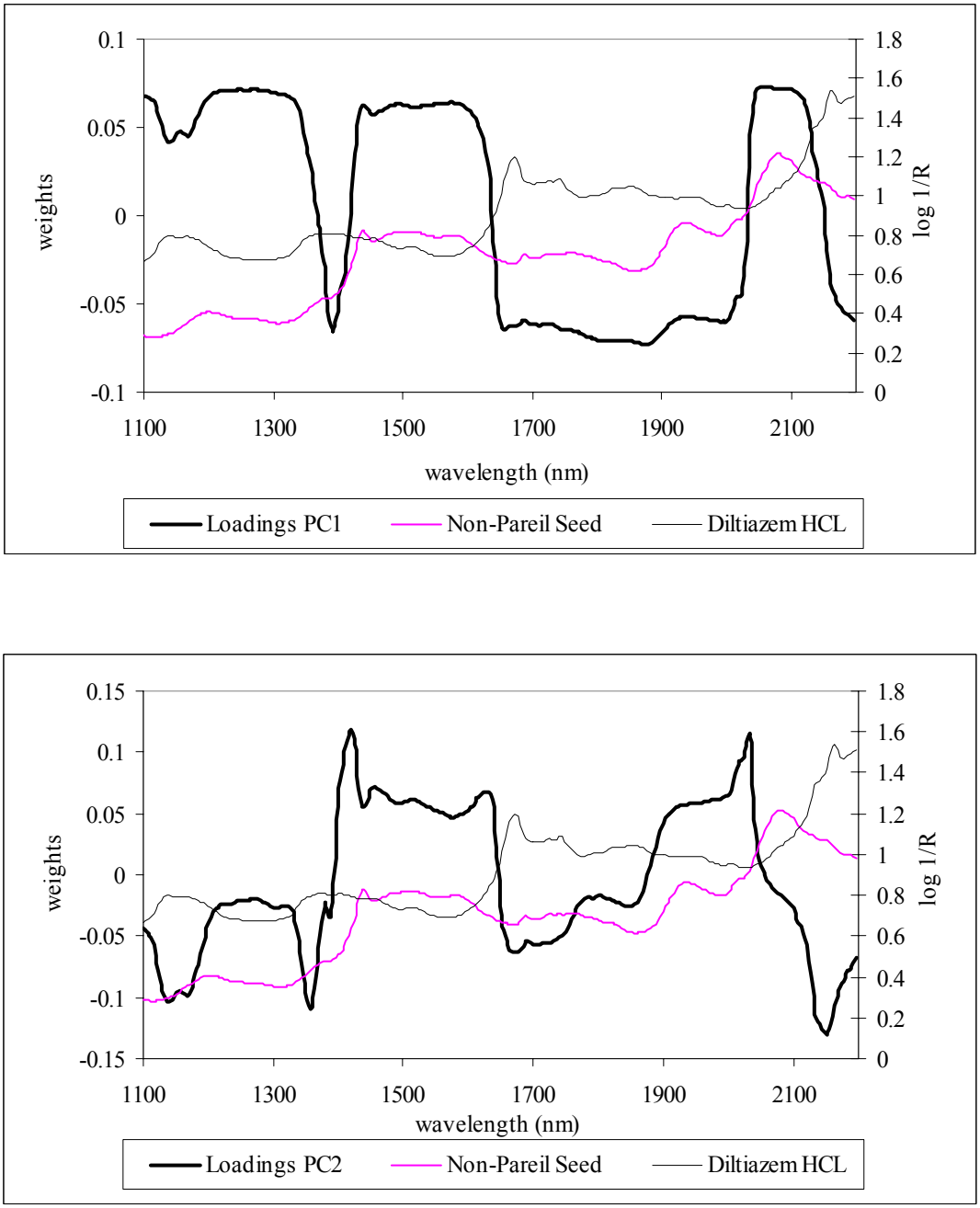

Figure 25. Loadings Spectrum of at-line 150mg/g Diltiazem HCl Pellets PC-1 (top) and PC-2 (bottom)

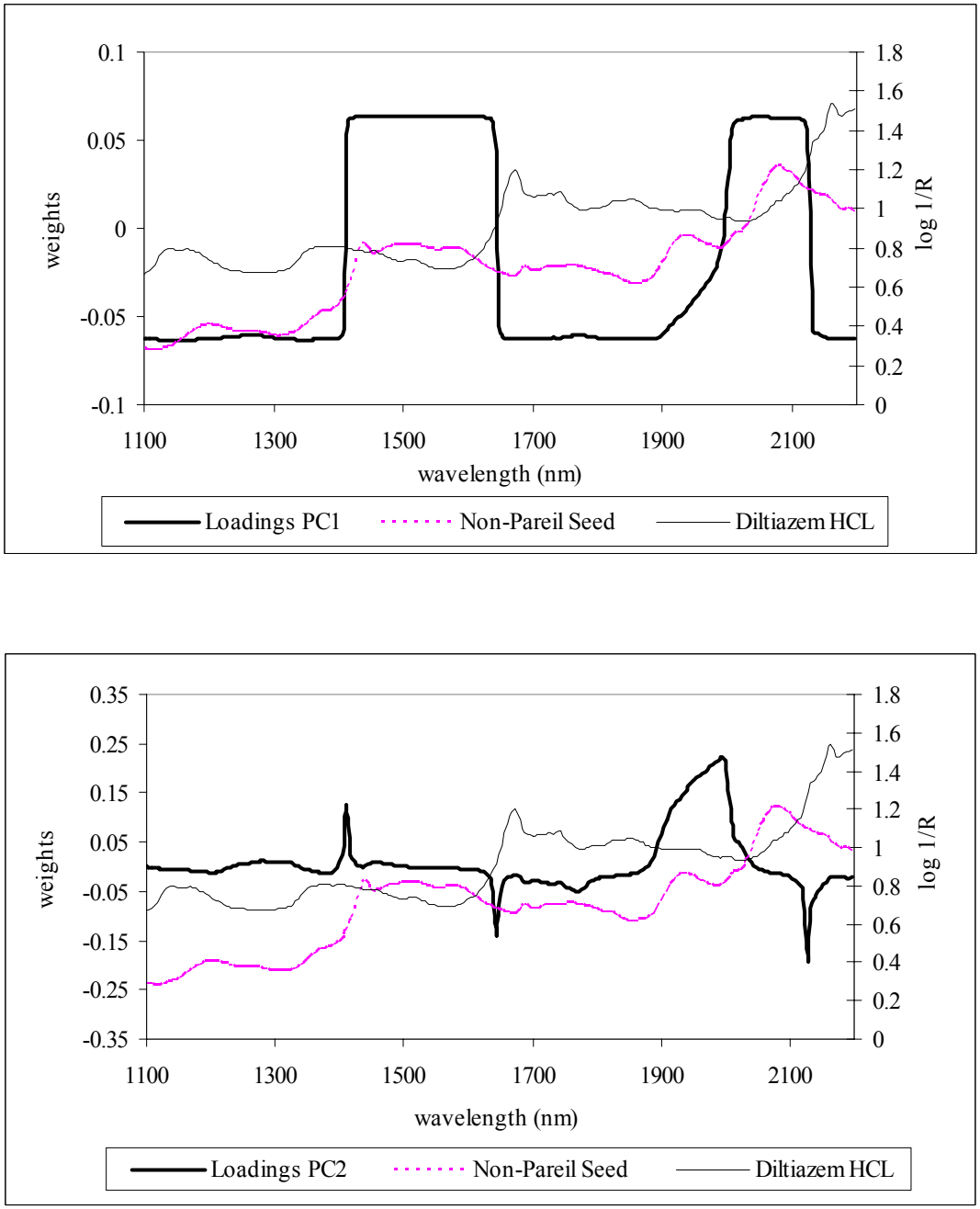

Figure 26. Loadings Spectrum of at-line 550mg/g Diltiazem HCl Pellets C-1 (top) and PC-2 (bottom)

Table 15. Principal component regression results for at-line analysis of diltiazem HCl drug-layered pellets.

MSC						2nd Derivative					
150mg/g						**150mg/g**					
PCs Used	T-Statistic		R^2	SEC	SEP	PCs Used	T-Statistic		R^2	SEC	SEP
1	PC-1	-7.98	0.55	2.47%	2.87%	1	PC-1	-8.94	0.70	2.17%	2.62%
2	PC-1	-18.52	0.92	0.92%	0.75%	2	PC-1	-27.3	0.97	0.63%	0.55%
	PC-2	-15.16					PC-2	-16.82			
300mg/g						**300mg/g**					
PCs Used	T-Statistic		R^2	SEC	SEP	PCs Used	T-Statistic		R^2	SEC	SEP
1	PC-1	-27.98	0.94	0.92%	0.87%	1	PC-1	-22.10	0.91	1.14%	1.29%
2	PC-1	-29.33	0.96	0.72%	0.66%	2	PC-1	-32.74	0.96	0.63%	0.65%
	PC-2	-3.17					PC-2	-7.95			
550mg/g						**550mg/g**					
PCs Used	T-Statistic		R^2	SEC	SEP	PCs Used	T-Statistic		R^2	SEC	SEP
1	PC-1	-48.08	0.98	0.66%	0.53%	1	PC-1	-18.22	0.97	0.65%	0.54%
2	PC-1	-51.60	0.98	0.61%	0.58%	2	PC-1	-15.07	0.96	0.63%	0.59%
	PC-2	-2.98					PC-2	-1.65			

SEC and SEP were inversely related to pellet strength. In general at-line analysis had SEC and SEP values about 0.5% lower than those obtained from in-line methods. A detailed discussion of the factors contributing to the observed differences in calibration and prediction errors between in-line and at-line analyses is provided later in this manuscript.

3.1.2.3 Partial Least Squares Regression

Partial least squares regression results of D2 spectra for all pellet strengths are summarized in **Table 16**. The results were similar to those obtained using PCR, with SEPs less than 1% achieved, and an inverse relationship between pellet strength and SEP observed In general, the PLS models used one additional regression factor as compared to PCR, which may be attributed to inclusion of sources of analyte error in the model. The addition of such information may have allowed slightly lower SEPs to be achieved without overfitting. The ratio of current MSECV value to the minimum value in the calibration was again effective at identifying an ideal number of factors to prevent overfitting.

3.1.2.4 Summary of At-Line Regression Model Performance

A summary of the performance of optimized single wavelength, multiple wavelength, PCR and PLS models for at-line analysis of all pellet strengths is presented in **Table 17**. In addition, a plot of both the calibration and prediction results obtained by principal component regression of second derivative spectra for 150mg/g pellets is presented in **Figure 27**. Similar calibration results were obtained for 150mg/g, 300mg/g,

Table 16. Partial least squares regression results for at-line analysis of diltiazem HCl drug-layered pellets.

		150 mg/g		
Factor	MSECV	R	SEC	SEP
1	1.353	0.79	2.24 %	2.55%
2	0.267	0.96	0.96 %	1.12%
<3>	0.187	0.98	0.77%	0.80%
4	0.156	0.98	0.66 %	NT
5	0.117	0.99	0.56%	NT
		300 mg/g		
Factor	MSECV	R	SEC	SEP
1	0.357	0.95	1.12%	1.23%
2	0.222	0.98	0.64%	0.69%
3	0.178	0.99	0.62%	0.65%
<4>	0.162	0.99	0.56%	0.55%
5	0.138	0.99	0.53%	0.57%
		550 mg/g		
Factor	MSECV	R	SEC	SEP
<1>	0.109	0.9902	0.66%	0.55%
2	0.108	0.9920	0.61%	0.53%
3	0.129	0.9935	0.58%	0.68%
4	0.150	0.9940	0.53%	NT
5	0.138	0.9946	0.52%	NT

< > - factors recommended by NSAS®
NT - not tested.

Table 17. Summary of regression results for at-line assessment of pellet potency.

150mg/g Diltiazem HCl Pellets			Potency (%)	
Regression Model	PCs	R^2	SEC	SEP
PCR – MSC	2	0.92	0.92	0.75
PCR – D2	2	0.97	0.63	0.55
PLS – D2	3	0.98	0.77	0.80
Multiple Wavelength	--	0.99	0.54	0.56
Single Wavelength	--	0.98	0.76	0.84

300mg/g Diltiazem HCl Pellets			Potency (%)	
Regression Model	PCs	R^2	SEC	SEP
PCR – MSC	2	0.96	0.72	0.66
PCR – D2	2	0.96	0.63	0.65
PLS – D2	4	0.99	0.56	0.55
Multiple Wavelength	--	0.98	0.70	0.78
Single Wavelength	--	0.99	0.55	0.52

550mg/g Diltiazem HCl Pellets			Potency (%)	
Regression Model	PCs	R^2	SEC	SEP
PCR – MSC	1	0.98	0.66	0.53
PCR – D2	1	0.97	0.65	0.54
PLS – D2	1	0.99	0.66	0.55
Multiple Wavelength	--	0.99	0.48	0.53
Single Wavelength	--	0.99	0.49	0.56

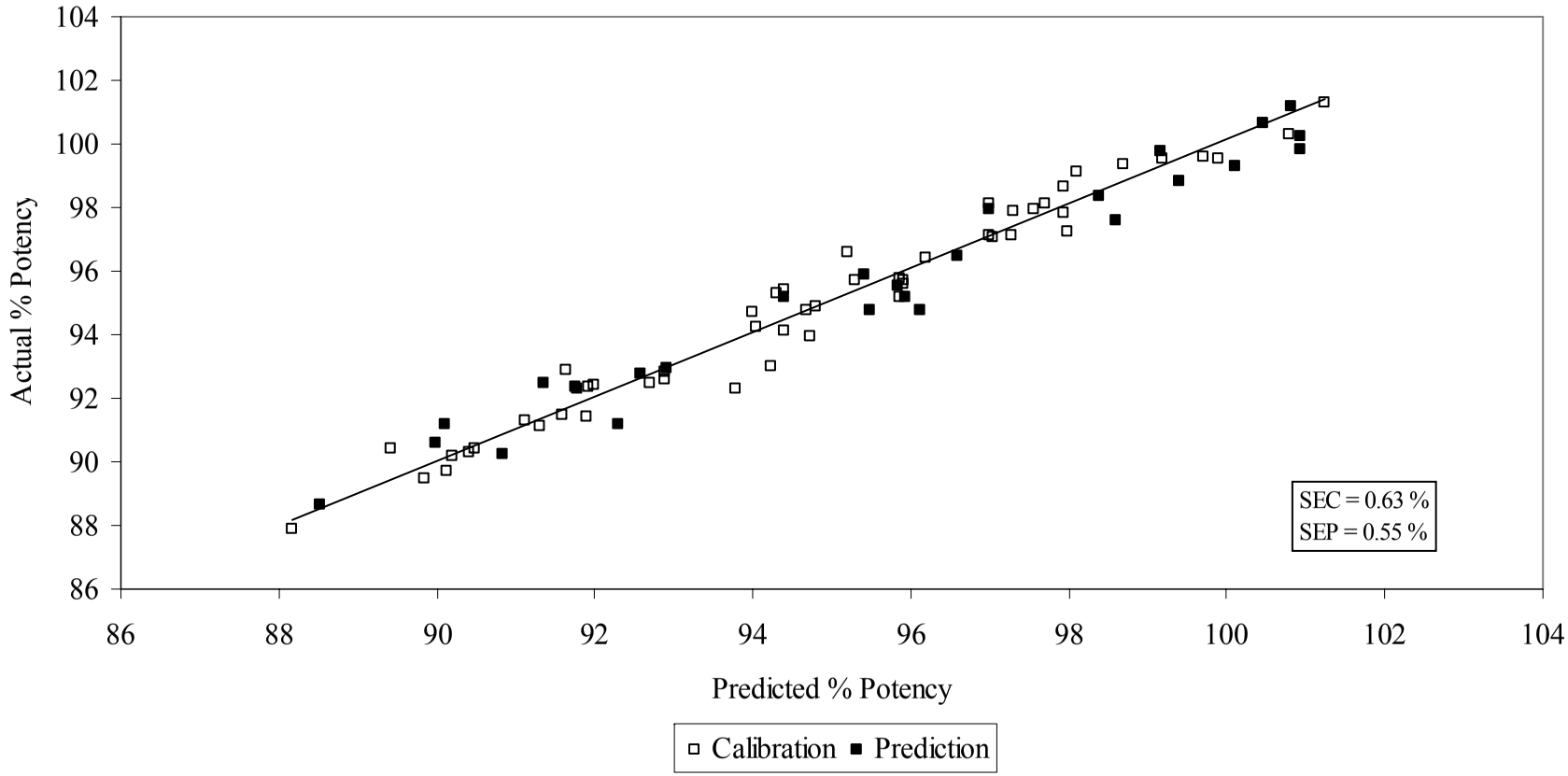

Figure 27. Potency Calibration and Prediction -- Diltiazem HCl 150mg/g Pellets At-line Analysis

and 550mg/g drug layered pellets. At-line analysis produced significantly better calibration and prediction results than the in-line system. All multivariate calibration models demonstrated R^2 values of 0.94 or greater and standard errors of calibration no greater than 1.0%. The simplistic single and multiple wavelength models also demonstrated their ability to predict pellet potency within 1% of actual HPLC values. As previously discussed, such results indicate that it may be possible to employ inexpensive single filter instruments for on-line monitoring of drug layering operations. However, the numerous advantages of full-spectrum methods should be strongly considered during near-IR method development.

3.1.3 Comparison of In-line and At-line Near-IR Methods for Monitoring Drug Layering

A comparison between in-line and at-line calibration model prediction errors is presented in **Table 18**. Using PCR or PLS, the average in-line and at-line SEPs for pellet potency were 1.11% and 0.63%, respectively, with a maximum SEP exhibited by the 150mg/g strength PLS-D2 in-line model. The use of single or multiple wavelength models allowed potency prediction with average SEPs of 1.09% and 0.63%, for in-line and at-line analyses, with a maximum value of 1.72% exhibited in the 500mg/g in-line model. Such results are reasonable in terms of the ability to control the drug loading process, and acceptable with respect to the 0.46% SEL value of the reference method.

Overall, at-line analyses demonstrated lower calibration and prediction errors than in-line methods. Several contributing factors to the robust performance of the at-line method may include: (i) the stationary nature of the sample; (ii) normalized particle size

Table 18. Comparison of in-line and at-line regression model performance for potency prediction.

150mg/g Diltiazem HCl Pellets

Regression Model	Standard Error Of Prediction (%)	
	In-line	At-line
PCR – D2	1.09	0.55
PLS – D2	1.52	0.80
Multiple Wavelength	1.25	0.56
Single Wavelength	1.33	0.84

300mg/g Diltiazem HCl Pellets

Regression Model	Standard Error Of Prediction (%)	
	In-line	At-line
PCR – D2	0.96	0.65
PLS – D2	0.96	0.55
Multiple Wavelength	0.36	0.78
Single Wavelength	0.31	0.52

550mg/g Diltiazem HCl Pellets

Regression Model	Standard Error Of Prediction (%)	
	In-line	At-line
PCR – D2	1.02	0.54
PLS – D2	0.71	0.55
Multiple Wavelength	1.61	0.53
Single Wavelength	1.72	0.56

and morphology due to removal of pellets from the process stream and sieving prior to analysis; (iii) the use of a larger number of samples for calibration development to encompass inherent variability in the sample pellet population; and (iv) differences between the spectral acquisition systems.

The number of samples for calibration development and prediction for the in-line system was unavoidable given the rate of potency change during processing and the operations that needed to be performed between each sample point. Within the potency range used for calibration development, theoretical potency increased by approximately 1% every 1.5, 3 or 4 min for the 150mg/g, 300mg/g, and 550mg/g lots, respectively. The following operations, which required approximately 65 – 70 sec to complete, were performed between the acquisition of each sample: (i) obtain a 20 scan spectrum [~30 seconds]; (ii) thief pellet sample from processor for reference potency analysis and at-line analysis [~10 sec]; (iii) sieve pellet sample through upper and lower sieve to remove agglomerates [~15 sec]; (iv) transfer pellet sample to labeled sample vial [~10 sec].

For the 300mg/g and 550mg/g strengths, the relative non-active time available between sample time points was approximately 1.5 and 2.5 min, respectively. For 150mg/g pellet processing, there was only about 20 sec of non-active time. Additional samples were not obtained because the sampling scheme was designed to assess samples at predefined process points corresponding to theoretical coating levels based on traditional weight gain monitoring methods. If the study were to be repeated, a larger number of samples in the calibration set would be investigated by both increasing the potency range being investigated, and increasing the number of batches to be included in the calibration set.

To investigate the effect of increasing both the calibration range and the number of samples in the calibration set, a regression model was developed using 162 spectra collected at-line from a total of nine rotogranulation batches (3 lots per strength) for 150mg/g, 300mg/g, and 550mg/g pellets. In order to develop the calibration across all pellet strengths, potency values were converted to percentage of diltiazem HCl content per pellet sample, 15%, 30%, 55%, respectively. A scatter plot of the calibration obtained following principal component regression of MSC spectra is presented in **Figure 28**. To test the calibration, the drug content of 108 samples from six additional batches (2 lots per strength) was assessed. Using two principal components an R^2 value of 0.998, an SEC of 0.66%, and an SEP of 0.71% were achieved.

Although it was possible to develop a single calibration across the studied range of pellet strengths, differences in slope between individual pellet strength categories can be seen in Figure 28. These deviations are a manifestation of non-linearity between the response of the near-IR method and drug concentration across the broad range of the single calibration model. Such non-linearity may result in erroneous estimation of pellet potency, and could adversely affect the ability to validate such a method for routine use. Therefore, the development of individual potency calibrations within specific pellet strength categories, as conducted in this study, is preferred. An additional limitation of this model is the time required to perform the processing steps described above relative to the rate of potency change occurring during processing. In such cases, unique calibration models with a reduced number of scans would be required. Alternatively, though not preferred due to increased cost and process inefficiency, the drug layering suspension

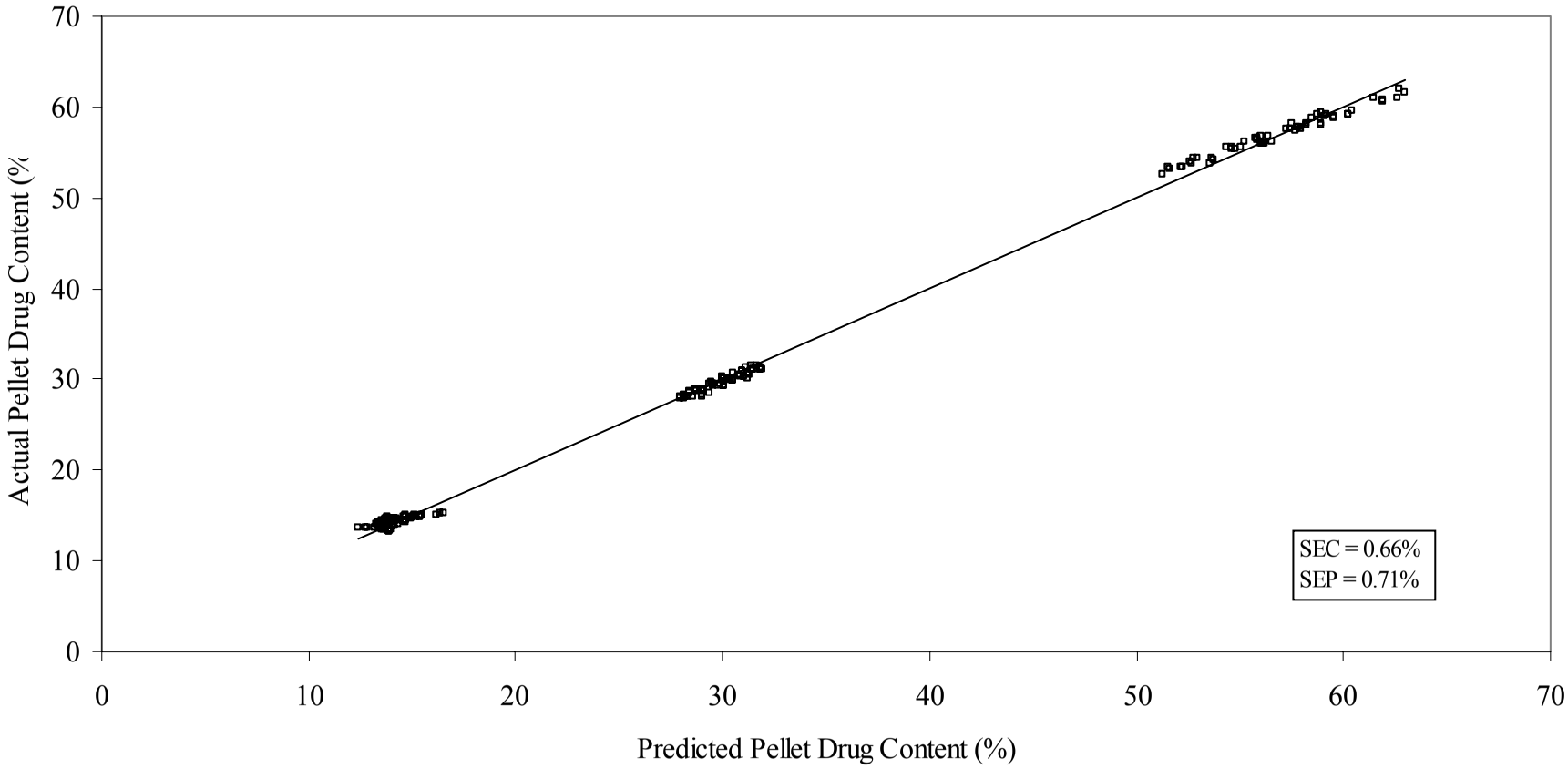

Figure 28. Potency Calibration for Across All Diltiazem HCl Pellet Strengths

could be diluted or the spray rate decreased to slow the rate of potency change during processing.

Differences between the potency range characteristics for the studied pellet strengths are also exemplified in Figure 28. This graphic clearly demonstrates that the 96% to 106% potency range becomes broader as drug content increases from 150 mg/g to 550mg/g. In terms of drug content, studied potency ranges were 144 mg/g to 159 mg/g for the 15% pellets, 288 mg/g to 312 mg/g for the 30% pellets and 528 mg/gram to 572 mg/g for the 55% strength. Such differences also help to explain why there exists a rank order difference in rate of potency change over the 150mg/g to 550mg/g strength range.

The grouping of pellet samples according to drug content is also apparent in **Figure 29** which is a principal component scores plot of the first PC versus the second PC, obtained following PCA of MSC spectra. Data from such plots may be used in pattern recognition tests in a quality control environment for qualitative classification of samples according to pellet strength. Such classification could be particularly beneficial as a quality control procedure during encapsulation of multiple types of pellets by ensuring that the different pellet types or strengths are correctly placed into their respective hoppers.

Within each strength category, pellets could also be qualitatively classified according to coating level. A principal component scores plot of the first PC versus the second PC obtained following PCA of MSC at-line spectra for 55% diltiazem HCl pellets is presented in **Figure 30**. Such classification, when used in combination with various pattern recognition algorithms, could also be used to identify desired rotogranulation

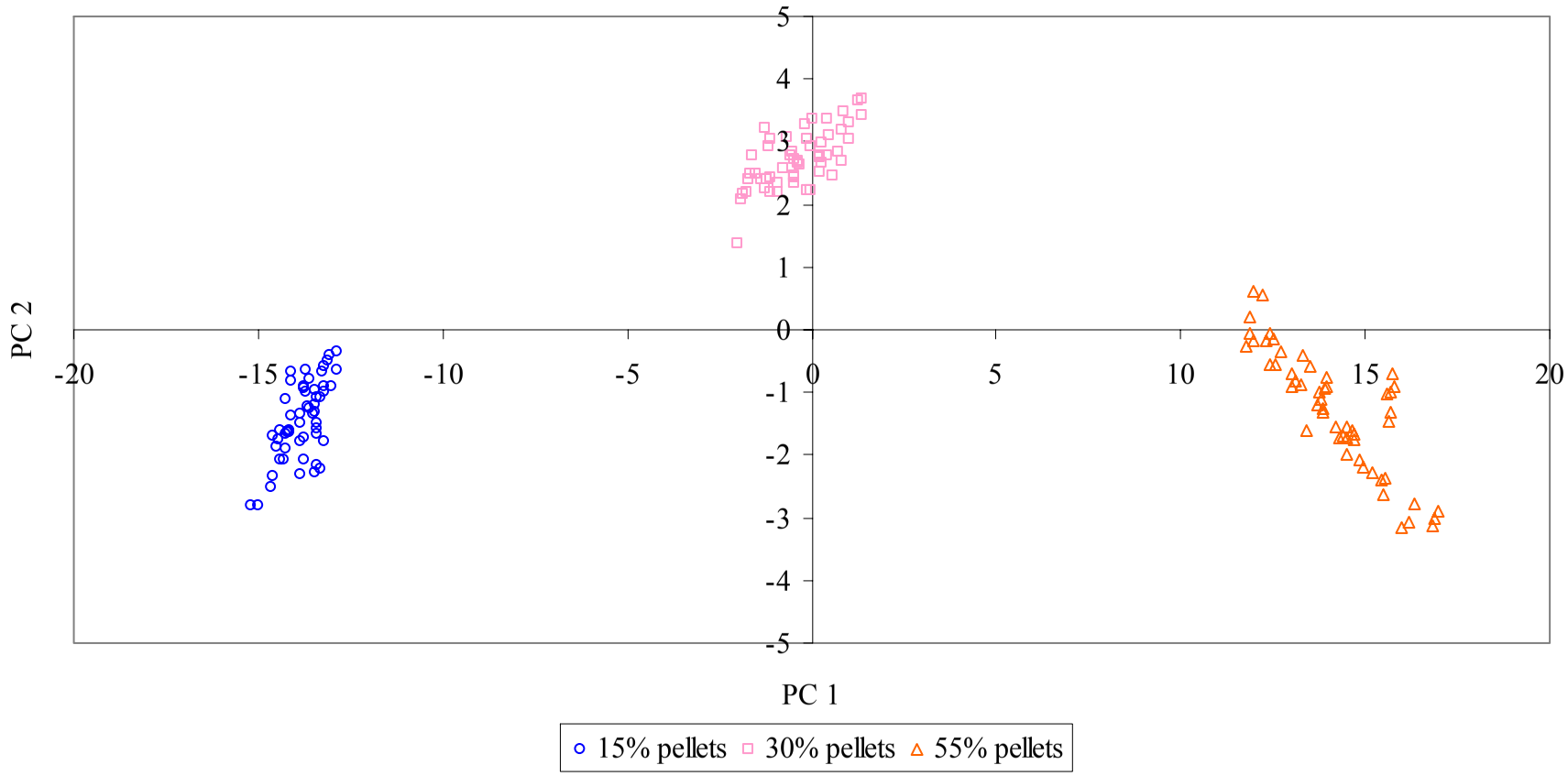

Figure 29. Principal Component Plot for 15% , 30%, and 55% Diltiazem HCl Pellets

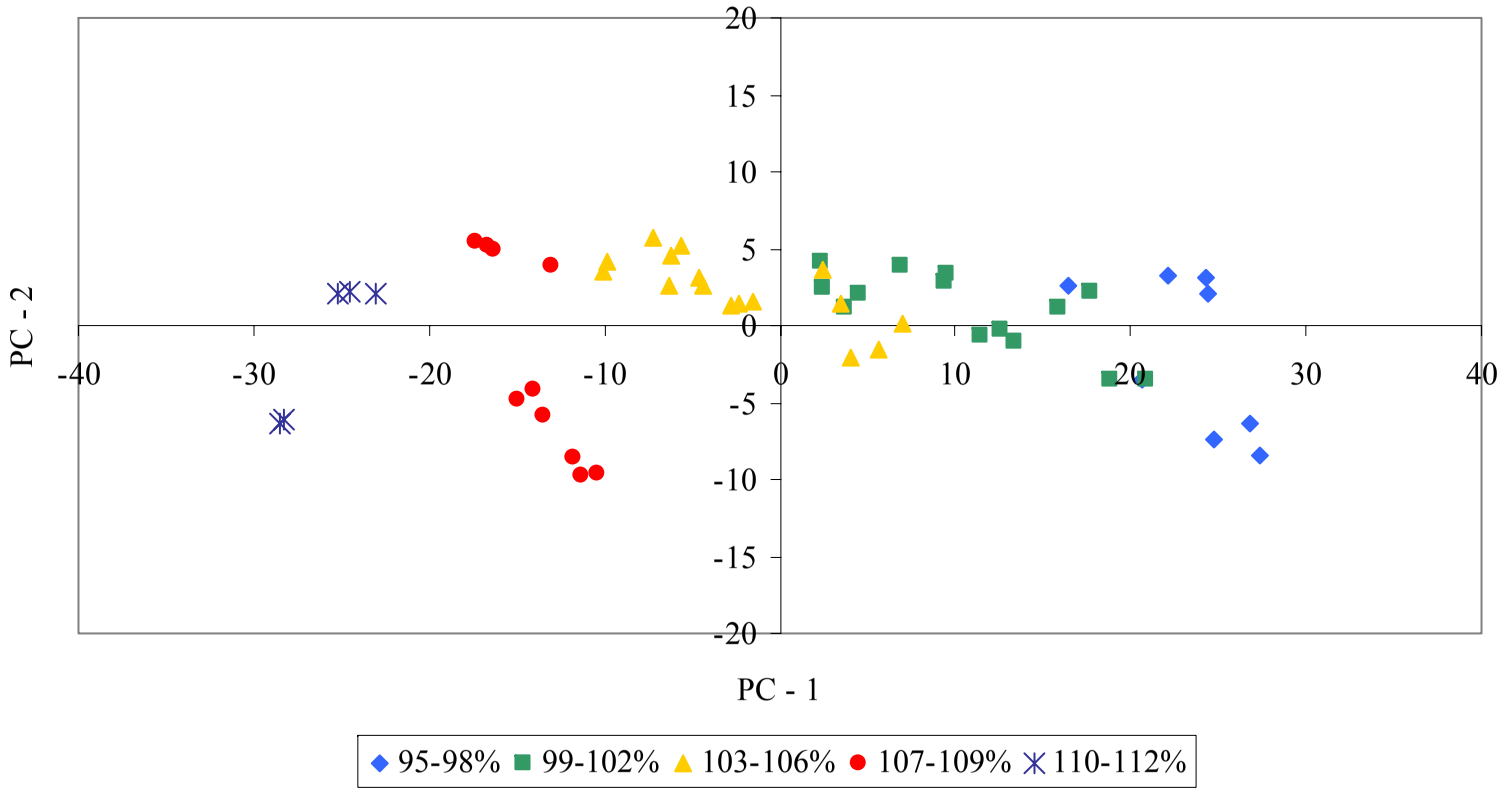

Figure 30. Principal Component Scores Plot for 55% Diltiazem HCl Pellets

process endpoints. An example of this type of application is discussed later in this manuscript.

Another significant factor governing the robust performance of the at-line method for assessing pellet potency is the configuration of spectral data collection systems. For at-line analysis, a NIRSystems Rapid Content Analyzer® module was used for spectral collection, while in-line analysis utilized a NIRSystems fiber optic Smart Probe®. Although both the Rapid Content Analyzer and the Smart Probe utilize fiber bundles for transmitting excitation light to the sample, there are significant differences in their bundle configurations. The RCA utilizes 420 fibers to transmit near-IR excitation energy from the source to the sample over a distance of 10 in. The Smart Probe, which is also composed of 420 fibers, however, utilizes 210 fibers to transmit excitation energy to the sample and 210 fibers to return reflected light to the detector over a distance of 5 ft.

Since the Smart Probe, as compared to the RCA, utilizes fewer fibers to carry light to and from the sample and the distance the energy must travel is much greater, significant energy loss over the length of the fiber occurs. This energy loss translates to lower absorbance values for spectra collected using the probe. This difference is exemplified in **Figure 31,** which depicts spectra of 100% potent 150mg/g diltiazem HCl pellets collected using either the RCA or the SmartProbe. Such absorption differences are likely to translate to a lower signal to noise ratio for the SmartProbe, which may contribute to the higher and more variable SEC and SEP results obtained during in-line assessment of pellet potency. This increase in noise can be observed in **Figure 32,** which shows the loadings spectrum for PC-1 following PCA analysis of MSC spectra for a 150mg/g rotogranulation trial analyzed using the Smart

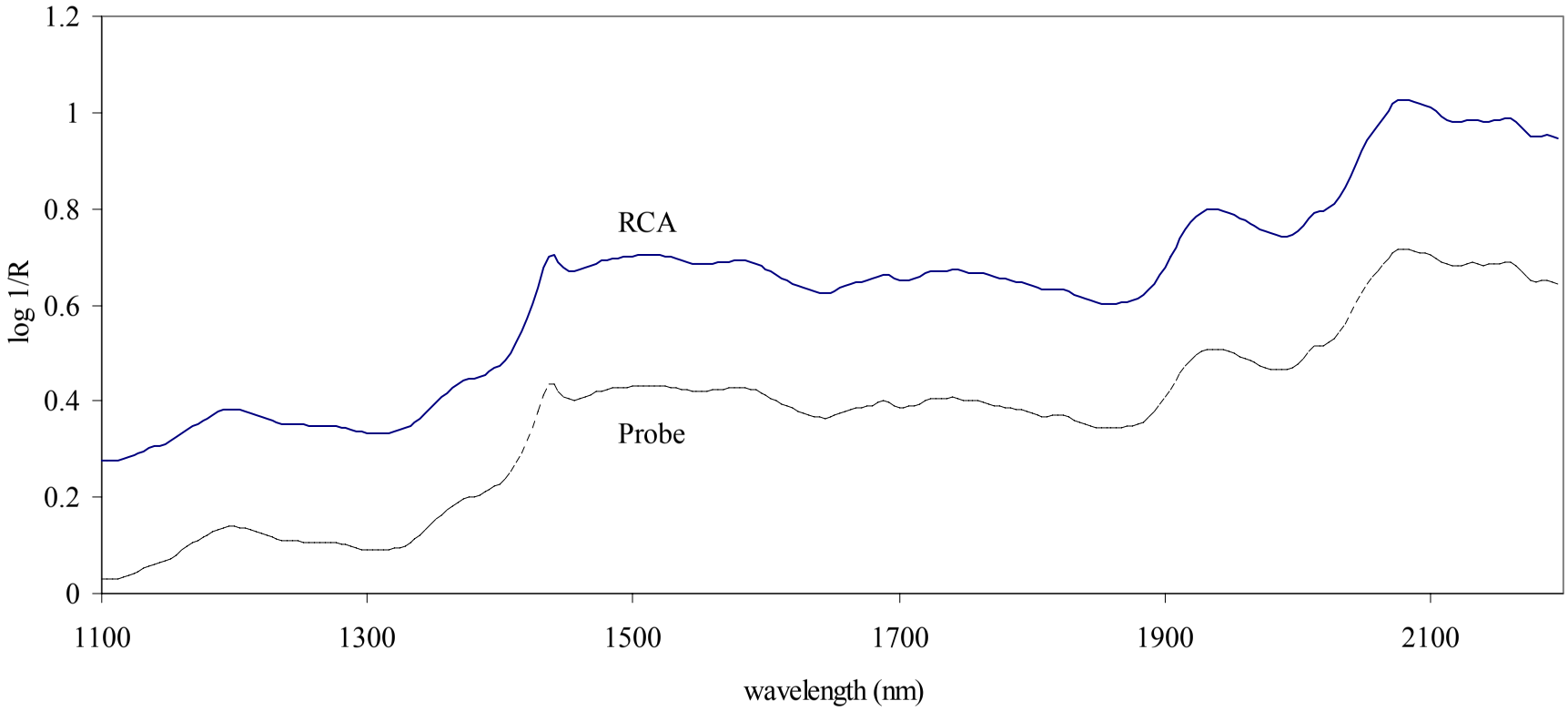

Figure 31. Comparison of 150mg/g Diltiazem HCl Pellet Spectra RCA versus SmartProbe Sampling

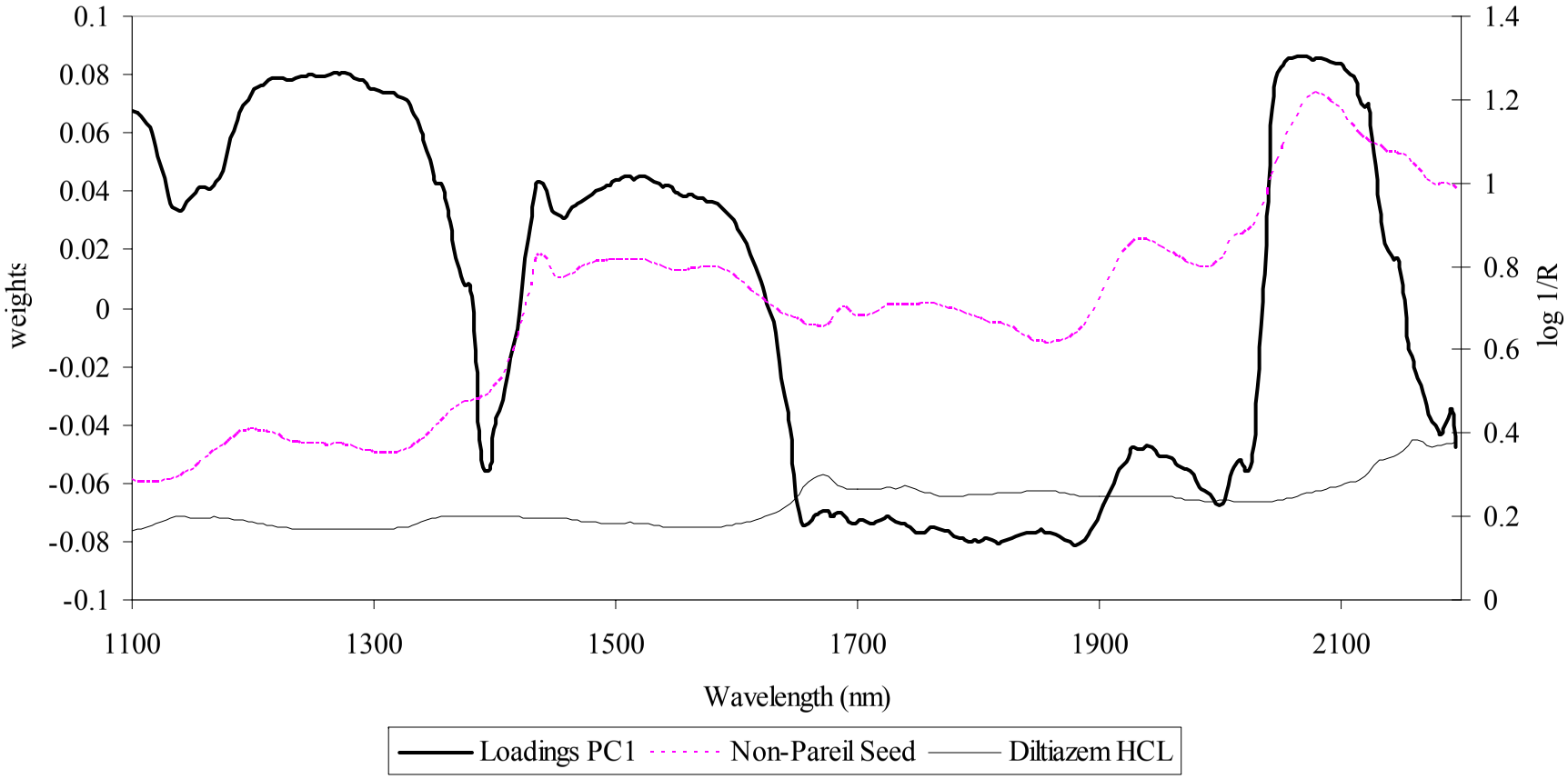

Figure 32. PC-1 Loadings for 15% Diltiazem HCl Pellets - Analysis via Smart Probe

Probe. A much smoother loadings spectrum for the same samples analyzed using the RCA is shown **Figure 33.**

Two additional factors that may have contributed to increased noise in the in-line spectra are sample presentation and pellet morphology and size distribution. In-line analysis assessed the characteristics of moving particles, whereas the at-line technique involved analysis of stationary samples. Prior to at-line analysis, agglomerates and fines were removed from the sample via a simple sieving process. During in-line analysis, however, there was no opportunity to remove out-of-specification particles from the batch.

3.1.4. Practical Considerations Regarding Near-infrared Monitoring of Drug Layering

Numerous processing and formulation factors such as rotor speed, inlet air temperature, process airflow, atomization air pressure, dew point, solids content of layering suspension, binder level, and drug solubility characteristics can dramatically affect the potency and morphology of pellets produced via rotogranulation. Although typical drug layering processes utilize lengthy and expensive manufacturing schemes, operations typically rely on theoretical determinations of applied solids to indirectly predict drug layering endpoints.

During this study, the accuracy of the theoretical applied solids method for assessing pellet potency was evaluated. **Table 19** is a summary of the theoretical (based on applied suspension solids) versus actual potency (as determined by HPLC) for 150mg/g, 300mg/g, and 550mg/g diltiazem HCl pellets. These data demonstrate that

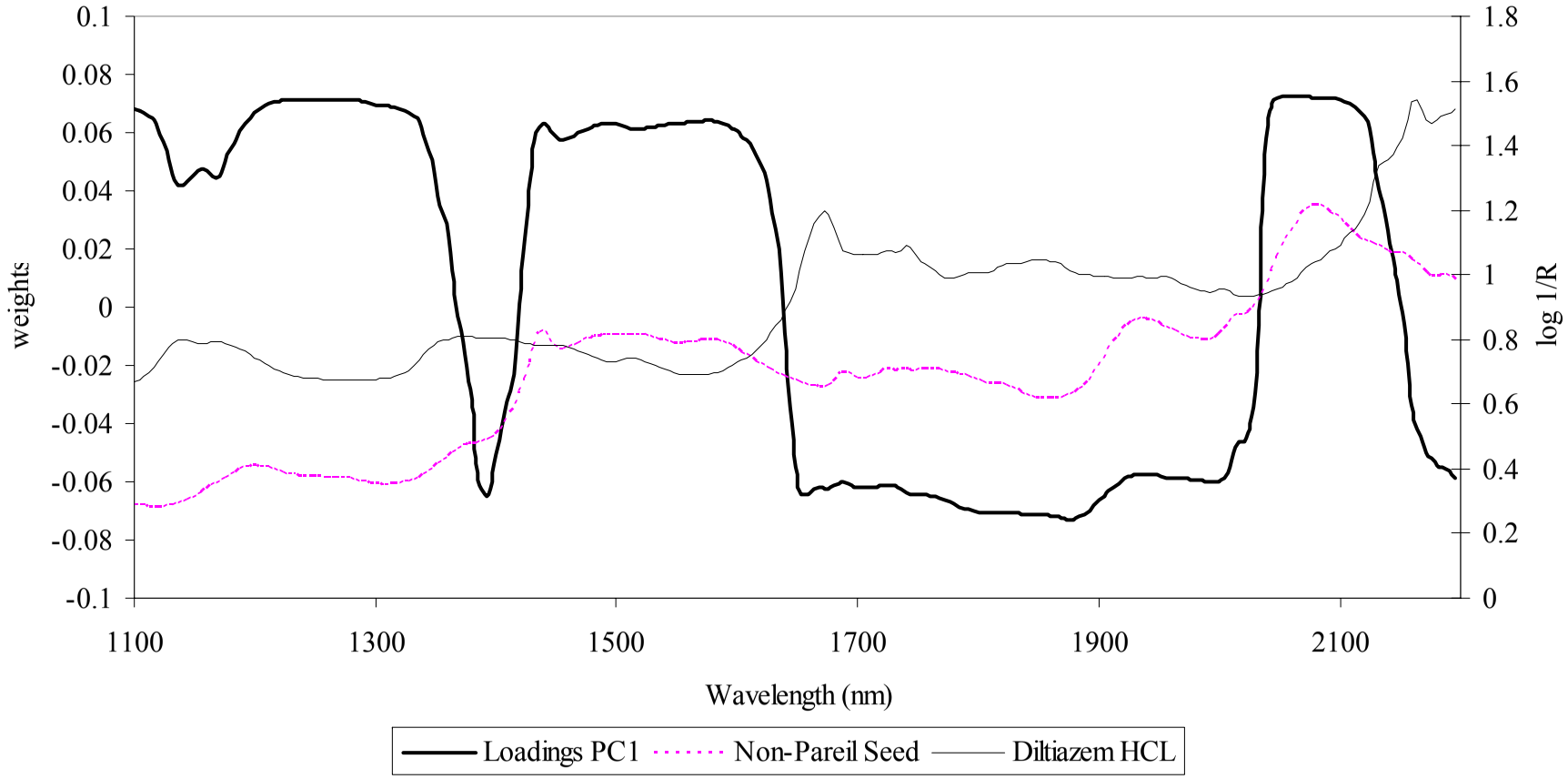

Figure 33. PC-1 Loadings for 15% Diltiazem HCl Pellets - Analysis via Rapid Content Analyzer

Table 19 Theoretical versus Actual Pellet Potency

150mg/gram Diltiazem HCl Pellets

Trial #1*			Trail #2			Trial #3		
Theoretical Potency (%)	HPLC Potency (%)	delta (%)	Theoretical Potency (%)	HPLC Potency (%)	delta (%)	Theoretical Potency (%)	HPLC Potency (%)	delta (%)
87	81.8	-5.2	87	84.5	-2.5	87	84.6	-2.4
90	84.9	-5.1	90	87.6	-2.4	90	87.6	-2.4
93	87.7	-5.3	93	90.5	-2.5	93	90.3	-2.7
96	90.1	-5.9	96	93.4	-2.6	96	93.4	-2.6
98	92.5	-5.5	98	95.6	-2.4	98	95.6	-2.4
100	94.8	-5.2	100	98.0	-2.0	100	97.9	-2.1
102	97.1	-4.9	102	100.0	-2.0	102	99.8	-2.2
104	98.9	-5.1	104	102.1	-1.9	104	102.0	-2.0
106	101.0	-5.0	106	104.1	-1.9	106	104.2	-1.8

* *nozzle problems encountered during processing*

300mg/gram Diltiazem HCl Pellets

Trial #1			Trail #2			Trial #3		
Theoretical Potency	HPLC Potency	delta	Theoretical Potency	HPLC Potency	delta	Theoretical Potency	HPLC Potency	delta
96	93.5	-2.5	96	93.6	-2.4	96	93.8	-2.2
98	95	-3.0	98	96.2	-1.8	98	96	-2.0
100	97.8	-2.2	100	98.5	-1.5	100	98.1	-1.9
102	99.5	-2.5	102	100.7	-1.3	102	99.6	-2.4
104	101.6	-2.4	104	102.8	-1.2	104	101.1	-2.9
106	104.0	-2.0	106	104.8	-1.2	106	103.5	-2.5

550mg/gram Diltiazem HCl Pellets

Trial #1*			Trial #2			Trial #3		
Theoretical Potency	HPLC Potency	delta	Theoretical Potency	HPLC Potency	delta	Theoretical Potency	HPLC Potency	delta
96	102.3	6.3	96	97.2	1.2	96	96.4	0.4
98	104.8	6.8	98	98.4	0.4	98	98.7	0.7
100	106.2	6.2	100	101.1	1.1	100	100.9	0.9
102	107.7	5.7	102	102.5	0.5	102	102.7	0.7
104	110.5	6.5	104	105.1	1.1	104	105	1.0
106	111.9	5.9	106	107.2	1.2	106	107.4	1.4

* *Uncoated seeds noted in plenum at process end*

there was an approximate 2% difference between theoretical and actual pellet potency, with actual potency being less than theoretical values in most instances. For this type of unit operation, such losses are expected, and would be addressed by adjusting the capsule fill weight to compensate for the loss. However, during this study, trial #1 of the 150mg/g strength and trial #1 of the 550mg/g strength pellets demonstrated -5% and +6% deviations from theoretical potency. These deviations were attributed to assignable processing issues, which are not uncommon in routine pharmaceutical manufacturing operations.

For the 150mg/g batch, several nozzle clogs during processing caused localized over-wetting and generated approximately 10% agglomerates (>16 mesh) within the batch. The agglomerates were subsequently removed from the batch via the screening process. The screened pellets, although sub-potent, would conform to USP assay specifications of 90.0% - 110% at the theoretical target process endpoint (100% theoretical potency). Since actual HPLC potency values, not theoretical values, are used in the development of calibration models, inclusion of these data in the model was deemed acceptable.

For the 550mg/g batch, a significant quantity of non-pareil seeds was observed in the air plenum below the rotor after processing. The beads were assayed and found to contain no diltiazem. The absence of drug substance on the beads indicates that the beads fell into the plenum during start-up which can occur with this rotogranulation operation. This resulting decrease in the quantity of non-pareil seeds available for drug layering subsequently resulted in the production of super-potent beads. These beads, were also deemed acceptable for use in the development of calibration models.

The data summarized in the table above demonstrates that traditional methods of monitoring applied coating suspension solids during rotogranulation are neither optimal nor reliable. True batch potency, as measured by HPLC, and weight gain methods differed by as much as 7% due to potential systematic problems that occurred during processing, i.e., nozzle clogs or pellet loss to the plenum during start-up. Even when no process anomalies were encountered, pellet potency as determined by weight gain differed from HPLC values by an average of 3%. Hence, there is a need for an in-line method to monitor such pelletization processes.

Because near-IR methods for determining pellet potency are less affected by changes in processing conditions than traditional weight gain monitoring techniques, such methods can provide a higher degree of confidence in identifying process endpoints. With such methods in place, the development of near-IR in-process release specifications could reduce production cycle-time by allowing subsequent batch processing to proceed prior to receiving analytical laboratory results, or prevent the loss of an entire batch due to an unexpected process anomaly.

3.1.5 Pilot Plant Applications

Because of the favorable results obtained in the laboratory scale study, an experiment was conducted to assess the ability to predict the potency of pilot scale pellets using data obtained from experiments performed in the laboratory. A comparison of laboratory versus pilot-scale processing parameters, including rationale for scale-up parameter selection is presented in **Table 20**. Although quantitatively identical laboratory and pilot-scale 550mg/ml formulations were evaluated in this study,

Table 20. Processing parameters for drug suspension layering – laboratory versus pilot scale.

Parameter	Laboratory	Pilot Scale	Scale-up Rationale
Batch Size	3.3. kg	75 kg	to provide 100% equipment fill at process endpoint
Inlet Air Temperature	60 ± 5° C	67 ± 7° C	adjusted to maintain product temperature within target 40 – 50ºC range
Product Temperature	40 ± 2° C	48 ± 12° C	target 40 – 50 ºC based on laboratory scale data
Exhaust Air Temperature	46 ± 3° C	37 ± 6° C	dependent variable
Number of Spray Guns	1	4	proportional increase based on equipment design
Nozzle Size	1.2 mm	1.2 mm	identical to development
Total Spray Rate	10 – 27 g/min	244 - 464 g/min	linear increase based on solution delivery rate, bowl charge, and atom. air pressure, product performance
Atomization Air Pressure	40 psi	50 ± 10 psi	proportional increase based on solution delivery rate
Rotor Speed	550 ± 25 rpm	90 ± 15 rpm	experimentally determined to prevent attrition during processing
Angular Velocity	~29 ft/sec	~12 ft/sec	experimentally determined to prevent pellet attrition during processing
Air Flow	120 ± 10 cfm	700 ± 200 cfm	adjusted to maintain sufficient fluidization and adequate rate of solvent evaporation
Process Time	5 hours	5 hours	identical

theoretically determined process parameters were adjusted, as necessary, to provide a finished product with desirable physical (narrow particle size distribution, minimal agglomerates and fines, smooth surface) and chemical (assay, content uniformity) characteristics. Near-IR analyses were conducted once final process parameters were defined.

The MSC/PCR calibration developed for the 550mg/g laboratory scale pellets was used to predict the potency of a 75 kg pilot scale batch. **Figure 34** shows a plot of predicted versus actual potency. The prediction error for this study, 1.04%, although acceptable, was slightly higher than in the laboratory study. This error may be attributed to differences in pellet surface characteristics and density differences between laboratory and pilot scale pellets.

The application of near-IR for predicting the endpoint of clinical or production scale batches based on calibration models developed in the laboratory may prove to be very important to the pharmaceutical manufacturer. When drug layering or polymer coating efficiencies vary, as they do, from lab scale equipment to larger equipment used for manufacturing, the availability of a rapid on-line or at-line measurement for prediction of process endpoints may potentially save millions of dollars in time and materials. Although the standard error of prediction may not match the values obtained when calibration and validation data arise from product manufactured on the same equipment, the results may be good enough to prevent loss from the initial batches of clinical production lots of product while saving valuable time.

An additional study was conducted to assess the ability to monitor clinical batch pellet production and predict pellet potency. From each of the initial 75 kg batches,

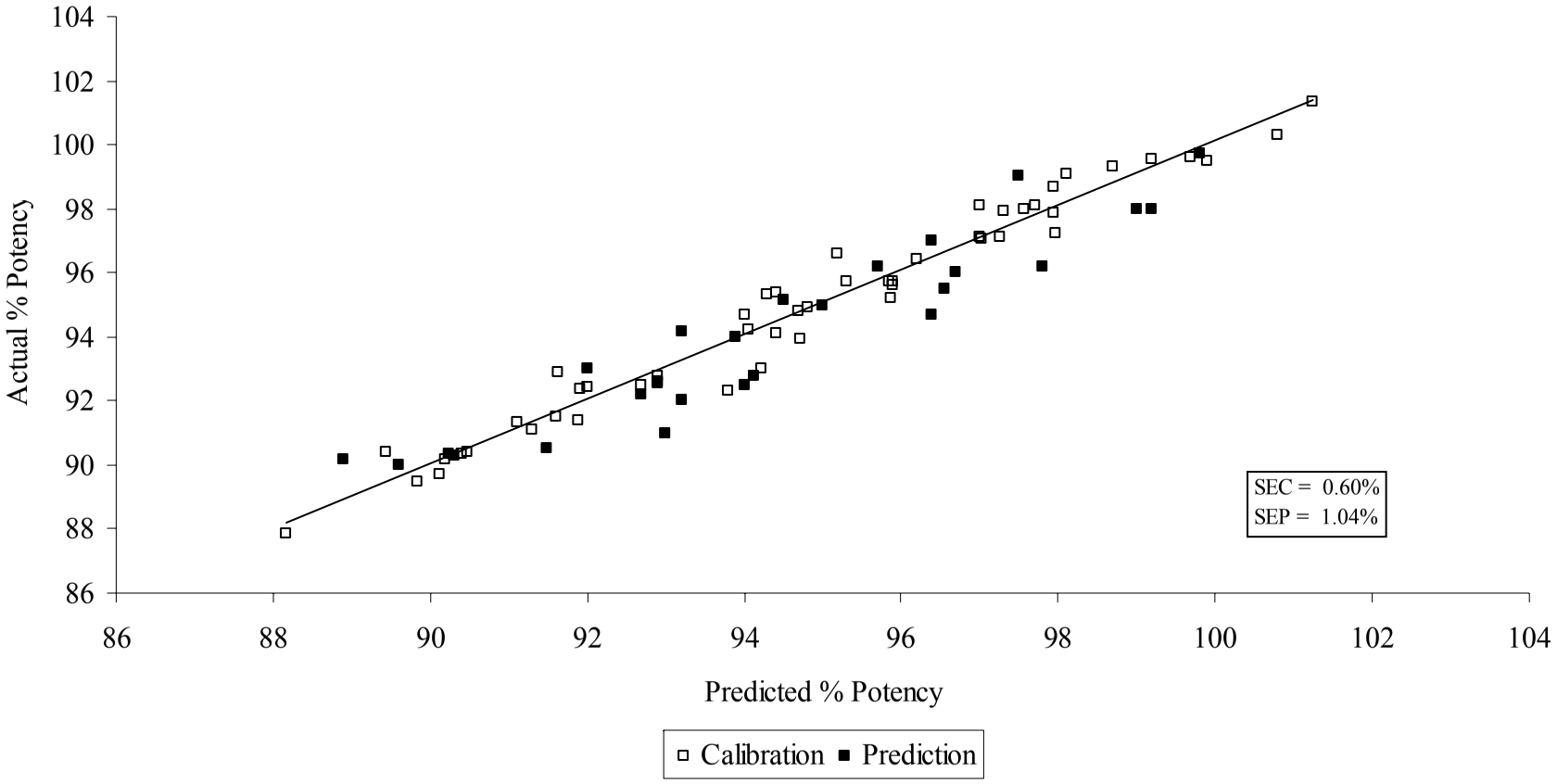

Figure 34. Pilot-Scale Potency Prediction using Laboratory-scale Data 75 kg Batch Size

eighteen samples ranging from 90% to 100% theoretical potency were analyzed according to previously described at-line methods, and used to develop potency calibrations. Samples from two additional 75 kg pilot-scale batches, processed using similar conditions to those used for calibration, were used to test the model. The regression results for PCR, PLS, and single wavelength calibration provided SEP values ranging from 0.32% to 0.53% which were similar to those observed in laboratory-scale at-line analysis. Such results are not surprising since both the training samples and the test samples were processed under the same conditions, handled similarly, and tested via the same at-line procedures. Because these batches were part of a clinical batch manufacturing campaign, it was not possible to conduct in-line analysis due to cGMP concerns. However, the at-line results clearly demonstrate that near-IR analysis can be an efficient tool for accurately monitoring the potency of drug layered beads in a production environment.

3.2 Quantitative Prediction of Eudragit RS30D Coating Level

Wurster coating studies utilized diltiazem HCl pellets from each potency class prepared during initial rotogranulation studies. The pellets were coated with an aqueous dispersion of Eudragit RS30D (ERS) which was plasticized with triethyl citrate and contained talc as an anti-tacking agent. **Figure 35** (baselines off-set for clarity) shows the spectra of a core 550mg/g diltiazem pellet, a cast ERS film, and coated pellets containing 5% to 16% theoretical applied polymer solids. Although the spectra appear to

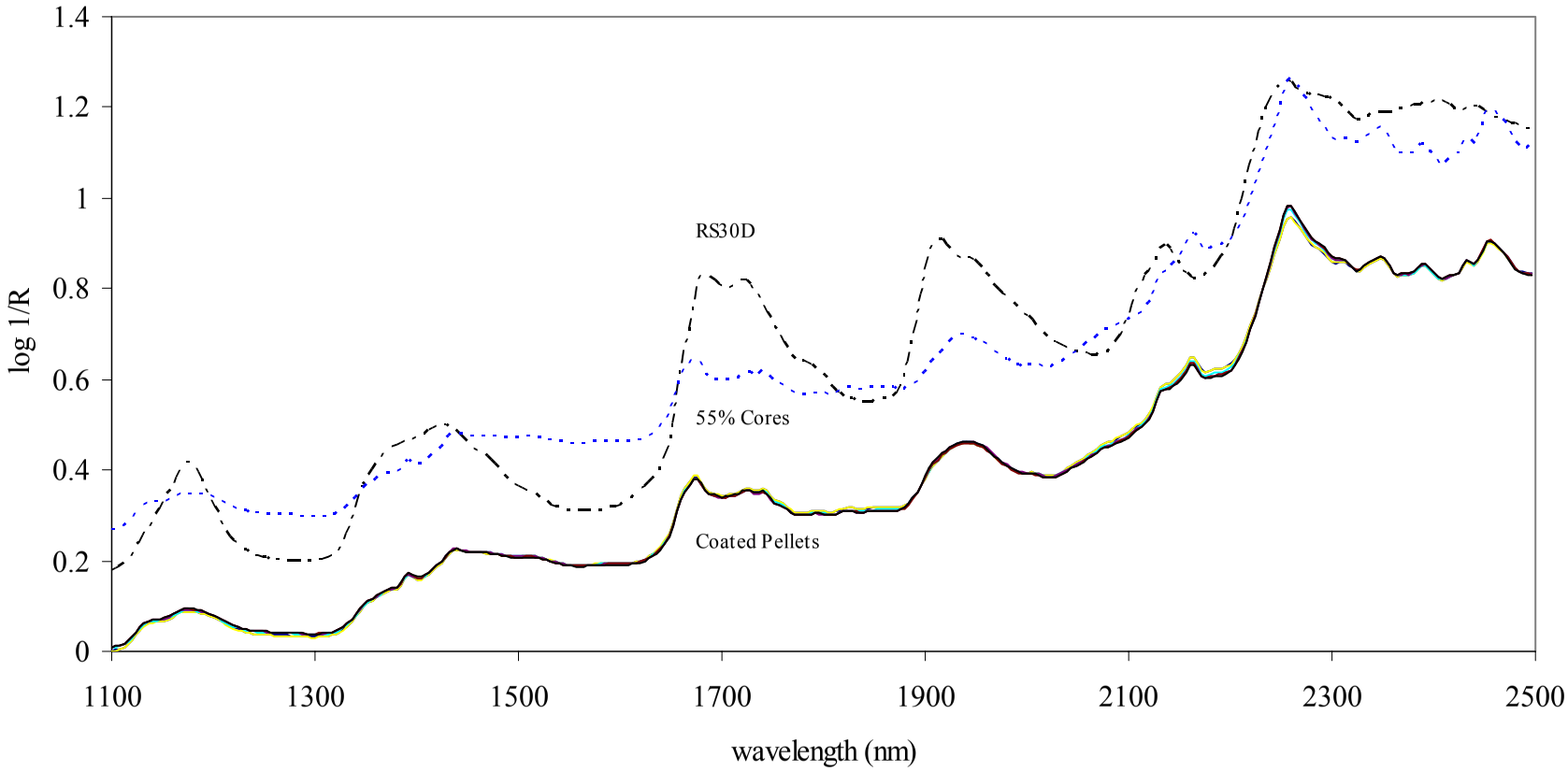

Figure 35. 550mg/g Diltiazem Pellets -- Coated 6% to 16% Applied Polymer Solids

be very similar, minor spectral changes can be observed in regions characteristic of the Eudragit RS30D polymer and core pellets. Chemical structures of the primary coating system and core pellet components were presented in **Figure 17** and **Figure 20**, respectively.

Truncated regions of the coated bead spectra, presented in **Figure 36**, demonstrate that absorbance increases with applied coating in regions characteristics of the coating material, while absorbance decreases in regions characteristic of the core pellet. The increasing absorbance in the 1680 to 1700 nm is attributed to C-H stretching in the first overtone region due to the influence of the poly(ethylacrylate, methylmethacrylate) trimethyl-ammonio-ethylmethacrylate chloride polymer, the primary component of the ERS system. The decreasing absorbance observed in a region characteristic of the core pellet, 2156 nm to 2180 nm, are likely the result of a combination bands arising from amine stretching associated with diltiazem HCl.

3.2.1 In-Line Analysis of Coated Pellets

Duplicate coating batches were processed for each of the three different potency types of diltiazem HCl core beads. The same calibration techniques used to build models for the prediction of pellet potency were employed to develop an in-line near-IR method for determining applied ERS solids during Wurster coating.

Single wavelength, multiple wavelength, and principal component calibrations were developed using both scatter corrected and second derivative spectra. A PLS calibration model was also developed using second derivative spectra. The choice of spectral preprocessing, MSC or D2, was based on the programs used to perform

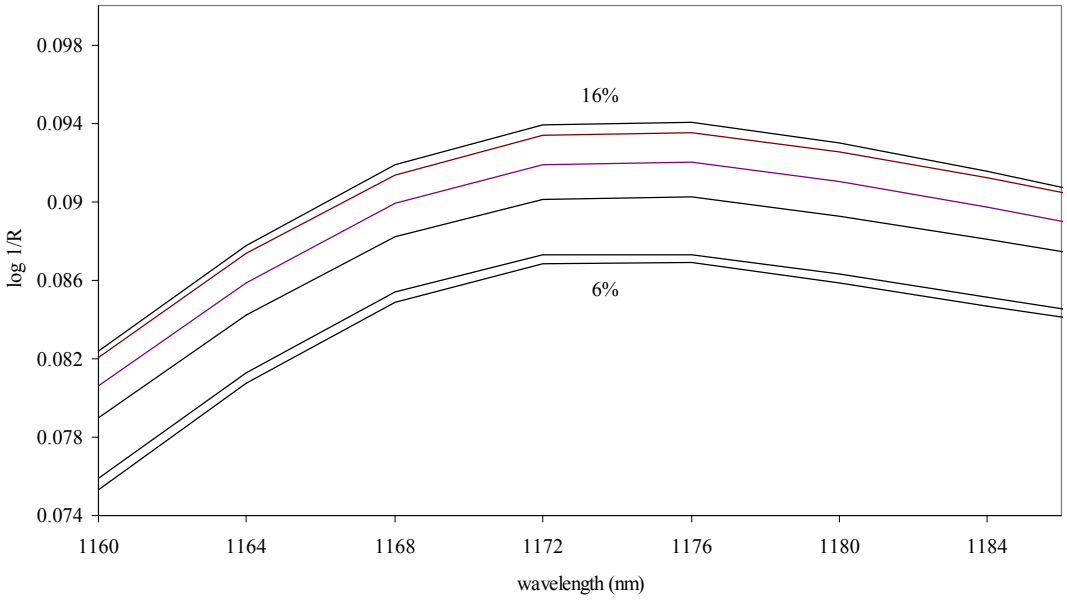

A. Spectral Region Characteristic of Eudragit RS30D

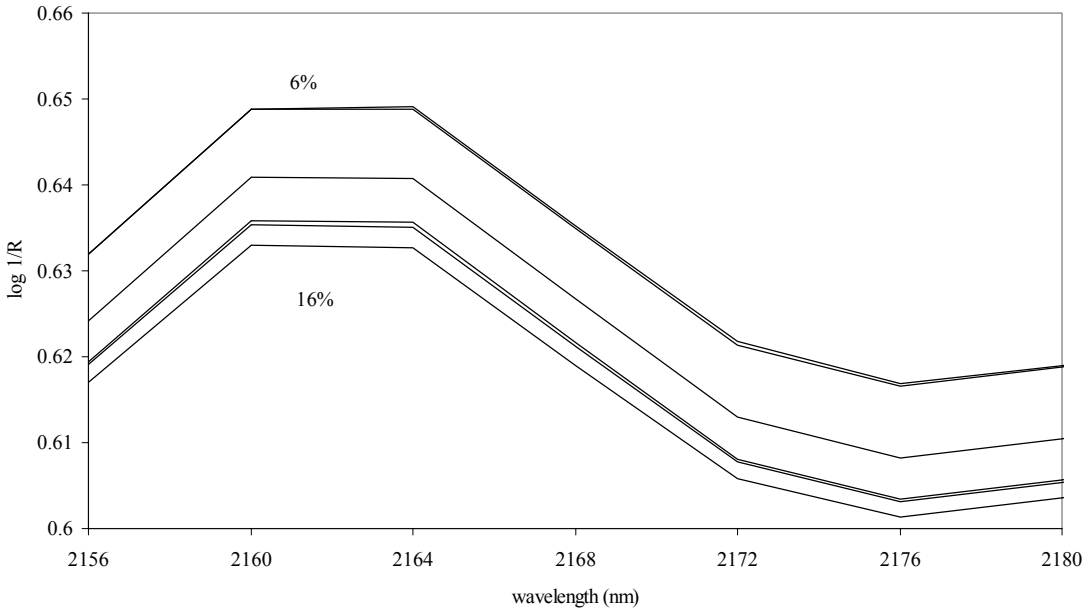

B. Spectral Region Characteristics of Diltiazem HCl

Figure 36: 550mg/g Diltiazem Pellets Coated with 6% - 16% Polymer Solids Truncated Spectral Regions

chemometric analysis. Single wavelength, multiple wavelength, and PCR analyses were performed on both MSC and D2 using SPEAKEASY® chemometric routines. PLSR was, however, performed using NSAS® software which offered only derivative-based spectral preprocessing. Because spectra were collected during processing, calibration model development was limited to one spectral scan per batch at each time point.

A total of 4 batches were processed for each pellet strength. Two batches were processed per day with complete set-up and tear-down of the fluid bed processor occurring between lots. Calibrations were developed using 24 samples within the 5% to 16% theoretical applied polymer solids range from two of the four batches for each formulation. Two batches from each formulation were processed to assess the predictive power of the developed calibrations.

3.2.1.1 Single and Multiple Wavelength Regression

For the single and multiple wavelength models, the most robust calibrations were developed using wavelengths from spectral regions characteristic of the ERS polymer or the drug-layered pellet. A single wavelength calibration was developed using absorbance values at 1616 nm which was highly correlated with ERS. A two-wavelength model was developed using 1616 nm and 2086 nm, which correlated with ERS and drug-layered pellets, respectively. For all strengths, both single- and multiple-wavelength models had R^2 values of 0.99, and SEC and SEP values of <0.5% were achieved.

3.2.1.2 Principal Component Regression

Principal component regression of spectra collected in-line was used following MSC or D2 treatment of the NIR data. Initially, spectra were transformed into principal component axis space. **Table 21** summarizes the sequences of principal components and their percentages of contribution to the total variations of spectral data. The first principal component accounts for the largest amount of the total variations which, for MSC spectra, is about 60%. For D2 spectra, a greater number of PCs were required to explain total spectral variation. In these spectra, the amount of total variation explained by the first PC is about 50%.

The correlation of the first two PCs to the ERS and drug-layered pellet components of 150 mg/g, 300mg/g, and 550 mg/g beads coated with 16% w/w ERS can be observed in **Figures 37 and 38**, which present the loadings of these PCs for MSC spectra. In general, a smother loading spectra is observed for the at-line samples relative to spectra collected in-line which may be attributed to: (i) the stationary nature of the sample; (ii) normalized particle size and morphology due to removal of pellets from the process stream and sieving prior to analysis; (iii) more uniform sample moisture; and (iv) differences between the spectral acquisition systems.

The principal components used for regression were limited to those that contributed significantly to the model (t-statistic >3.0). Regression results are summarized in **Table 22**. Two PCs were significant for all models (t-statistic > 3.0) with the exception of 300mg/g D2/PCA, in which only one PC was significant. All models demonstrated that applied polymer solids could be predicted within 0.7% of laboratory values for all pellet strengths. The inclusion of additional PCs was also investigated

Table 21. Principal components of in-line ERS polymer coating onto diltiazem HCl pellets.

MSC				Second Derivative			
150 mg/g				150 mg/g			
Root No.	Roots	Proportional Variance	Cumulative Variance	Root No.	Roots	Proportional Variance	Cumulative Variance
1	141.5	0.5662	0.5662	1	116.16	0.4646	0.4646
2	90.2	0.3607	0.9269	2	17.93	0.0717	0.5469
3	11.5	0.0461	0.9731	3	11.28	0.0451	0.5815
4	3.3	0.0130	0.9861	4	8.66	0.0345	0.6162
5	1.52	0.0061	0.9922	5	8.18	0.0327	0.6489
300 mg/g				300 mg/g			
Root No.	Roots	Proportional Variance	Cumulative Variance	Root No.	Roots	Proportional Variance	Cumulative Variance
1	165.52	0.6620	0.6620	1	146.48	0.5859	0.5859
2	70.531	0.2821	0.9441	2	17.08	0.0683	0.6542
3	10.18	0.0407	0.9842	3	14.57	0.0583	0.7125
4	1.63	0.0065	0.9914	4	12.47	0.0499	0.7624
5	0.66	0.0026	0.9941	5	11.88	0.0475	0.8099
550 mg/g				550 mg/g			
Root No.	Roots	Proportional Variance	Cumulative Variance	Root No.	Roots	Proportional Variance	Cumulative Variance
1	155.64	0.6225	0.6225	1	140.7	0.5628	0.5628
2	74.161	0.2966	0.9192	2	25.25	0.1010	0.6638
3	16.05	0.0642	0.9834	3	13.25	0.0530	0.7168
				4	12.75	0.0510	0.7678
				5	11.39	0.0455	0.8134

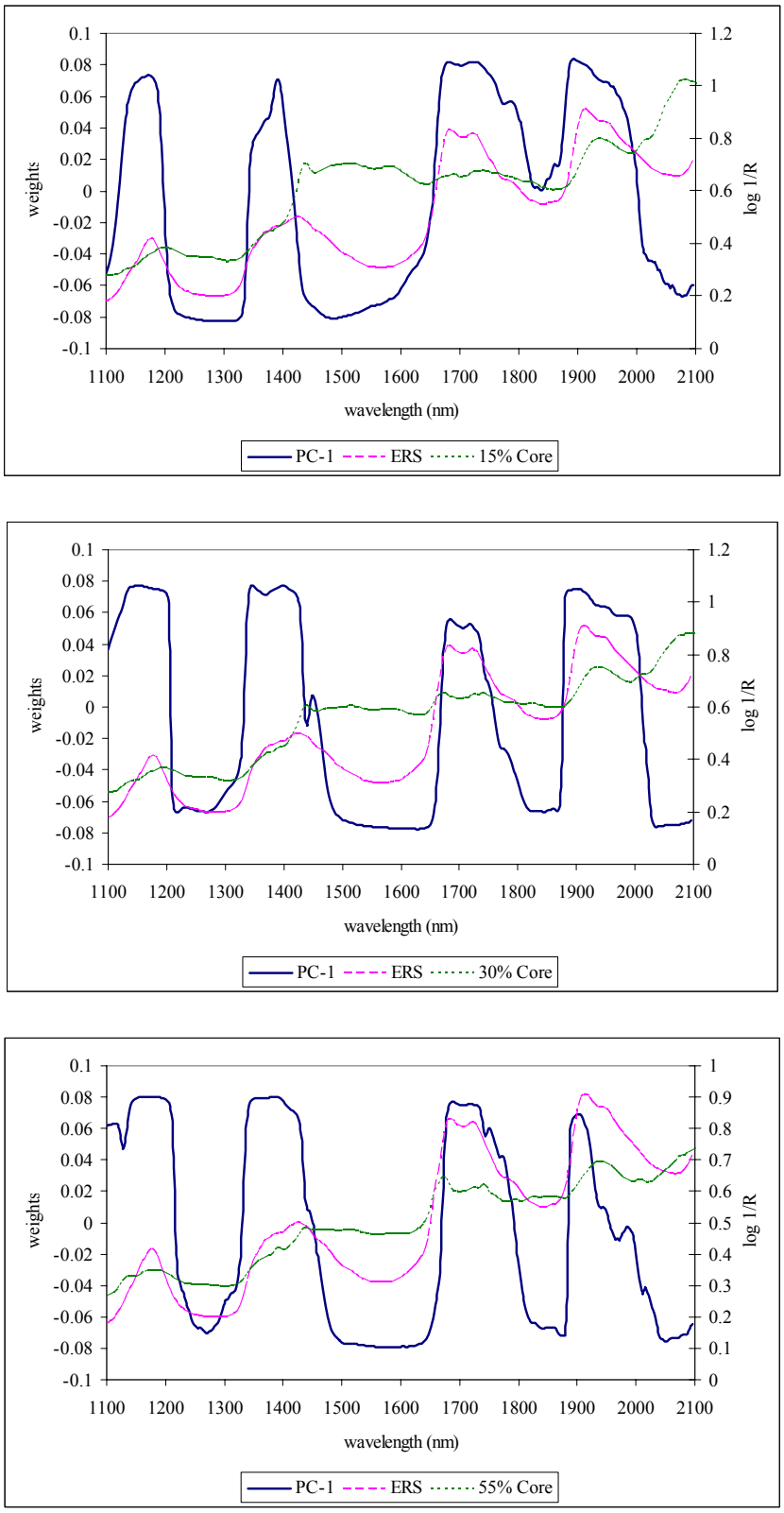

Figure 37. First PC Loadings for 16% ERS Coated Pellets – in-line sampling 150mg/g (top), 300mg/g (middle), 550mg/g (bottom)

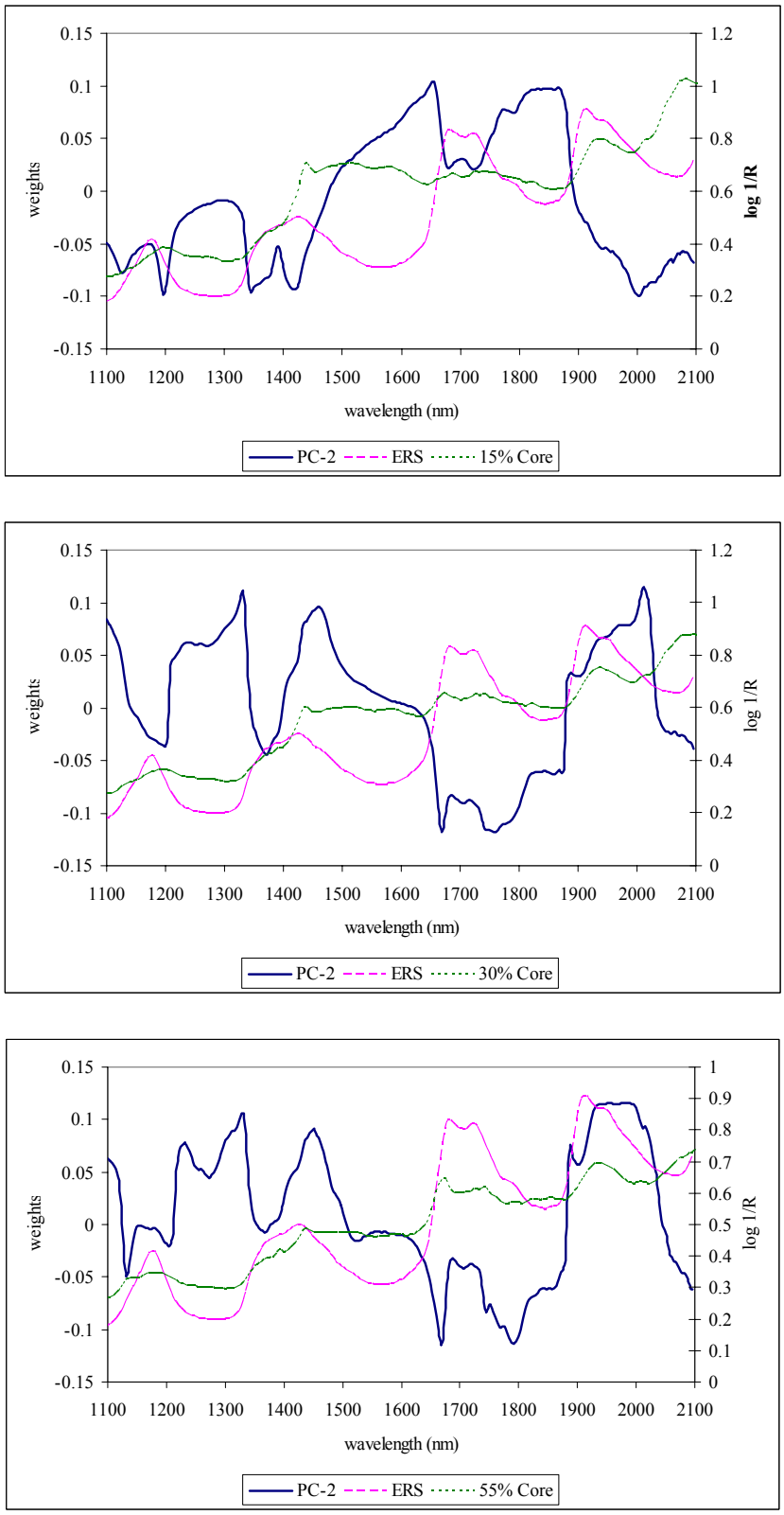

Figure 38. Second PC Loadings for 16% ERS Coated Pellets – in-line sampling 150mg/g (top), 300mg/g (middle), 550mg/g (bottom)

Table 22. Principal component regression results for in-at-line analysis of ERS coated diltiazem HCl pellets.

MSC						2nd Derivative					
150mg/g						**150mg/g**					
PCs Used	T-Statistic		R^2	SEC	SEP	PCs Used	T-Statistic		R^2	SEC	SEP
1	PC-1	11.47	0.93	0.98%	0.73%	1	PC-1	-27.75	0.98	0.63%	1.22%
2	PC-1	20.44	0.98	0.55%	0.61%	2	PC-1	-19.2	0.98	0.43%	0.70%
	PC-2	-4.76					PC-2	-8.73			
300mg/g						**300mg/g**					
PCs Used	T-Statistic		R^2	SEC	SEP	PCs Used	T-Statistic		R^2	SEC	SEP
1	PC-1	18.71	0.94	0.88%	0.83%	1	PC-1	-32.74	0.98	0.51%	0.55%
2	PC-1	58.54	0.99	0.28%	0.33%	2	PC-1	-32.35	0.98	0.52%	0.56%
	PC-2	-13.63					PC-2	-0.703			
550mg/g						**550mg/g**					
PCs Used	T-Statistic		R^2	SEC	SEP	PCs Used	T-Statistic		R^2	SEC	SEP
1	PC-1	27.86	0.99	0.42%	0.74%	1	PC-1	-24.65	0.98	0.47%	0.38%
2	PC-1	65.78	0.98	0.34%	0.48%	2	PC-1	-39.67	0.99	0.29%	0.31%
	PC-2	-6.84					PC-2	-4.11			

during calibration development. Although such models provided lower SEC values, they demonstrated higher SEP values, which may indicate overfitting of the data. The calibrations utilized in this study were based on PCs which provided SEC and SEP values that were similar and as low as possible, thus maximizing the model robustness.

3.2.1.3 Partial Least Squares Regression

Partial least squares regression results of D2 spectra for all pellet strengths are summarized in **Table 23**. Performance of the PLSR was similar or slighlty better than PCR, with SEPs of less than ~0.5% achieved for all pellet strengths. In some instances, SEP values were lower than SEC. Since only a limited number of samples were available for model development, such behavior was not unexpected.

3.2.1.4 Summary of In-Line Regression Model Performance

A summary of the performance of optimized single wavelength, multiple wavelength, PCR and PLS models for in-line analysis of applied polymer solids during Wurster coating is presented in **Table 24**. Similar calibration results were obtained for 150 mg/g, 300mg/g, and 550mg/g drug layered pellets. All calibration models demonstrated R^2 values of 0.98 or greater and standard errors of calibration less than 0.70%. A scatter plot of the calibration and prediction results obtained by D2/PCR regression of second derivative 150mg/g pellet spectra pellets is presented in **Figure 39.** This model demonstrated an R^2 value of 0.98, an SEC of 0.63%, and an SEP of 0.35%. Standard error of the laboratory (SEL) for the reference method, as previously reported, was approximately 0.47%.

Table 23. Partial least squares regression results for in-line ERS polymer coating onto diltiazem HCl drug-layered pellets.

		150 mg/g		
Factor	MSECV	R	SEC	SEP
1	2.25	0.99	0.59%	0.52%
2	1.72	0.99	0.52%	0.42%
<3>	1.17	0.99	0.37%	0.25%
4	1.15	0.99	0.32%	NT
5	1.29	0.99	0.25%	NT
		300 mg/g		
Factor	MSECV	R	SEC	SEP
1	6.28	0.98	0.71%	0.87%
2	2.41	0.98	0.38%	0.42%
3	1.66	0.99	0.29%	0.36%
<4>	1.38	0.99	0.23%	0.34%
5	1.12	0.99	0.17%	0.39%
		550 mg/g		
Factor	MSECV	R	SEC	SEP
1	2.34	0.99	0.65%	0.72%
2	1.84	0.99	0.51%	0.54%
<3>	1.29	0.99	0.47%	0.50%
4	1.27	0.99	0.42%	NT
5	1.39	0.99	0.41%	NT

< > - factors recommended by NSAS®
NT - not tested.

Table 24. Summary of regression results for in-line assessment of applied ERS polymer.

	150mg/g Diltiazem HCl Pellets			
			Applied Polymer (%)	
Regression Model	PCs	R^2	SEC	SEP
PCR – MSC	2	0.98	0.55	0.61
PCR – D2	2	0.98	0.43	0.70
PLS – D2	3	0.99	0.37	0.25
Multiple Wavelength	--	0.99	0.36	0.39
Single Wavelength	--	0.99	0.40	0.20

	300mg/g Diltiazem HCl Pellets			
			Applied Polymer (%)	
Regression Model	PCs	R^2	SEC	SEP
PCR – MSC	2	0.99	0.28	0.33
PCR – D2	1	0.98	0.51	0.55
PLS – D2	3	0.99	0.29	0.36
Multiple Wavelength	--	0.99	0.20	0.25
Single Wavelength	--	0.99	0.14	0.21

	550mg/g Diltiazem HCl Pellets			
			Applied Polymer (%)	
Regression Model	PCs	R^2	SEC	SEP
PCR – MSC	2	0.98	0.34	0.48
PCR – D2	2	0.99	0.29	0.31
PLS – D2	2	0.99	0.47	0.50
Multiple Wavelength	--	0.99	0.21	0.33
Single Wavelength	--	0.99	0.25	0.28

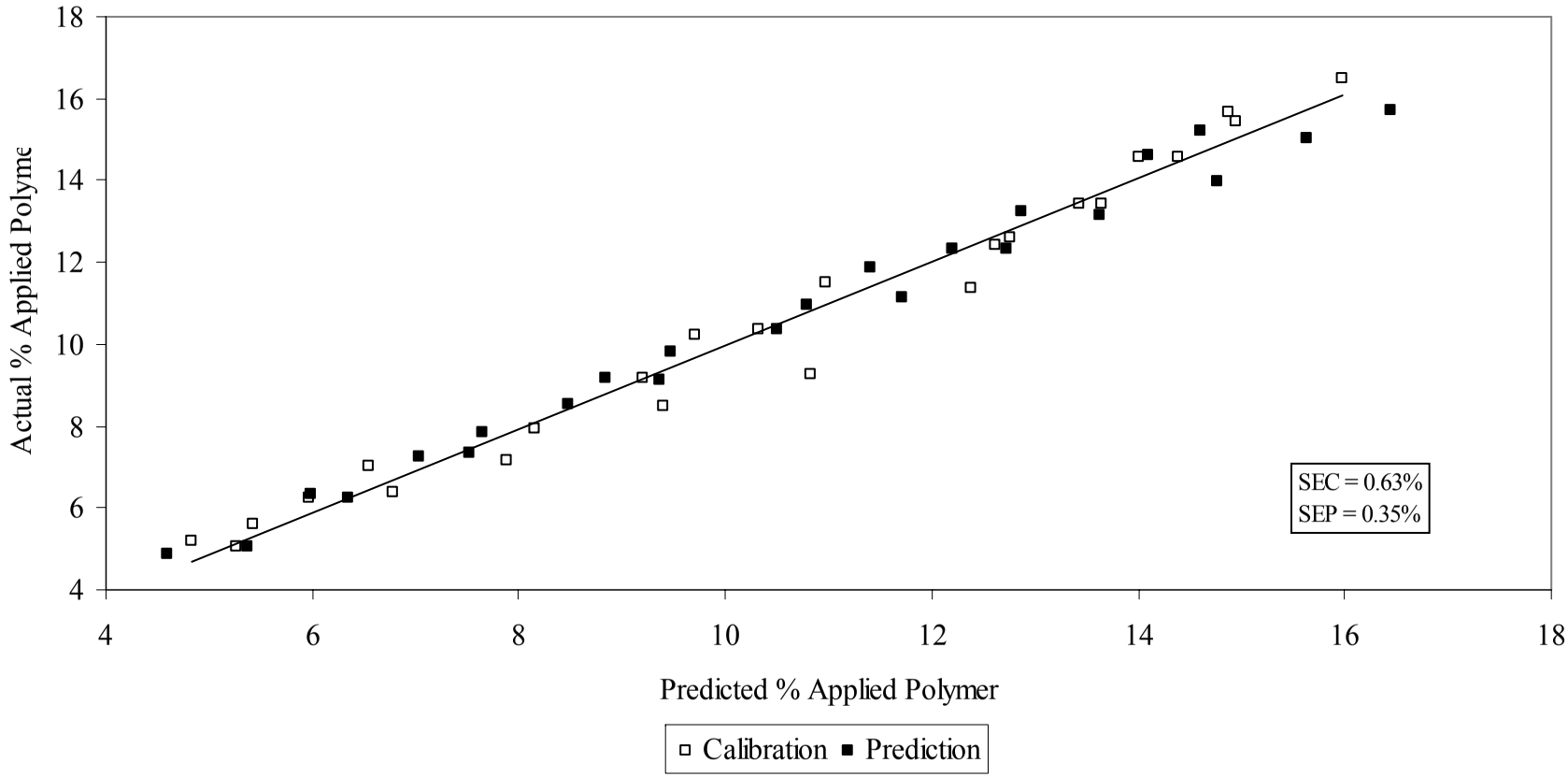

Figure 39. Applied Polymer Solids Calibration and Prediction -- Diltiazem HCl 150mg/g Pellets In-line Analysis

As observed in the rotogranulation study, the simplistic single and multiple wavelength models also demonstrated their ability to accurately predict applied polymer solids content within ~0.75% of actual values. Therefore, it may be possible to employ simple filter-based instruments to monitor coating operations in-line. However, the merits and shortcomings of both full-spectrum and single or multivariate modeling techniques, as previously discussed, should be thoroughly investigated to assure consistent model accuracy for a routine commercial environment (134).

3.2.2 At-line Analysis of Coated Pellets

At-line spectra of unit-dose samples were obtained in triplicate by scanning through the base of the glass sample vials using a NIRSystems Rapid Content Analyzer and model 6500 spectrometer. **Table 25** provides a summary of the calibration models developed using coated pellet spectra collected at-line. Additionally, a plot of both the calibration and prediction results obtained by principal component regression of second derivative spectra for 150mg/gram pellets is presented in **Figure 40**. Overall, the performance of the at-line methods was similar to the in-line models with SEP values of less than of ~0.6% achieved for all models.

3.2.3 Comparison of In-line and At-line Near-IR Methods for Monitoring Wurster Coating

A comparison between on-line and at-line coating prediction errors is presented in **Table 26**. For all calibration models, it was possible to predict potency within 0.6% of reference laboratory values. Interestingly, the in-line model, in some instances, provided

Table 25. Summary of regression results for at-line assessment of applied ERS polymer.

	150mg/g Diltiazem HCl Pellets			
			Applied Polymer (%)	
Regression Model	PCs	R^2	SEC	SEP
PCR – MSC	2	0.99	0.43	0.59
PCR – D2	2	0.99	0.37	0.48
PLS – D2	2	0.99	0.38	0.42
Multiple Wavelength	--	0.99	0.33	0.39
Single Wavelength	--	0.99	0.39	0.42

	300mg/g Diltiazem HCl Pellets			
			Applied Polymer (%)	
Regression Model	PCs	R^2	SEC	SEP
PCR – MSC	2	0.99	0.37	0.49
PCR – D2	2	0.99	0.27	0.49
PLS – D2	2	0.99	0.29	0.34
Multiple Wavelength	--	0.99	0.27	0.34
Single Wavelength	--	0.99	0.31	0.37

	550mg/g Diltiazem HCl Pellets			
			Applied Polymer (%)	
Regression Model	PCs	R^2	SEC	SEP
PCR – MSC	2	0.99	0.23	0.53
PCR – D2	2	0.99	0.26	0.59
PLS – D2	2	0.99	0.23	0.41
Multiple Wavelength	--	0.99	0.21	0.32
Single Wavelength	--	0.99	0.25	0.28

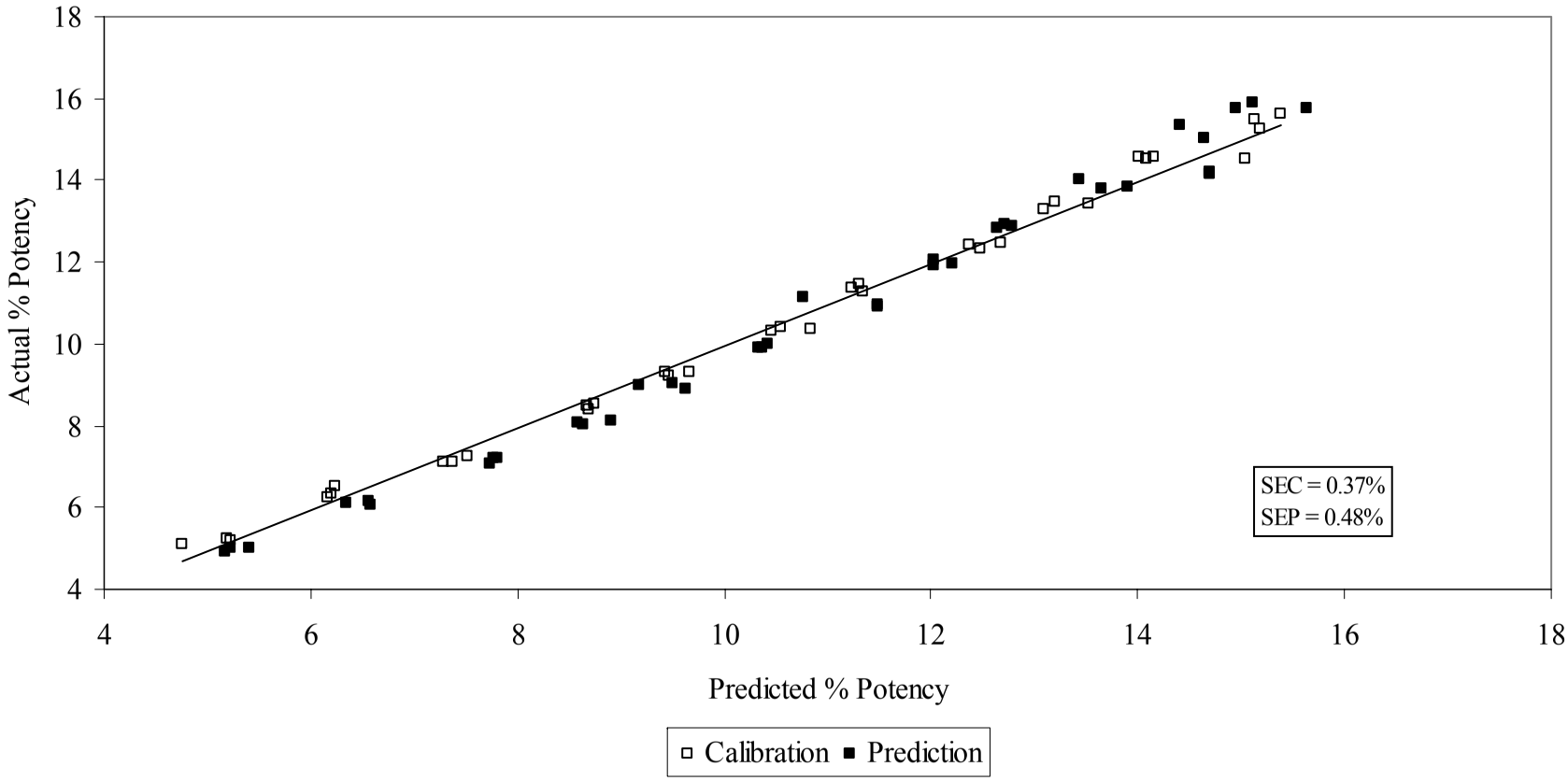

Figure 40. Coating Calibration and Prediction -- Diltiazem HCl 150mg/g Pellets At-line Analysis

Table 26. Comparison of in-line and at-line regression model performance for applied ERS polymer coating prediction.

150mg/g Diltiazem HCl Pellets

Regression Model	Standard Error Of Prediction (%)	
	In-line	At-line
PCR – D2	0.70	0.48
PLS – D2	0.25	0.42
Multiple Wavelength	0.39	0.39
Single Wavelength	0.20	0.42

300mg/g Diltiazem HCl Pellets

Regression Model	Standard Error Of Prediction (%)	
	In-line	At-line
PCR – D2	0.55	0.49
PLS – D2	0.36	0.34
Multiple Wavelength	0.25	0.34
Single Wavelength	0.21	0.37

550mg/g Diltiazem HCl Pellets

Regression Model	Standard Error Of Prediction (%)	
	In-line	At-line
PCR – D2	0.31	0.59
PLS – D2	0.50	0.41
Multiple Wavelength	0.33	0.32
Single Wavelength	0.28	0.28

better prediction results than did the at-line method. This may be attributed to the fact that in-line spectra were obtained by scanning through a

stationary sapphire window which is transparent in the near-IR region. During at-line analysis, error may be introduced from variations in sample packing, sample repositioning, and variability in the base of the glass vial through which spectra are collected. Such results are reasonable in terms of the ability to control the drug loading process, and acceptable with respect to the 0.41% SEL of the reference method.

With respect to sample presentation, Yoon *et al.,* (135) in their analysis of sample presentation effect on the spectra of pharmaceutical excipients, demonstrated that sample thickness and sample presentation diameter had considerable effects on near-IR spectral characteristics while spectral changes associated with sample packing was less pronounced. In the current study, the depth of the pellets in the sample vials and the depth of the pellets moving past the direct reflectance in the in-line method were similar (~5 cm). Since the beads analyzed in this study are free-flowing, have a relatively narrow particle size distribution, and do not considerably consolidate when tapped, variations in packing differences were also not likely significantly contribute to at-line measurement error. However, to mitigate risk associated with packing differences and the potential for sample segregation to occur, each vial was inverted 3 times between scans and replicate scans were averaged to obtain one composite spectrum for each sample time point.

One aspect of the sampling that potentially contributed to better prediction results for the in-line method, as compared to at-line analysis was sample presentation diameter. The sapphire window in direct reflectance probe used for in-line analysis had a diameter of 10 mm, while the base diameter of the sample vials used for at-line analysis was

18 mm. In addition, both the Direct Reflectance Probe and the RCA utilize 420 fibers (200 μm diameter) to carry near-IR radiation to the sample. Therefore, since the sapphire window diameter in the direct reflectance probe is smaller than the base of the sample vials, and the distance the near-IR radiation travels through the fibers in the probe is significantly greater than for the RCA, lower absorbance values for the in-line samples would be expected. However, as seen in **Figure 41,** which depicts spectra of 150mg/g diltiazem HCl pellets coated with 16% ERS collected using either the RCA or the fiber optic probe, higher absorbance values were associated with the probe sampling system. Such absorption differences are likely to translate to a lower signal to noise ratio for the RCA, which may contribute to the higher and more variable SEC and SEP results obtained during at-line assessment of pellet potency. In addition, the loadings spectra for PC-1 and PC-2 of MSC spectra for 150mg/g diltiazem HCl pellets coated with 6% to 16% ERS, presented in **Figure 42** and **Figure 43**, demonstrate good correlation to spectral features of interest in predicting coating level. Despite minor performance differences between the in-line and at-line systems, both were quite effective in providing a non-invasive technique for monitoring the Wurster coating process.

3.2.4 Prediction of Dissolution of Eudragit RS30D Coated Pellets

Prior to final blending or encapsulation, intermediate pellets lots are often tested to ensure that they meet product specifications such as potency and dissolution. Since the production of most extended-release pellet products usually involves time consuming and expensive manufacturing operations, in-house quality control mechanisms are commonly employed to prevent the combination of sub-standard intermediates with acceptable

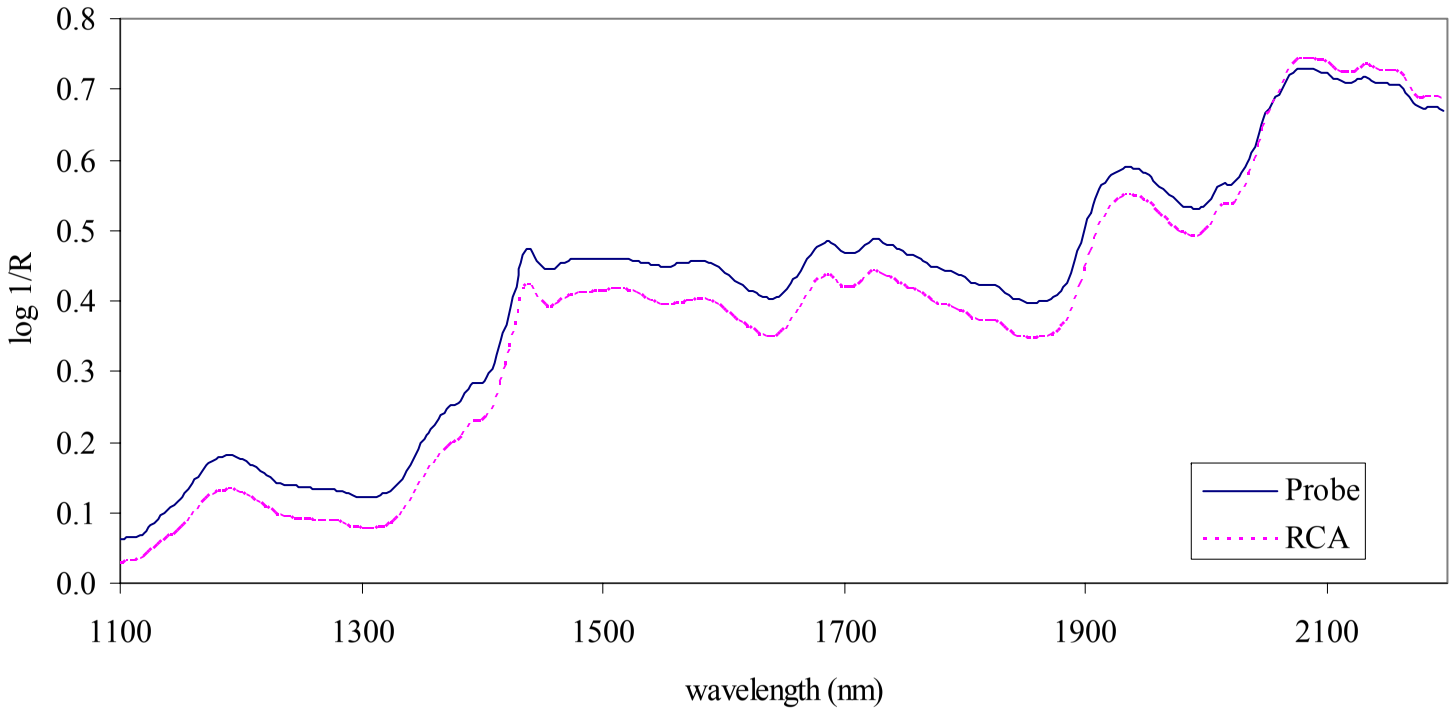

Figure 41. 150mg/g Diltiazem + 16% ERS Coat
RCA versus Direct Reflectance Sampling

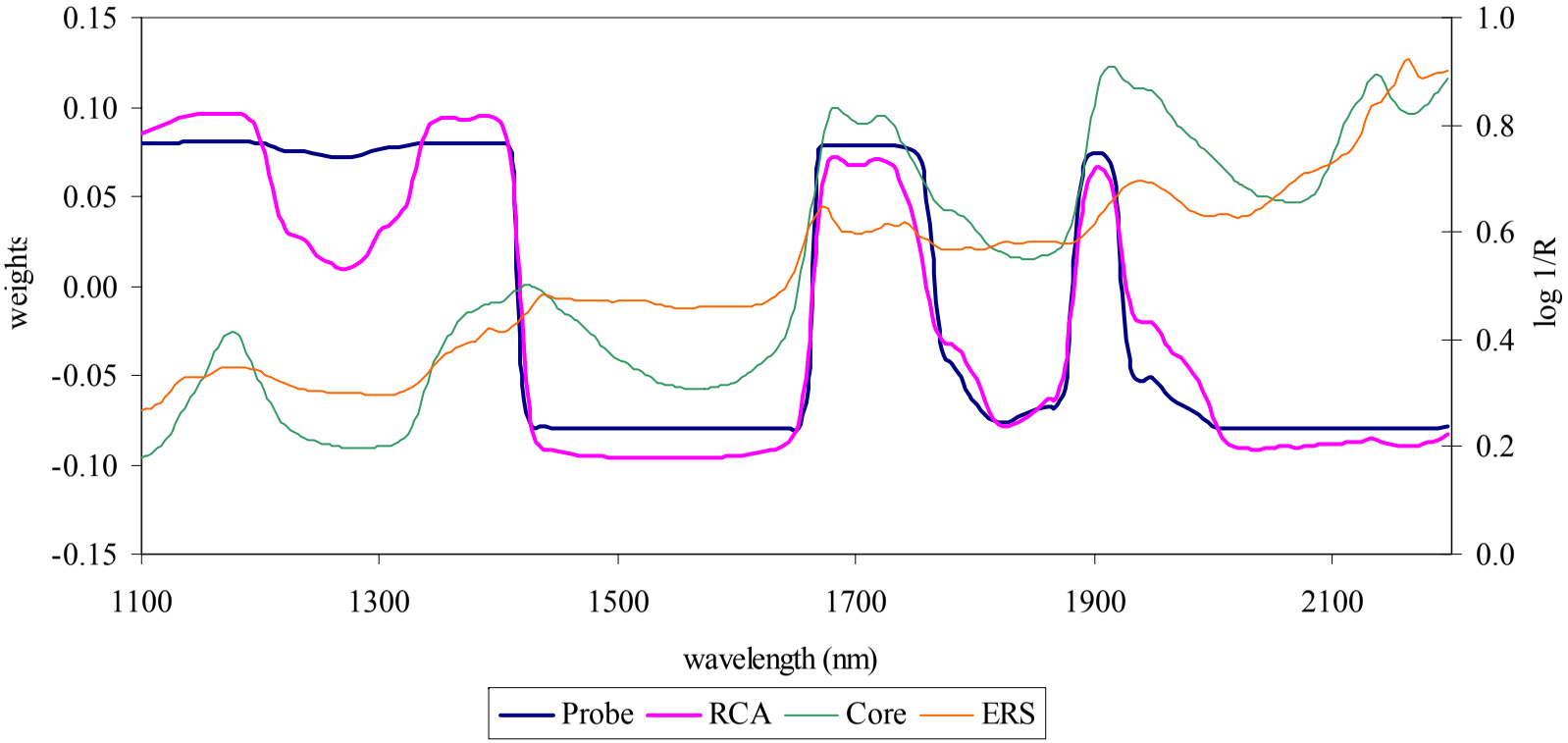

Figure 42. PC-1 Loadings for 15% Diltiazem HCl Pellets + 16% ERS Coat RCA versus Direct Reflectance Probe

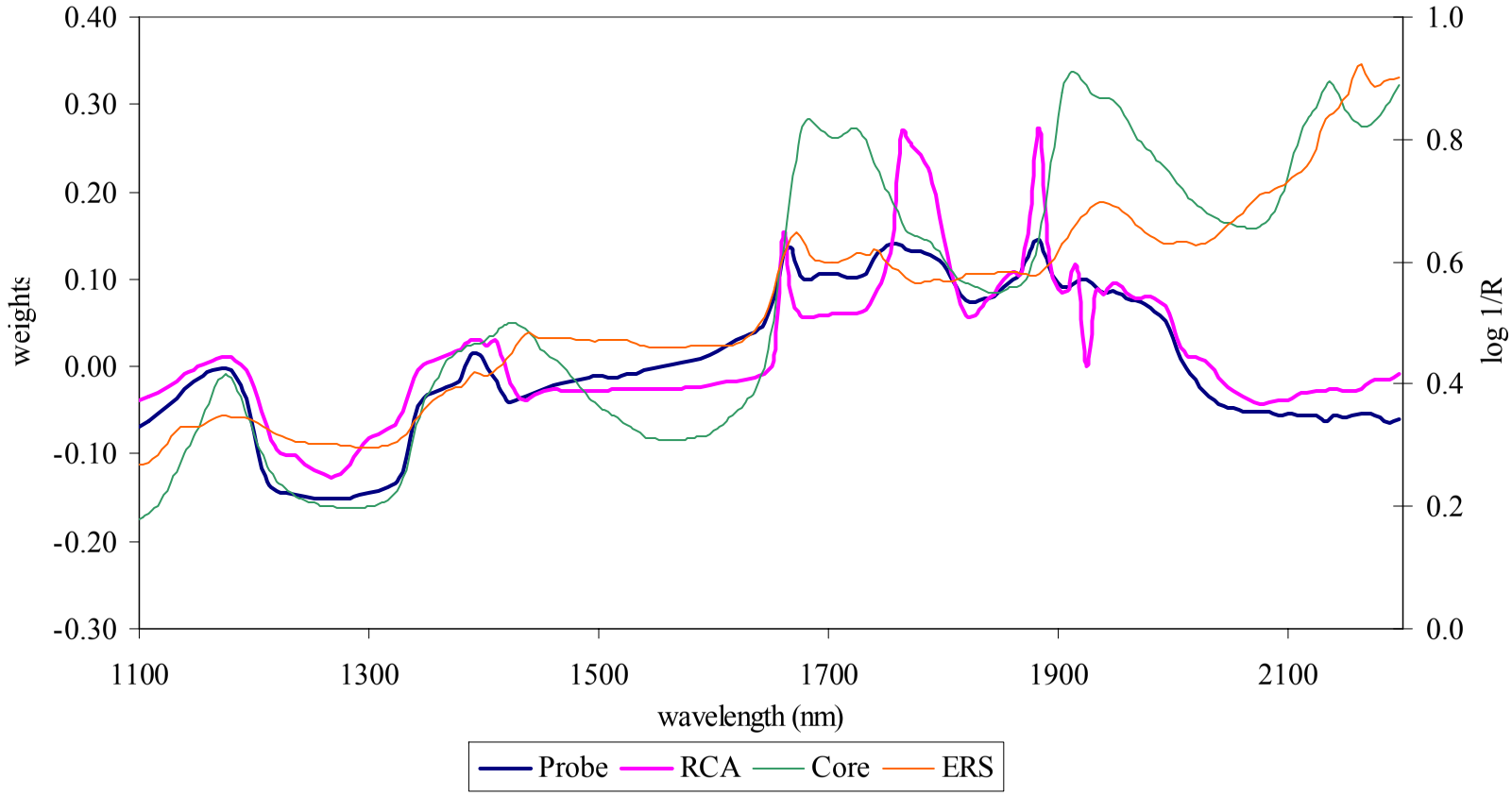

Figue 43. PC-2 Loadings for 15% Diltiazem HCl Pellets + 16% ERS Coat RCA versus Direct Reflectance Probe

product. Once identified, sub-standard material may either be reworked (if possible) or removed entirely from subsequent manufacturing operations. Although such quality mechanisms may potentially save companies millions of dollars, intermediate testing procedures may be costly and time consuming, especially for extended-release products intended to provide twenty-four hour drug release. The development of near-infrared spectroscopic methods to predict extended-release pellet dissolution characteristics could potentially reduce production cycle down-time associated with the acquisition of intermediate laboratory results. Furthermore, such methods would allow product quality to be assessed prior to completing the manufacture of an entire batch.

In this study, drug release from 120 mg doses of 55% diltiazem HCl pellets, coated with either 12%, 14% or 16% Eudragit RS30D, was evaluated over 8 h using a USP dissolution apparatus equipped with an automated UV sampling system (Varian/Cary, Palo Alto, CA). Dissolution conditions, as per the USP 24 monograph for Diltiazem Hydrochloride Extended-release Capsules (130), were: n = 12, 900 ml of 0.1N HCl, apparatus II, 50 rpm paddle speed, λ = 240 nm. The time required for 50% of drug release to occur (t50%) was determined by modeling the dissolution profiles using TableCurve 2D® software (Version 4.0., Systat Software, San Rafael, CA). The dissolution profiles, presented in **Figure 44**, were fit to the four parameter sigmoidal equation:

$$y = y_0 + a/\left(1 + e^{-((x-x_0)/b)}\right) \qquad \text{(Eq. 21)}$$

where: y_0 represents the lower bound in dissolution; a is the difference between the upper and lower bound in dissolution; x_0 is the time of the inflection point; and b is a

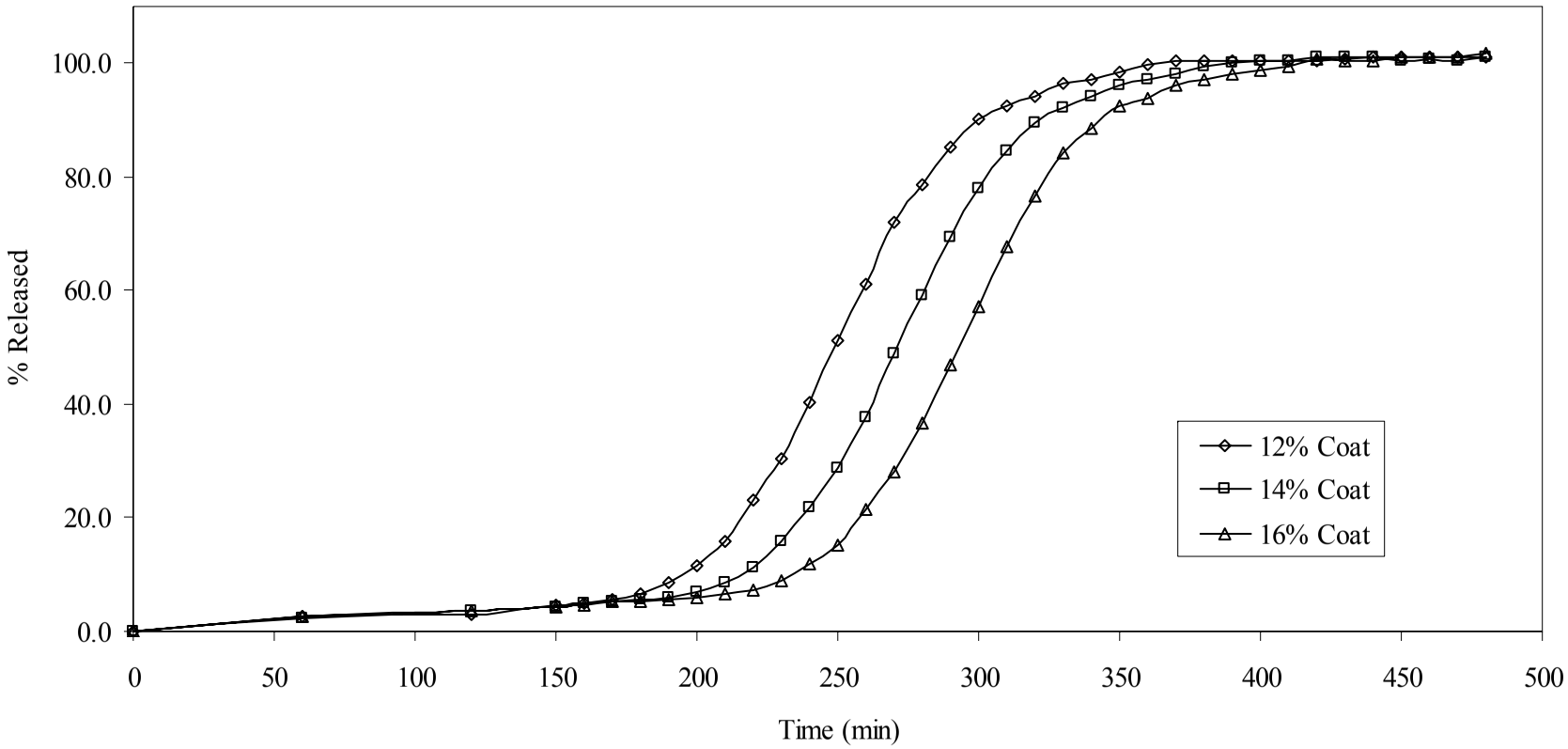

Figure 44. Dissolution Profile for Eudragit RS30D Coated Pellets

scale parameter (width in time in which most of the dissolution change occurs). Dissolution data and regression coefficients are summarized in **Appendices 3 – 5.**

Sigmoidal drug release patterns from Eudragit® RS coated pharmaceutical products have been well studied (136,137), and are best described by an ion exchange mechanism. As the dissolution medium dissolves the diltiazem HCl in the core, anionic counterions from both the drug substance and the dissolution media interact with the oppositely charged quaternary ammonium groups in the Eudragit RS polymer and increase the permeability of the hydrated polymer film. The lag time associated with this phenomenon is controlled by the rate of water influx through the coating, and increases with increasing thickness of the coat.

Prior to dissolution, near-IR spectra were collected from 1100 to 2200 nm using a NIRSystems 6500 spectrometer equipped with a Rapid Content Analyzer sampling system. The spectra were scatter corrected and reduced to 275 wavelengths prior to principal component analysis for calibration development. In this analysis, the first two principal components explained 99% of the variability in the spectral data and were used in the calibration model. **Figure 45** shows a plot of calibration and results obtained. The model had a R^2 of 0.997, an SEC of 6.9 minutes and an SEP of 8.1 min.

The results of this study demonstrate the potential of near-infrared spectroscopy as a rapid, non-destructive means for assessing the dissolution characteristics of extended-release pellets. Furthermore, the dissolution data generated shows that the coating applied to pellets within a target applied polymer solids range is uniform. For n=12 samples, t50% values varied by only by about 7 min (~3%) over a four to six hour time period.

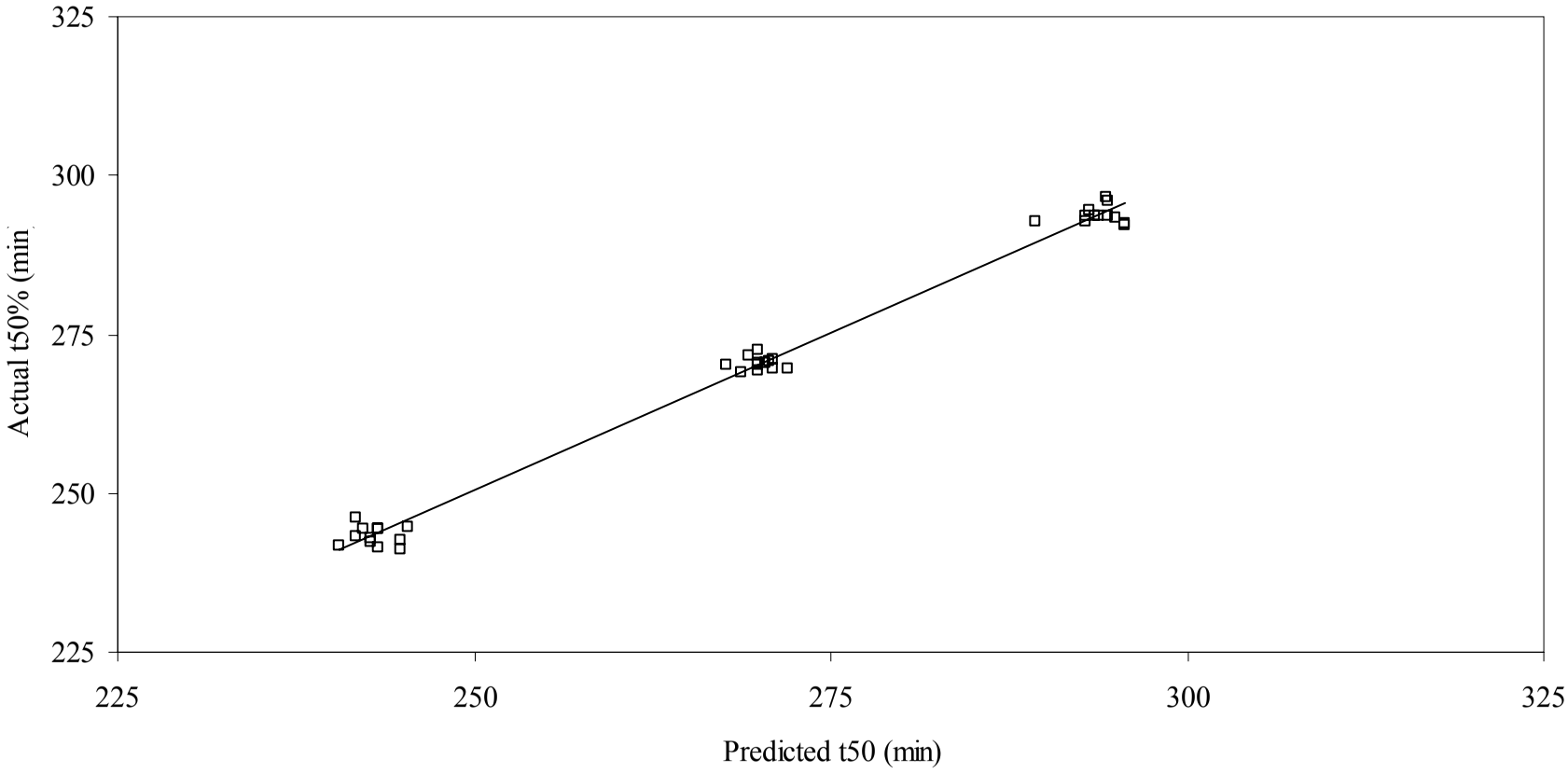

Figure 45. Prediction of t50% Diltiazem HCl Dissolved for Eudragit RS30D Coated Diltiazem HCl 550 mg/g Pellets

3.3 Qualitative Prediction of Eudragit RS30D Coating Endpoint

In addition to being a powerful tool for quantitative pharmaceutical analysis, near-IR spectroscopy has gained recognition for its qualitative analysis capabilities. Qualitative analysis involves classifying samples by comparing their spectral characteristics to those of a reference group. The most widely accepted methods for qualitative near-IR analysis utilize pattern recognition techniques. Such methods classify samples according to their similarity to a training set. Because pattern recognition techniques can only recognize the variability to which they accustomed, it is necessary to develop a training set that represents all expected sources of spectral variability. After training the computer to recognize the spectral qualities of acceptable material, pattern recognition algorithms can be employed to quickly identify and classify unknown test samples.

The ability of two pattern recognition methods to qualitatively predict coating process endpoints was assessed in this phase of study. The techniques under investigation included a MD calculation and a BEAST (Bootstrap Error-Adjusted Single-sample Technique). Of these methods, the BEAST has been previously shown to offer speed, accuracy and precision over the Mahalanobis distance metrics in qualitative analysis of near-IR data (78,138). Both methods classify samples according to their similarity to a training set. After training the computer to recognize the spectral qualities of pellet samples containing a desired level of applied polymer coating, the referenced pattern recognition algorithms were employed to identify and classify unknown test

samples as either acceptable or unacceptable with respect to a target applied coating level.

In this study, three different training sets, corresponding to 6%, 10% and 15% applied polymer solids, were developed from samples collected from two Wurster coating runs. Each target training set was comprised of 12 samples (six samples from each coating run). For each sample, triplicate spectra were collected by scanning through the base of the glass sample vials using a NIRSystems Rapid Content Analyzer and model 6500 spectrometer, then averaged. Following MSC treatment of the near-IR data, a principal-axis-transformation of the spectral data points was performed. Principal component analysis reduced 275 independent variables to 2 principal components which explained 99% of the variance in the data. Training sets development for both the Mahalanobis and BEAST analyses utilized two principal components and 1000 bootstrap replications.

During two subsequent coating trials, samples were collected at various time points over a range of 6% to 16% applied polymer solids. Using the bootstrap algorithm or Mahalanobis distance metric to assess test sample spectral similarity to the training set, a distance analogous to a standard deviation was calculated between the test sample and the center of the training cluster. Samples within 3 SDs from the training cluster were considered to contain the target coat and were classified as acceptable. Samples with SDs >3 were classified as outliers and were deemed unacceptable.

A graphic presentation of the classification results for BEAST and MD analyses of all investigated pellet strengths and target coating levels is presented in **Figure 46.**

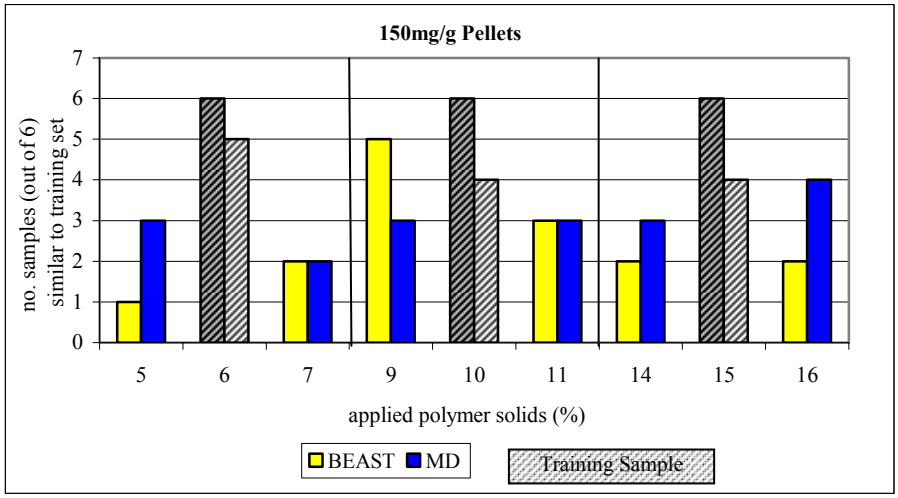

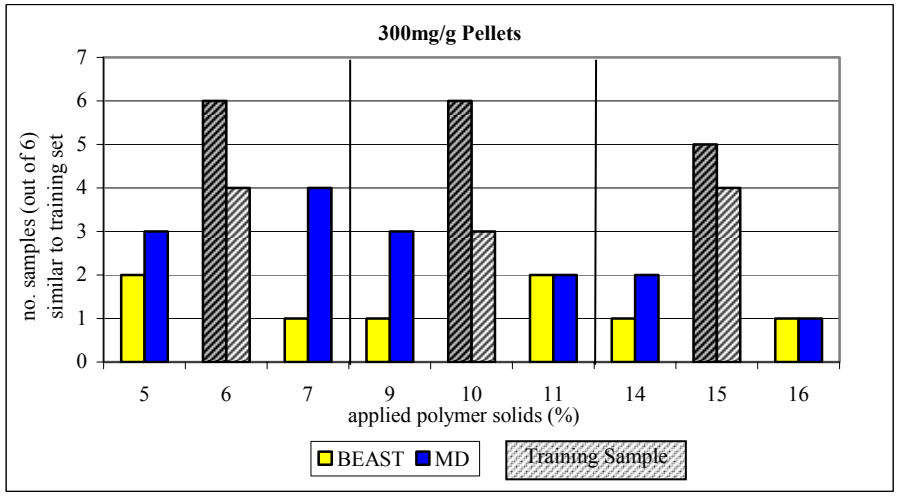

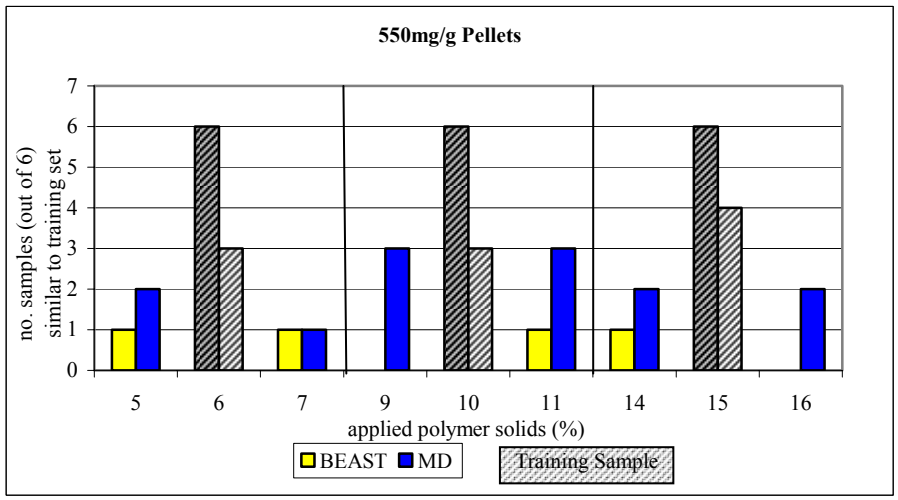

Figure 46. Qualitative Prediction of Target Applied Polymer Solids BEAST versus Mahalanobis Distance

In each graph, three training sets, 6%, 10% and 15%, are presented by the hatched bars. The height of the bars represents the number of test samples (out of six) classified by the BEAST and MD algorithms as similar (≤3 SDs) to the training set. Corresponding numerical values are displayed in **Appendix 6.** For all pellet strengths and coating levels, both the BEAST and MD metrics correctly classified all samples that deviated more than 1% from the training group as outliers. Therefore, these results are not presented in the graph. With respect to samples within ~1% of target coating level, the BEAST metric was more robust than the MD calculation in correctly identifying samples containing a desired target coating level. Furthermore, the BEAST was more effective at correctly classifying samples outside of the target coating range as outliers. However, it is important to note that for both algorithms, all false positive or false negative classifications had BEAST or MD distances that were borderline with respect to the 3 SD classification limit for spectral similarity. Possible sources for error include inherent size variability of individual pellets comprising a single sample, and variability of the reference method. Differences between the chemometric techniques may also provide some insight into the more robust performance of the BEAST metric in this application.

In a 1991 publication, Drennen and Lodder (138), provided an excellent comparison of the BEAST and MD methods. They demonstrated that the BEAST distance between the center of a training cluster and a sample spectrum is proportional to the concentration of the sample constituents that generate the vector connecting the center and sample spectral points. The direction of the vector provides the spectrum that identifies the constituents of the sample. The BEAST is nonparametric and makes no assumptions about the distribution of spectral points in hyperspace.

The MD metric assumes the spectral variations associated with both the calibration set and the test spectra are random. However, spectral noise is often not random, particularly in the analysis of complex samples. For the MD technique to function correctly, the spectral clusters must all share the same shape in hyperspace. Furthermore, these clusters must not be skewed. As a consequence, near-IR spectral discrimination using Mahalanobis distances is more likely to fail when the sample of interest is a complex mixture with many variables. Since multiparticulate systems are complex systems, which involve changing constituent concentrations, and are subject to scattering differences due to differences in particle sizes in the sample matrix, the BEAST metric may provide more reliability with regard to classification performance than the MD approach. Another explanation for these observed results involves the ability of the BEAST to account for skew and to provide an advantage in cases where limited training data is available.

Figures 47, 48, and 49 show calculated bootstrap distances versus % applied polymer for 150mg/g pellets coated with 6%, 10% and 14%, respectively. Note the increase in SD as the amount of applied polymer deviates from each respective target coating level. For each coating level, the bootstrap algorithm was effective in identifying when the desired coating level was achieved. All samples within 0.5% of each target coat were classified correctly by this pattern recognition technique. However, several samples containing ±1% applied polymer solids were also classified as acceptable. Such error is actually expected due to the fact that, within any given batch, the diameters of individual uncoated diltiazem HCl core pellets vary by as much 150 μm while the thickness of applied coating polymer varies by less than 2 μm within 1% of the target

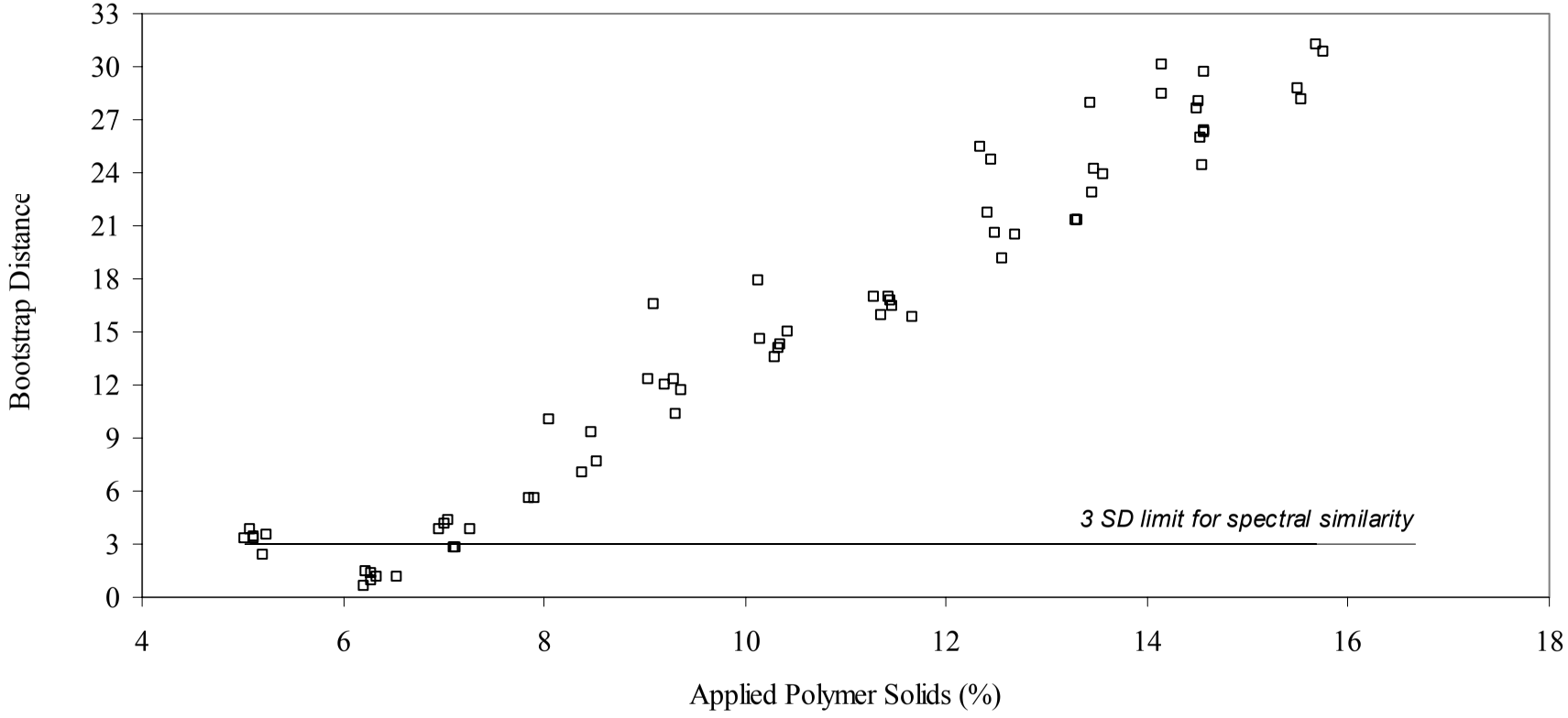

Figure 47. Qualitative Prediction of Applied Polymer Solids using the BEAST Algorithm. Target 6% coating level.

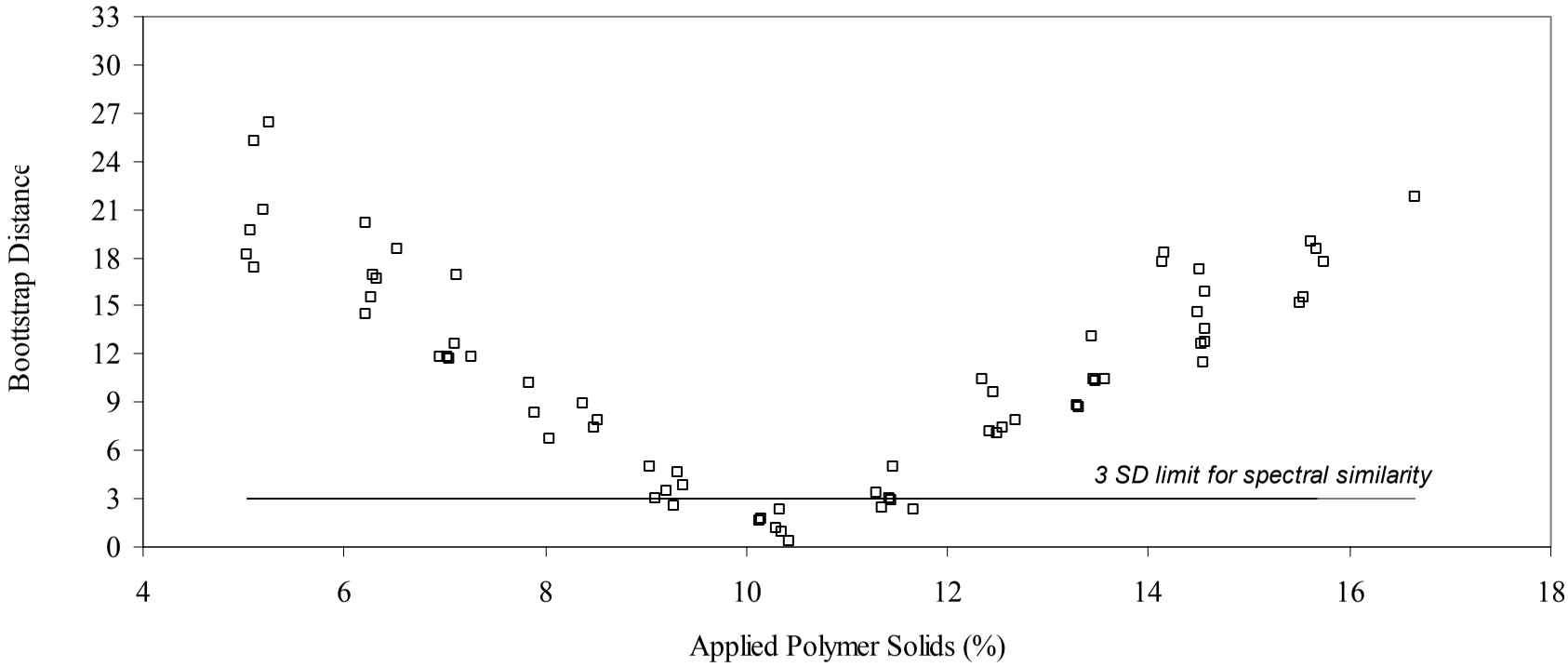

Figure 48. Qualitative Prediction of Applied Polymer Solids using the BEAST Algorithm. Target 10% Coating Level.

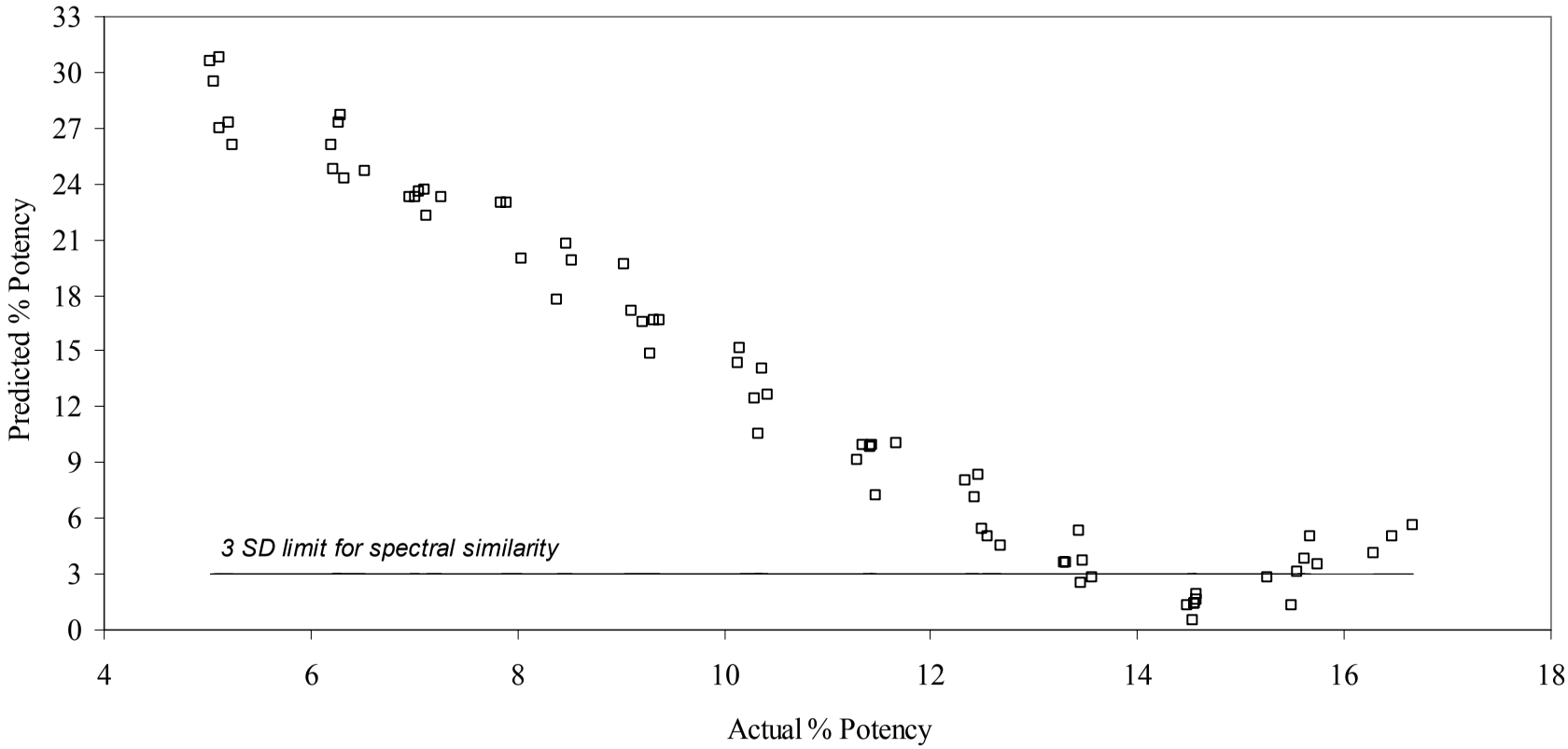

Figure 49. Qualitative Prediction of Applied Polymer Solids using the BEAST Algorithm. Target 14% Coating Level.

coat. Therefore, it is not unreasonable to have 1% variability in the actual polymer content of individual coated pellets or unit-dose samples. Nevertheless, qualitative near-IR techniques can provide a significant advantage over current methods of coating process monitoring, and errors of approximately 0.5% to 1% should be within acceptable limits for properly designed pellet products. In fact, FDA guidelines regarding scale-up and post-approval changes for modified release products (SUPAC-MR) (139). allows as much as 10% w/w change in quantity of drug release controlling polymer in a modified-release drug product, provided the dosage form meets application/compendial product release requirements and demonstrates dissolution similarity ($F2 > 50$) (140) with respect to the original ANDA or NDA exhibit lot formulation.

4 CONCLUSIONS

Controlled release pellet production often involves lengthy and expensive manufacturing operations in which there are no simple methods for accurately monitoring potency or applied polymer solids during processing. Typically, formulation scientists and manufacturing personnel rely solely on applied weight gain calculations to predict drug layering and coating process endpoints. In-process potency analysis is necessary to determine capsule fill weights needed to deliver a desired dose, and dissolution testing of the final dosage form is essential to ensure uniformity of the drug release rate. The availability of a rapid on-line or at-line measurement for prediction of process endpoints and evaluation of product quality characteristics may potentially save millions of dollars in time and materials. Therefore, the objective of this research was to develop and evaluate at-line and in-line near-infrared spectroscopic methods for assessing pharmaceutical pellet characteristics and to predict desired process endpoints.

The initial phase of this study demonstrated the utility of near-IR spectroscopy in the quantitative prediction of core pellet potency during rotogranulation operations. PCR or PLS based regression models were developed for predicting the potency of pellets containing diltiazem HCl over a range of 15% to 55% active drug content. Both in-line and at-line determination of pellet potency was effectively accomplished with average SEPs of 1.11% and 0.63%, respectively. The use of single or multiple wavelength

models also allowed acceptable potency prediction with average SEPs of 1.09% and 0.63%, for in-line and at-line analyses.

Although it was possible to develop a single calibration across the studied range of pellet strengths, non-linearity was noted between the response of the near-IR method and drug concentration across the broad range of the single calibration model. Such non-linearity may result in erroneous estimation of pellet potency, and could adversely affect the ability to validate such a method for routine use. Therefore, this study confirmed that the development of individual potency calibrations within specific pellet strength categories is preferred for this type of application.

The effective application of near-IR for predicting the endpoint of clinical or production scale batches was also demonstrated in this study. Prediction of pellet potency at pilot scale was accomplished using laboratory data. When process efficiencies vary, as they do, from lab scale equipment to larger equipment used for manufacturing, the availability of a rapid on-line or at-line measurement for prediction of process endpoints may potentially save millions of dollars in time and materials.

Perhaps one of the most important issues confirmed by this study is that traditional weight gain methods for monitoring rotogranulation operations are neither optimal nor reliable. True batch potency, as measured by HPLC and weight gain methods, differed by as much as 7% when systematic process problems were encountered during processing. Furthermore, even when no process issues were observed, actual pellet potency varied by an average of 3% from actual values. Such findings provide strong support for the development and routine use of in-line method for monitoring rotogranulation operations.

The second major phase of this study demonstrated the ability to monitor Wurster pellet coating operations and quantitatively predict applied coating level and dissolution characteristics. Calibrations for applied Eudragit RS30D polymer solids were developed for in-line or at-line analysis of a variety of pellet strengths using PCR, PLS, multiple wavelength and single wavelength models. All regression models demonstrated R^2 values of 0.98 or greater and standard errors of calibration less than 0.6%. As seen in the rotogranulation study, the simplistic single and multiple wavelength models also demonstrated their ability to accurately predict applied polymer solids content within 0.5% of laboratory values. Interestingly, the in-line model, in some instances, provided better prediction results than did the at-line method. This was attributed to the fact that in-line spectra were obtained by scanning through a stationary sapphire window sampling system which was developed for in-line monitoring of the Wurster coating operation.

Analysis of the dissolution characteristics of sustained release pellets was also explored in this study. Diltiazem HCl pellets containing 55% drug were coated with 12% to 16% Eudragit RS30D and subjected to dissolution testing in a USP II dissolution apparatus. The time to reach t50% was used as the reference value for near-IR calibration development. SEC and SEP values of approximately 7 minutes were obtained over a range of t50% values occurring between 4 h and 6 h. Implementation of such a method could dramatically reduce production cycle downtime by allowing production to proceed on the basis of acceptable near-IR results. Such applications would be particularly beneficial in the production of sustained-release products or products which have associated with them lengthy analytical testing procedures. However, the accuracy of the near-IR method cannot be better than the reference method from which it is built.

Therefore, representative samples, those which include all type of expected variation, must be included in the model to ensure method robustness.

In the final phase of this study, qualitative analysis of applied Eudragit RS30D polymer level was accomplished using either a Mahalanobis Distance (MD) calculation or a Bootstrap Error-Adjusted Single-sample Technique (BEAST). For all pellet strengths and coating levels studied, both the BEAST and MD metrics correctly classified all samples that deviated more than 1% from target as outliers. With respect to samples within ±1% of target coating level, the BEAST metric was more robust than the MD calculation in correctly identifying samples containing a desired target coating level. In agreement with findings of previous studies, the BEAST was more efficient than the MD metric in correctly classifying samples within or outside of the outside of the target coating range.

Using the BEAST metric for qualitative analysis of applied polymer coating, all samples within 0.5% of each target coat were classified correctly. However, several samples containing ±1% applied polymer solids were also classified as acceptable. Such error is actually expected due to inherent variability of the pellets being analyzed. Overall, both the BEAST and the MD algorithms were effective in qualitatively predicting pellet potency within about 1% of reference method values. Such results should be considered as acceptable for assessment of functional coating level of properly designed pellet systems.

This study has demonstrated the potential of near-infrared spectroscopy in quantitative and qualitative assessment of pelletized pharmaceutical product characteristics and in the identification of process endpoints at various stages of

manufacture. New at-line and in-line applications of near-IR analysis for monitoring and controlling pharmaceutical pellet production operations and assessing core and coated pellet characteristics were developed, and their practical limits investigated. Accurate near-IR assessment of core pellet potency and applied polymer solids during respective drug layering and coating operations, as well as qualitative identification of coating process endpoints was demonstrated utilizing both formulations and manufacturing processes that paralleled typical commercial pharmaceutical pellet production operations. Validation and implementation of the near-IR analysis techniques discussed in this manuscript could potentially reduce production cycle-times associated with the acquisition of laboratory test results while ensuring product quality compliance throughout various stages of the sustained-release pellet manufacturing process.

REFERENCES

1. I. Ghebre-Selassie. Pellets: A general overview. In I. Ghebre-Selassie (ed.), *Pharmaceutical Pelletization Technology*, Marcel Dekker, New York, 1989, pp. 1-13.

2. R. E. O'Connor and J. B. Schwartz. Drug release mechanism from a microcrystalline cellulose pellet system. *Pharm. Res.* **10**(3): 356 – 361 (1993).

3. M. Rabiskova and M. Chalabala. Slow release pellets containing beta-blocker. *Eur. J. Pharm. Sci.* **4**(101): 157 - 157 (1996).

4. R. Bodmier. Tableting of coated pellets. *Eur. J. Pharm. Biopharm.* **43**(1): 1 – 8 (1997).

5. B. Johansson, M. Wikberg, G. Alderborn, Compression behaviour and compactibility of microcrystalline cellulose in pellets in relationship to their pore structure and mechanical properties. *Int. J. Pharm.* **117**(1): 57 – 73 (1995).

6. T. E. Beckert, K. Lehmann, and P.C. Schmidt, Compression of enteric-coated pellets to disintegrating tablets. *Int J. Pharm.* **143**(1): 13 – 23 (1996)

7. K. Krogars, J. Heinamaki, J. Vesalahti, M. Marvola, O. Antikainen, and J. Yliruusi. Extrusion-spheronization of pH-sensitive polymeric matrix pellets for possible colonic drug delivery. *Int. J. Pharm*. **199**(2): 187 – 194 (2000).

8. W. Fischer, A. Boertz, S.S. Davis, R. Khosla, W. Cawello, K. Sandrock, and G. Cordes. Investigation of the gastrointestinal transit and i*n vivo* drug release of isosorbide-5-nitrate pellets, *Pharm. Res.* **4**(6): 480 – 485 (1987).

9. R. Cargill, L. J. Caldwel, K. Engle, J. A. Fix, P. A. Porter, and C.R. Gardner. Controlled gastric emptying. 1. Effects of physical properties on gastric residence times of nondisintegrating geometric shapes in beagle dogs. *Pharm. Res.* **5**(8): 533–536 (1988).

10. M. J. Gamlen. Pellet manufacture for controlled release. *Manuf. Chem*. **6**(6):55-59 (1985).

11. H**.** Ichikawa, Y. Fukumori, and C. M. Adeyeye. Design of prolonged-release microcapsules containing diclofenac sodium for oral suspensions and their preparation by the Wurster process. *Int. J. Pharm.* **156**(1): 39 – 48 (1997).

12. F. Goodhart. Centrifugal Equipment. In I. Ghebre-Selassie (ed.), *Pharmaceutical Pelletization Technology*, Marcel Dekker, New York, 1989, pp. 101-122.

13. D. M. Jones. Solution and suspension layering. In I. Ghebre-Selassie (ed.), *Pharmaceutical Pelletization Technology*, Marcel Dekker, New York, 1989, pp. 145-164.

14. C. Vecchio, F. Fabiani, M. E. Sangalli, L. Zema, A. Gazzaniga. Rotary tangential spray technique for aqueous film coating of ibuprofen pellets. *Drug Dev. Ind. Pharm.* **24**(3): 269 – 274 (1998).

15. Y. Fukumori. Coating of pharmaceutical powders by fluidized bed process. II. Microcapsules produced by layering of fine powder on coarse particles and subsequent aqueous enteric coating. *Chem. Pharm. Bull.* **36**(4): 1491-1501 (1988).

16. D. M. Jones. Factors to consider in fluid-bed processing. *Pharm. Tech.* **9:** 50-62 (1985).

17. B. N. Chukwumezie, M. Wojcik, P. Malak and C. M. Adeyeye. Feasibility studies in spheronization and scale-up of ibuprofen microparticulates using the rotor disk fluid-bed technology. *AAPS Pharm. Sci. Tech*. **3**(1): E2 (2003).

18. V. Rajan and S. Garg. Current status of drug delivery technologies and future directions. *Pharm. Tech. On-line*. **25**(2): 1-14 (2001).

19. V. Pillay and R. Fassihi. In vitro release modulation from crosslinked pellets for site-specific drug delivery to the gastrointestinal tract. I. Comparison of pH-responsive drug release and associated kinetics. *J. Control. Rel*. **59**(2):229-242 (1999).

20. Glatt Gmbh. Fluid Bed Coating. http://www.glatt.com /e/01_technologien/ 01_04_08.htm (accessed 09/06/08). part of The Glatt Group. http://www.glatt.com/ (accessed 09/06/08).

21. I. Ghebre-Saellassie, R. Gordon, M. B. Fawzi and R. U. Nesbitt. Evaluation of a high-speed pelletization process and equipment. *Drug Dev. Ind. Pharm.* **11**:1523-1541 (1985).

22. B. Gados. Rotary granulators – Evaluation of process technology for pellet production using factorial design. *Drugs Made Germ.* **27**:30-36 (1984).

23. R. Iyer, L. Augsburger, and D. Parikh. Evaluation of drug layering and coating: effect of process mode and binder level. *Drug Dev. Ind. Pharm.* **19**(9):981-998 (1993)

24. D. E. Wurster. Air suspension technique for coating drug particles: A preliminary report. *J. Pharm. Sci*. **48**: 451-455 (1959).

25. Guidance for Industry – PAT: A framework for innovative pharmaceutical development, manufacturing, and quality assurance. FDA. (September 2004).

26. J. E. Carroll, What does accelerating adoption of PAT-based approaches to pharmaceutical manufacturing mean for the makers of spectroscopic systems? *Spectrosc.* **20**(suppl. 1): 5-6 (2005).

27. J. Callis, D. Illman and B. Kowalski. Process analytical chemistry. *Anal. Chem.* **59**: 624A-637A (1987).

28. W. Blaser, R. Bredeweg, R. Harner, M. LaPack, A. Leugers, D. Martin, R. Pell, J. Workman, and L. Wright. Process analytical chemistry. *Anal. Chem.* **67** 47R-70R (1995).

29. D. Hassel and E. Bowman. Process analytical chemistry for spectroscopists. *Appl. Spectrosc.* **52:** 18A-29A (1998).

30. J. Workman, D. Veltkamp, S. Doherty, B. Anderson, K. Creasy, M. Koch, J. Tatera, A. Robinson, A. Bond, L. Burgess, G. Bokerman, A. Ullman, G. Darsey, F. Mozayeni, J. Bamberger, and M. Greenwood. Process analytical chemistry. *Anal. Chem.* **71**: 121R-180R (1999).

31. W. Herschel. Investigations of the powers of the prismatic colours to heat and illuminate objects; with remarks, that prove the different refrangibility of radiant heat. To which is added, an inquiry into the method of viewing the sun advantageously, with telescopes of large apertures and high magnifying powers. *Phil. Trans. Roy. Soc.* **90**: 255-283 (1800).

32. K. H. Norris. Design and development of a new moisture meter. *Agric. Eng.* **45**: 370-372 (1964).

33. P. Williams and K. Norris. *Near-infrared Technology in the Agricultural and Food Industries*, American Association of Cereal Chemists, St. Paul, MN, 1987.

34. D. A. Burns and E. W. Ciurczak. *Handbook of Near-infrared Analysis*. Marcel Dekker, New York, NY, 1992.

35. E. W. Ciurczak and J. K. Drennen. *Pharmaceutical and Medical Applications of NIR Spectroscopy*, Marcel Dekker, New York, NY, 2002.

36. K. A. Martin. Recent advances in near-infrared spectroscopy. *Appl. Spectrosc. Rev.* **27**(4): 325-383 (1992).

37. W. F. McClure. Near-infrared spectroscopy: The giant is running strong. *Anal. Chem.* **66**(1): 43A-53A (1994).

38. J. K. Drennen, E. G. Kraemer and R. A. Lodder. Advances and perspectives in near-infrared spectroscopy. *Crit. Rev. Anal. Chem.* **22**(6): 443-475 (1991).

39. E. Starck and K. Luchter. Near-infrared analysis (NIRA): A technology for quantitative and qualitative analysis. *Appl. Spectrosc. Rev.* **22**(4): 335-339 (1986).

40. E. W. Ciurczak. Uses of near-infrared spectroscopy in pharmaceutical analysis. *Appl. Spectrosc. Rev*. **23**: 143-163 (1987).

41. P. Corti, E. Dreassi, and F. Lonardi. Near infrared reflectance analysis: Feature and applications in pharmaceutical and biomedical analysis. *Il. Farmaco.* **48**: 3-20 (1993).

42. M. Josefson, I. Jedvert, S. Johansson and F. Langkilde. New opportunities with NIR spectrometry in the analysis of dosage forms. *Eur. J. Pharm. Sci.* **2**: 82-83 (1994).

43. W. Plugge and C. Van der Vlies. The use of near infrared spectroscopy in the quality control laboratory of the pharmaceutical industry. *J. Pharm. Biomed. Anal.* **10**: 797-803 (1992).

44. B. F. MacDonald and K. A. Prebble. Some applications of near-infrared reflectance analysis in the pharmaceutical industry. *J. Pharm. Biomed. Anal.* **11**: 1077-1085 (1993).

45. J. D. Kirsch and J. K. Drennen. Near-infrared spectroscopy: applications in the analysis of tablets and solid pharmaceutical dosage forms. *Appl. Spectrosc. Rev.* **30**(3), 139-174 (1995).

46. I. Murray and P.C. Williams. Chemcical principles of near-infrared technology. *In Near-infrared Technology in the Agricultural and Food Industries*. P. Williams and K. Norris (eds.), American Association of Cereal Chemists, St. Paul MN, pp 15-34.

47. E. W. Ciurczak. Principles of near-infrared spectroscopy. In *Handbook of Near-infrared Analysis*. D. A. Burns and E. W. Ciurczak (eds.), Marcel Dekker, New York, NY, 1992, pp. 7-12.

48. M. Blanco, J. Coello, H. Inturraiaga, S. Mospoch, and C. Pezuela. Near-infrared spectroscopy in the pharmaceutical industry. *Analyst*. **123**:135R-150R (1998).

49. C. A. Anderson, J. K. Drennen and Emil w. Ciurczak. Pharmaceutical applications of near-infrared spectroscopy. In D. A. Burns and E. W. Ciurczak (eds.), *Handbook of Near-infrared Analysis*, *Ed. 3,* Marcel Dekker, NY, 2007, pp 585 – 612.

50. S. D. Brown, T. B. Blank, S. T. Sum, and Lois G. Weyer. Chemometrics. *Anal. Chem.* **66**(12): 315R - 359R (1994).

51. S. Wold. Chemometrics, why, what and where to next. *J. Pharm. Biomed. Anal.* **9**(8): 589-596 (1991).

52. J. C. Berridge, P. Jones, and A. Roberts-McIntosh. Chemometrics in pharmaceutical analysis. *J. Pharm. Biomed. Anal.* **9**(8): 597-604 (1991).

53. P. Williams. Variables affecting near-infrared reflectance spectroscopic analysis. *In Near-infrared Technology in the Agricultural and Food Industries*. P. Williams and K. Norris (eds.), American Association of Cereal Chemists, St. Paul MN, pp. 143-167.

54. E. Ciurczak, R. Torlini and M. Demkowicz. Determination of particle size of pharmaceutical raw materials using near-infrared reflectance spectroscopy. *Spectrosc.* **1**: 36-39 (1987).

55. C. Bull. Compensation of particle size effects in near infrared reflectance. *Analyst* **116**: 781-786 (1991).

56. P. Frake, I. Gill, C. Luscombe, D. Rudd, J. Waterhouse and U. Jayasooriya. Near-infrared mass median particle size determination of lactose monohydrate, evaluating several chemometric approaches. *Analyst* **123**: 2043-2046 (1998).

57. A. O'Neil, R. Jee and A. Moffat. The application of multiple linear regression to the measurement of the median particle size of drugs and pharmaceutical excipients by near-infrared spectroscopy. *Analyst* **123**: 2297-2302 (1998).

58. O. Berntsson, T. Burger, S. Folestad, L. Daneilsson, J. Kuhn and J. Fricke. Effective sample size in diffuse reflectance near-IR spectroscopy. *Anal. Chem.* **71**: 617-623 (1999).

59. P. Kubelka and F. Munk. Ein beitrag zur optik der farbanstriche. *Z. Tech. Physik.* **12**:593 (1931).

60. G. S. Berth and H. G. Hecht. The physics of near-infrared reflectance. In P. Williams and K. Norris (eds.), *Near-Infrared Technology in the Agricultural and Food Industries*, American Association of Cereal Chemists, St. Paul, MN, 1987, pp. 1-15.

61. H.G. Hecht. The interpretation of diffuse reflectance spectra. *J. Res. Natl. Bur. Stand.* **80**(A):567 – 583 (1976).

62. M. Otsuka. Comparative particle size determination of phenacetin bulk powder by using Kubelka-Munk theory and principal component regression analysis based on near infrared spectroscopy. *Powd. Tech.* **141**: 244-250 (2004).

63. W. Hruschka. Data analysis: wavelength selection methods. In P. Williams and K. Norris (eds.), *Near-Infrared Technology in the Agricultural and Food Industries*, American Association of Cereal Chemists, St. Paul, MN, 1987, pp. 33-55.

64. R. Breretin. *Chemometrics. Data Analysis for the Laboratory and Chemical Plant*. Wiley, West Sussex, England, 2003; pp 147-163.

65. W. F. McClure. Analysis using fournier transforms. In D. A. Burns and E. W. Ciurczak (eds.), *Handbook of Near-infrared Analysis*, Marcel Dekker, New York, NY, 1992, pp 181 – 224.

66. T. Isaksson and T. Naes. The effect of multiplicative scatter correction (MSC) and linearity improvement in NIR spectroscopy. *Appl. Spectrosc.* **42**(7): 1273 - 1284 (1988).

67. E. W. Ciurczak. NIR Analysis of Pharmaceuticals. In D. A. Burnsand E. W. Ciurczak (eds.), *Handbook of Near-infrared Analysis*, Marcel Dekker, New York, NY, 1992, pp 549 – 563.

68. I. A. Cowe and J. W. McNichol. The use of principal components in the analysis of near-infrared spectra. *Appl. Spectros.* **39**(2): 257-266 (1985).

69. J. J. Workman. NIR spectroscopy calibration basics. In D. A. Burns and E. W. Ciurczak (eds.), *Handbook of Near-infrared Analysis*, Marcel Dekker, New York, NY, Ed. 3, 2007, pp 123-150.

70. James K. Drennen [a]; Elizabeth G. Kraemer [b]; Robert A. Lodder. Advances and perspectives in near-infrared spectrophotometry, *Critical Reviews in Analytical Chemistry*, **22**(6):443 – 475 (1991).

71. M. K. Boysworth and K. S. Booksh. Aspects of multivariate calibration applied to near-infrared spectroscopy. In D. A. Burns and E. W. Ciurczak (eds.), *Handbook of Near-infrared Analysis*, Marcel Dekker, New York, NY, Ed. 3, 2007, pp 207-231.

72. K. H. Erbensen, D. Guyot, F. Westad, and L. P. Houmoller. *Multivariate data analysis in practice: An introduction to multivariate data analysis and experimental design*. 5th Edition. Camo, Olso, Norway, 2002, pp 115 – 153.

73. R. Brereton. *Chemometrics: Applications of Mathematics and Statistics to Laboratory Systems*, Ellis Horwood, Sussex, UK, 1990.

74. M. Sharaf, D. Illman, and B. Kowalski. *Chemometrics*, Wiley, New York, NY, 1986., P. Geladi and B. R. Kowalski. Partial least-squares: A tutorial. *Anal. Chim. Acta.* **185**: 1-17 (1986).

75. H. Martens and T. Naes. *Multivariate Calibration*, Wiley, Chichester, UK, 1989.

76. H. L. Mark and D. Tunnell. Qualitative near-infrared reflectance analysis using Mahalanobis distances. *Anal Chem*. **57**(7): 1449-1456.

77. P. J. Gemperline, L. D. Webber, and F. O. Cox. Raw materials testing using soft independent modeling of class analogy analysis of near-infrared reflectance spectra. *Anal Chem*. **61**(2): 138-144.

78. R. A. Lodder and G. M. Hieftje. Quantile BEAST attacks the false-sample problem in near-infrared reflectance analysis. *Appl. Spectrosc.* **42**(8): 1351-1365 (1988).

79. B. Efron and R. Tibshirani. Bootstrap measures for standard errors, confidence intervals, and other measures of statistical accuracy. *Stat. Sci.* **1**(1): 54-77.

80. R.A Lodder, M. Selby, and G.M. Heiftje. Detection of capsule tampering by near-infrared spectroscopy. *Appl. Spectrosc.*, **59**: 1921-1930 (1987).

81. R..A Lodder and G.M. Heiftje. Analysis of intact tablets by near-infrared spectroscopy. *Appl. Spectrosc*., **42**: 556-558 (1988).

82. S. Katju, Kreft, B. Kozamernik and U. Urleb. Qualitative determination of polyvinylpyrrolidone type by near-infrared spectrometry. *Int. J. Pharm.*, **177**(1): 1-6 (1999).

83. J. D Kirsch and J. K. Drennen. Near-infrared spectroscopic monitoring of the film coating process. *Pharm. Res*., **13**(2): 234-237 (1996).

84. A. S. El-Hagrasy, H. R. Morris, F. D'Amico, R. A. Lodder, J. K. Drennen. Near-infrared spectroscopy and imaging for the monitoring of powder blend homogeneity. *J. Pharm. Sci.* 90(9): 1298-1307 (2001).

85. J. D. Kirsch, and J. K. Drennen. Nondestructive tablet hardness testing by near-infrared spectroscopy: a new and robust spectral best-fit algorithm. *J. Pharm. Biomed. Anal*. **19**(3-4): 351-362 (1999).

86. R. Jensen, E. Peuchant, I. Castagne, A. M. Boirac, G. Roux. One-step quantification of active ingredient in pharmaceutical tablets using near-infrared spectroscopy. *Spectros. Int. J.* **6**: 63-72 (1988).

87. P. Corti, E. Degrassi, G. Corbini, S. Lonardi and S. Gravina. Application of near infrared reflectance spectroscopy to pharmaceutical control: I. Preliminary investigation of the uniformity of tablets content. *Analusis* **18**: 112-116 (1990).

88. R. G. Buice, T. B. Gold, R. A. Lodder and G. A. Digenis. Determination of moisture in intact gelatin capsule by near-infrared spectrophotometry. *Pharm. Res.* **12**(1): 160-163 (1995).

89. P. Corti, E. Dreassi, G. Corbini, L. Montecchi, and J. Paggi. Application of near-infrared spectroscopy to pharmaceutical quality control. II: Assay of cloxacillin benzatine in creams. *Analusis* **18**: 117-121 (1990).

90. E. W. Ciurczak and R. P. Torlini. Analysis of solid and liquid dosage forms via NIRS. *Spectrosc.* **2**(3), 36-39 (1987).

91. J. Lin and C. Brown. Near-IR fiber-optic probe for electrolytes in aqueous solution. *Anal. Chem.* **65**: 287-292 (1993).

92. L. J. Galante, M. A. Brinkley, and R. A. Lodder. Bacterial monitoring in vials using a spectrophotometric assimilation method. *Pharm. Res.* **9**(3): 357-364 (1992).

93. L. J. Galante. M. A. Brinkley, J. K. Drennen. and R. A. Lodder. Near-infrared spectrometry of microorganisms in liquid pharmaceuticals. *Anal. Chem.* **62**: 2514-2521 (1990).

94. Near-infrared Spectrometry. In *The United States Pharmacopeia 27*, United States Pharmacopeial Convention, Rockville, MD, 2004, pp. 2569-2573.

95. Guidance for Industry – Analytical procedures and methods validation chemistry: manufacturing, and controls documentation. FDA. (September 2004).

96. J. E. Sinsheimer and A. M. Keuhnelian. Near-infrared spectroscopy of amine salts. *J. Pharm Sci.* **55**: 1240-1244 (1966).

97. N. Odu and E. Inaba. Determination of allylisopropylacetireide and phenacetin in pharmaceutical preparations by near-infrared absorption spectroscopy. *Yakugaku Zasshi* **87**: 213-215 (1967).

98. S. Lonardi, R. Viviani, L. Masconi, M. Bernuzzi, P. Corti, E. Dreassi,. C. Murratzu and G. Corbini. Drug analysis by near-infrared reflectance spectroscopy: Determination of the active ingredient and water content in antibiotic powders. *J. Pharm. Biomed. Anal.* **7**(3): 303-308 (1989).

99. E. W. Ciurczak. Pharmaceutical mixing studies using near-infrared spectroscopy. *Pharm. Tech.* **15**(9): 140-145 (1991).

100. B. G. Osborne. Determination of nicotinamide in pre-mixes by near-infrared spectroscopy. *Analyst* **112**(3): 313-315 (1987).

101. D. J. Wargo and J. K. Drennen. Near-infrared characterization of powdered blends. *J. Pharm. Biomed. Anal*. **14**(11): 1415-1423 (1996).

102. J. C. Chasseur. On-line assay of cimetidine granules by near infrared reflectance spectroscopy. *Chim. Oggi.* **6**: 21-24 (1987).

103. S. Watano, H. Takashima, Y. Sato, K. Miyanami, and T. Yasumoto. IR absorption characteristics of a near-IR moisture sensor and mechanism of water transfer in fluidized bed granulation. *Adv. Pwdr. Technol.*, **90**: 153-159 (1997).

104. J. White. On-line moisture detection for a microwave vacuum dryer. *Pharm. Res.*, **11**: 728-732 (1994).

105. R. Jensen, E. Peuchant, I. Castagne, A. M. Boirac, G. Roux. One-step quantification of active ingredient in pharmaceutical tablets using near-infrared spectroscopy. *Spectros. Int. J*. **6**: 63-72 (1988).

106. J. Lin and C. Brown. Near-IR fiber-optic probe for electrolytes in aqueous solution. *Anal. Chem.* **65**: 287-292 (1993).

107. L. J. Galante, M. A. Brinkley, and R. A. Lodder. Bacterial monitoring in vials using a spectrophotometric assimilation method. *Pharm. Res.* **9**(3): 357-364 (1992).

108. L. J. Galante. M. A. Brinkley, J. K. Drennen. and R. A. Lodder. Near-infrared spectrometry of microorganisms in liquid pharmaceuticals. *Anal. Chem.* **62**: 2514-2521 (1990).

109. K. Morisseau and C. Rhodes. Pharmaceutical uses of near-IR spectroscopy. *Drug Dev. Ind. Pharm.* **21**: 1071-1090 (1995).

110. K. Marshall and E. M. Rudnic. Tablet dosage forms. In G. Banker and C. T. Rhodes (eds.), *Modern Pharmaceutics*, Marcel Dekker, New York, 1990, pp. 355-425.

111. S. Han and P. Faulkner. Determination of SB 216469-S during tablet production using near-infrared spectroscopy. *J. Pharm. Biomed. Anal.* **14:** 1681-1689 (1996).

112. D. D. MacLaren and R. G. Hollenbeck. A high performance liquid chromatographic method for the determination of the amount of hydroxpropyl methylcellulose applied to tablets during an aqueous film coating operation. *Drug Dev. Ind. Pharm.* **13**: 2179-2197 (1987).

113. L. Scattergood, K. Fegely, P. Rege, D. Ferrizzi and A. Rajabi-Siohbooi. Comparative study of theoretical versus actual weight gain for Surelease barrier membrane pellets. Presented at AAPS Annual Meeting, November 2004.

114. J. D. Kirsch and J. K. Drennen. Determination of film-coated tablet parameters by near-infrared spectroscopy. *J. Pharm. Biomed. Anal.* **13**: 1273-1281 (1995).

115. J. K. Drennen and J. D. Kirsch. Apparatus for nondestructively inspecting a coated article and associated method. US Patent 5,750,996. (May 12, 1998).

116. B. R. Buchanan, M. A. Baxter, T. S. Chen, X. A. Qin, P. A. Robinson. Use of near-infrared spectroscopy to evaluated an active in a film coated tablet, *Pharm. Res.* **13**: 616-621 (1996).

117. M. Andersson, M. Josefson, F. Langkilde and K. G. Wahlund. Monitoring of film coating process for tablets using near infrared reflectance spectroscopy. *J. Pharm. Biomed. Anal*. **20:** 27-37 (1999).

118. G. A. Duff, S. A. Thornton, B. R. Buchanan and M. A. Baxter. On-line monitoring of pelletized product uniformity by remote reflectance near-infrared spectroscopy. *STP Pharma. Pratiques* **4**(1): 1-4 (1994).

119. M. Andersson, S. Folestad, J. Gottfires, M. O. Johansson, M. Josefson, and K. G. Wahlund. Quantitative analysis of film coating in a fluidized bed process by in-line NIR spectrometry and multivariate batch calibration. *Anal. Chem.*, **72**: 2099-2108 (2000).

120. M. Andersson, B. Holmquist, J. Linquist, O. Nilsson and K. G. Wahlund. Analysis of film coating thickness and surface area of pharmaceutical pellets using fluorescence microscopy and image analysis. *J. Pharm. Biomed. Anal.* **22**: 325-339 (2000).

121. O. Berntsson, L. G. Danielsson and S. Folestad. Characterization of diffuse reflectance fiber probe sampling moving solids using a Fourier transform near-infrared spectrometer. *Anal. Chim. Acta.* **431**: 125-131 (2001).

122. S. Sekulic, H. Ward, D. Brannegan, E. Stanley, C. Evans, S. Sciavolino, P. Hailey and P. Aldridge, On-line monitoring of powder blend homogeneity by near-infrared spectroscopy. *Anal.Chem.* **68:** 509-513 (1996).

123. P. Hailey, P. Doherty and P. Tapsell, T. Oliver and P. Aldridge. Automated system for the on-line monitoring of powder blending processes using near-infrared spectroscopy Part I. System development and control. *J. Pharm. Biomed. Anal.* **14:** 551-559.

124. T. Burger, J. Kuhn, R. Caps and J. Fricke. Quantitative determination of the scattering and absorption coefficients from diffuse reflectance and transmittance measurements. *J. Appl. Spectrosc.* **51**: 309-317 (1997).

125. T. Burger, J. Fricke and J. Kuhn. NIR radiative transfer investigations to characterize powders and their mixtures. *J. Near Infrared Spectrosc*. **6**: 33-40 (1998).

126. G. Kemeny, T. Pokorny, E. Nagy, G. Istok and E. Doromby. Optical analysis instrument having rotating optical standards. PCT Patent Application, WO 8503575 A1 (1985).

127. J. W. MacTaggert. Infrared constituent analyzer and control system. UK Patent GB2147413A (1985).

128. J. A. Sumen, J. S. Tornberg. Procedure for measuring components of a coating on a moving base material. United States Patent 5,914,490 (1999).

129. M. Andersson, O. Svensson, S. Folestad, M. Josefson, and K. G. Wahlund. Near-IR spectroscopy on moving solids using a scanning grating spectrometer – Impact on multivariate process analysis. *Chemomet. Intel. Lab. Syst*. **75**: 1-11 (2005).

130. Diltiazem HCl Extended-release Capsules, *U.S. Pharmacopeia 24*, US Pharmacopeial Convention: Rockville, MD, 2000, p. 75.

131. C. D. Melia, B. R. Hansjaj, K. A. Khan, and I. R. Wilding. A simple and rapid method for the quantification of Eudragit RS100 and RL100 poly(methacrylates) in sustained-release dosage forms. *Pharm. Res.* **8**(7): 899-902 (1991).

132. Manual for Near Infrared Spectral Analysis Software (NSAS V. 3,23), NIRSystems, Silver Spring, MD, 1990.

133. H. Mark and J. Workman. Chemometrics in spectroscopy. *Spectrosc.*, **13**(6): 19-21 (1998).

134. (<612> Chromatography, *U.S. Pharmacopeia 24,* US Pharmacopeial Convention: Rockville, MD, 2000, p. 2281.

135. W. L. Yoon, R. D. Jee and A. C. Moffat. Optimization of sample presentation for the near-infrared spectra of pharmaceutical excipients. *Analyst*, **123**:1029-1034 (1998).

136. R. Bodmier, X. Guo, R. Sarabia and P. Skultety. The influence of buffer species and strength on diltiazem HCl release from beads coated with aqueous cationic polymers dispersions, Eudragit RS, RL 30D. *Pharm. Res.* **13**(1); 52-56 (1996),

137. S. Narisawa, M. Nagata, C. Danyoshi, H. Yoshino, K. Murata, Y. Hirakawa, and K. Noda. An organic acid-induced sigmoidal release system for oral controlled-release preparations. *Pharm. Res*. **11**(1):111-116 (1994)

138. J. K. Drennen and R. A. Lodder. Qualitative analysis using near-infrared spectroscopy. A comparison of discriminant methods in dissolution testing. *Spectrosc*. **6**(8): 34-39 (1991).

139. Guidance for Industry – SUPAC-MR: Scale-up and post-approval changes: Modified release solid oral dosage forms. FDA. (September 1997).

140. Guidance for Industry – SUPAC-IR: Scale-up and post-approval changes: Immediate release solid oral dosage forms. FDA. (November 1995).

APPENDICES

Appendix 1. Laboratory-scale diltiazem HCl pellet particle size distribution via sieve analysis.

Mesh Size	Aperture (μm)	Aperture Midpoint (μm)	Trial #1 (% retained)	Trial #2 (% retained)	Trial #3 (% retained)
		150 mg/g			
14	1400	1550	2	0	0
16	1180	1290	2.4	0	0
18	1000	1090	0.4	0.4	0.4
20	850	925	52.4	56	57.9
25	710	780	42.8	43.6	41.7
30	600	655	0	0	0
40	425	513	0	0	0
		300 mg/g			
14	1400	1550	0	0	0
16	1180	1290	0	0	0
18	1000	1090	8	8.8	9.2
20	850	925	90.4	89.2	88.8
25	710	780	1.6	2	2
30	600	655	0	0	0
40	425	513	0	0	0
		550 mg/g			
14	1400	1550	0.4	0.8	3.6
16	1180	1290	0.8	0.4	0.4
18	1000	1090	90	79.2	77
20	850	925	8	19.6	19
25	710	780	0.4	0	0
30	600	655	0.4	0	0
40	425	513	0	0	0

Appendix 2. Pilot-scale diltiazem HCl 550mg/g pellet particle size distribution via sieve analysis

Mesh Size	Aperture (μm)	Aperture Midpoint (μm)	Trial #1 (% retained)	Trial #2 (% retained)
14	1400	1550	0.9	1.5
16	1180	1290	1.5	3.1
18	1000	1090	81.7	77.1
20	850	925	14.9	17.6
25	710	780	1.0	0.7
30	600	655	0	0
40	425	513	0	0

Appendix 3. Dissolution Data for Eudragit RS30D Coated Pellets – 12% w/w Coat

	% Diltiazem HCl Released															
Time (min)	1	2	3	4	5	6	7	8	9	10	11	12	min	max	mean	SD
0	0	0	0	0	0	0	0	0	0	0	0	0	0	0	0	
60	2	2	3	3	3	2	2	3	1	3	3	3	1	3	2.5	0.7
120	3	3	4	4	4	3	3	3	2	2	3	3	2	4	3.1	0.7
150	5	5	5	5	5	5	5	5	4	3	5	5	3	5	4.8	0.6
160	5	5	5	5	5	5	6	5	4	4	5	5	4	6	4.9	0.5
170	5	6	6	6	5	6	6	6	5	4	6	5	4	6	5.5	0.7
180	6	6	7	7	7	7	7	7	7	6	7	7	6	7	6.8	0.5
190	7	7	10	9	9	9	8	9	9	7	10	9	7	10	8.6	1.1
200	10	12	12	11	13	10	10	11	12	11	13	13	10	13	11.5	1.2
210	13	15	16	15	18	14	14	18	16	18	17	18	13	18	16.0	1.8
220	21	22	23	22	26	22	22	25	22	24	24	24	21	26	23.1	1.5
230	28	29	30	30	33	30	29	32	29	31	32	31	28	33	30.3	1.5
240	38	39	39	40	42	41	40	43	40	41	41	40	38	43	40.3	1.4
250	49	49	50	50	52	51	51	52	51	53	53	52	49	53	51.1	1.4
260	59	60	60	61	61	63	63	65	60	62	61	60	59	65	61.3	1.7
270	70	70	71	72	72	73	72	74	71	73	73	73	70	74	72.0	1.3
280	77	76	75	80	79	80	79	80	79	79	79	79	75	80	78.5	1.6
290	83	83	82	84	85	87	87	86	86	86	86	87	82	87	85.2	1.7
300	88	89	88	89	90	92	92	91	90	90	91	91	88	92	90.1	1.4
310	91	92	90	91	92	93	94	94	93	92	94	94	90	94	92.5	1.4
320	94	95	92	96	96	96	97	96	95	94	96	95	92	97	95.2	1.3
330	95	95	94	97	96	97	98	98	97	96	97	96	94	98	96.3	1.2
340	96	96	95	98	96	98	98	97	97	98	96	98	95	98	96.9	1.1
350	97	98	98	99	97	99	100	98	98	99	98	99	97	100	98.3	0.9
360	99	100	101	100	99	101	100	99	100	101	99	99	99	101	99.8	0.8
370	100	100	101	99	100	100	100	101	101	100	102	100	99	102	100.3	0.8
380	100	101	100	101	99	100	99	102	100	102	101	100	99	102	100.4	1.0
390	101	101	102	100	100	100	99	100	100	101	102	101	99	102	100.6	0.9
400	100	101	101	100	101	101	100	101	99	100	101	101	99	101	100.5	0.7
410	101	100	101	101	101	101	100	100	100	101	100	100	100	101	100.5	0.5
420	101	101	101	100	100	100	101	100	100	100	101	101	100	101	100.5	0.5
430	101	100	102	100	101	100	101	100	101	101	102	100	100	102	100.8	0.8
440	101	102	101	100	102	100	102	100	102	102	101	101	100	102	101.2	0.8
450	101	102	100	101	102	101	101	100	102	101	101	101	100	102	101.1	0.7
460	101	102	100	101	102	101	101	100	102	100	100	101	100	102	100.9	0.8
470	100	101	101	101	102	100	100	101	102	100	101	102	100	102	100.9	0.8
480	100	101	102	101	102	101	101	101	102	101	100	102	100	102	101.2	0.7

Data fit to $y = y_0 + a/\left(1 + e^{-((x-x_0)/b)}\right)$ for t50% dissolution analysis where:

a = 98.4757

b = 23.3649

x_o = 250.6261

y_o = 2.0915

Appendix 4. Dissolution Data for Eudragit RS30D Coated Pellets – 14% w/w Coat

	% Diltiazem HCl Released															
Time (min)	1	2	3	4	5	6	7	8	9	10	11	12	min	max	mean	SD
0	0	0	0	0	0	0	0	0	0	0	0	0	0	0	0	
60	1	2	3	3	2	2	3	3	1	3	2	3	1	3	2.3	0.8
120	3	4	5	4	3	4	3	2	3	3	3	5	2	5	3.5	0.9
150	4	5	3	4	5	5	4	5	5	4	3	5	3	5	4.3	0.8
160	5	5	4	6	4	4	5	5	6	5	4	6	4	6	4.9	0.8
170	6	6	5	6	6	6	5	4	6	5	5	4	4	6	5.3	0.8
180	6	6	6	6	5	6	5	4	7	6	6	5	4	7	5.7	0.8
190	6	6	7	7	5	6	6	5	6	6	6	5	5	7	5.9	0.7
200	7	8	8	6	6	7	6	6	7	7	7	7	6	8	6.8	0.7
210	8	10	10	8	8	8	7	8	9	10	9	9	7	10	8.7	1.0
220	10	12	12	10	13	10	10	11	12	11	13	12	10	13	11.3	1.2
230	15	16	17	14	15	13	14	16	17	16	18	18	13	18	15.8	1.6
240	20	22	23	20	21	20	22	23	22	21	24	23	20	24	21.8	1.4
250	26	29	30	28	27	27	29	29	30	26	32	30	26	32	28.6	1.8
260	36	37	39	37	39	35	38	35	38	35	41	40	35	41	37.5	2.0
270	46	49	52	47	49	47	51	49	46	46	51	52	46	52	48.8	2.3
280	55	60	62	58	60	57	60	60	58	57	60	62	55	62	59.1	2.1
290	67	69	73	69	71	68	69	68	68	66	71	73	66	73	69.3	2.2
300	76	78	81	77	80	78	78	75	77	75	80	81	75	81	78.0	2.1
310	84	85	87	85	85	84	83	81	82	84	87	86	81	87	84.4	1.8
320	89	91	92	90	89	90	88	87	87	89	90	92	87	92	89.5	1.7
330	91	93	94	94	91	92	92	90	89	93	94	94	89	94	92.3	1.7
340	93	95	93	96	93	94	94	93	91	96	96	96	91	96	94.2	1.6
350	96	97	96	98	95	95	96	94	93	97	99	97	93	99	96.1	1.7
360	97	97	98	99	96	96	97	94	96	98	100	98	94	100	97.2	1.6
370	99	97	98	100	98	97	97	96	97	98	101	99	96	101	98.1	1.4
380	99	99	100	100	100	98	98	98	99	100	101	101	98	101	99.4	1.1
390	101	99	102	101	100	99	100	99	100	101	100	100	99	102	100.2	0.9
400	100	101	101	100	101	101	100	101	99	100	101	101	99	101	100.5	0.7
410	101	100	101	101	101	101	100	100	100	101	100	100	100	101	100.5	0.5
420	101	102	100	101	102	101	101	100	102	101	101	101	100	102	101.1	0.7
430	100	101	101	101	102	100	100	101	102	100	101	102	100	102	100.9	0.8
440	100	101	100	101	102	101	101	101	102	101	100	102	100	102	101.0	0.7
450	101	101	101	100	100	100	101	100	100	100	101	101	100	101	100.5	0.5
460	101	102	100	101	101	101	101	100	102	100	100	101	100	102	100.8	0.7
470	101	100	101	101	101	101	100	100	100	101	100	100	100	101	100.5	0.5
480	100	101	102	100	102	101	101	101	102	101	100	102	100	102	101.1	0.8

Data fit to $y = y_0 + a/\left(1 + e^{-((x-x_0)/b)}\right)$ for t50% dissolution analysis where:

a = 97.5053

b = 23.0576

x_o = 273.1917

y_o = 3.0055

Appendix 5. Dissolution Data for Eudragit RS30D Coated Pellets – 16% w/w Coat

	% Diltiazem HCl Released															
Time (min)	1	2	3	4	5	6	7	8	9	10	11	12	min	max	mean	SD
0	0	0	0	0	0	0	0	0	0	0	0	0	0	0	0	
60	1	3	2	3	4	2	1	3	2	4	3	3	1	4	2.6	1.0
120	3	4	4	4	5	3	3	4	3	5	4	3	3	5	3.8	0.8
150	4	4	5	4	5	4	4	5	3	5	5	3	3	5	4.3	0.8
160	4	5	5	4	5	5	4	6	4	5	5	4	4	6	4.7	0.7
170	5	5	6	5	5	5	5	6	5	5	6	4	4	6	5.2	0.6
180	5	5	6	5	5	6	5	6	5	5	6	4	4	6	5.3	0.6
190	5	5	6	6	5	6	5	6	5	5	7	5	5	7	5.5	0.7
200	6	5	7	6	5	6	5	6	6	6	7	6	5	7	5.9	0.7
210	7	6	7	7	6	7	6	7	6	6	7	7	6	7	6.6	0.5
220	7	7	8	8	7	8	7	7	7	7	8	8	7	8	7.4	0.5
230	8	9	10	9	9	10	9	8	9	8	9	9	8	10	8.9	0.7
240	11	12	12	12	12	13	12	10	12	11	13	12	10	13	11.8	0.8
250	15	15	16	15	16	16	15	13	15	14	16	15	13	16	15.1	0.9
260	20	21	21	22	22	23	23	20	22	20	21	21	20	23	21.3	1.1
270	26	28	27	29	30	30	29	27	28	27	29	28	26	30	28.2	1.3
280	34	37	35	38	38	38	37	35	36	36	38	38	34	38	36.7	1.4
290	46	48	45	47	49	48	46	44	47	46	48	49	44	49	46.9	1.6
300	57	57	56	57	60	58	56	55	56	57	59	58	55	60	57.2	1.4
310	68	67	65	69	71	69	67	66	65	68	70	66	65	71	67.6	1.9
320	78	76	74	78	79	78	76	75	75	76	78	75	74	79	76.5	1.6
330	84	83	82	86	87	86	84	83	83	83	87	82	82	87	84.2	1.9
340	89	87	87	91	91	91	89	87	88	87	90	86	86	91	88.6	1.8
350	92	93	94	93	92	92	92	90	90	93	94	94	90	94	92.4	1.4
360	91	95	94	96	92	94	93	93	91	96	95	96	91	96	93.8	1.9
370	95	98	97	98	95	95	96	94	93	98	98	97	93	98	96.2	1.7
380	96	98	98	99	96	96	97	95	96	98	100	98	95	100	97.3	1.5
390	97	97	98	100	97	99	99	98	97	99	97	99	97	100	98.1	1.1
400	98	98	99	100	98	99	99	100	99	100	97	99	97	100	98.8	0.9
410	99	98	99	100	99	99	99	102	101	100	98	100	98	102	99.5	1.2
420	100	99	100	101	100	101	100	103	102	102	99	101	99	103	100.7	1.2
430	100	100	100	102	100	99	100	102	101	101	100	100	99	102	100.4	0.9
440	99	100	100	101	99	100	101	103	100	101	100	101	99	103	100.4	1.1
450	100	100	101	100	100	101	101	103	100	102	101	102	100	103	100.9	1.0
460	101	100	100	99	100	101	100	103	101	103	101	102	99	103	100.9	1.2
470	101	101	100	100	100	102	101	103	102	102	101	101	100	103	101.2	0.9
480	102	103	101	99	101	103	102	102	101	101	102	102	99	103	101.6	1.1

Data fit to $y = y_0 + a/\left(1 + e^{-((x-x_0)/b)}\right)$ for t50% dissolution analysis where:

a = 96.9432

b = 23.1678

x_o = 294.9015

y_o = 3.6087

Appendix 6. Qualitative prediction of target applied polymer solids. Comparison of BEAST and Mahalanobis distance metrics.

150mg/gram Pellets

Applied Polymer Solids	Total Samples	BEAST Classification		MD Classification	
		Acceptable	Unacceptable	Acceptable	Unacceptable
5%	6	1	5	3	3
6%*	6	6	0	5	1
7%	6	2	4	2	4
9%	6	5	1	3	3
10%*	6	6	0	4	2
11%	6	3	3	3	3
14%	6	2	4	3	3
15%*	6	6	0	4	2
16%	6	2	4	4	2

300mg/gram Pellets

Applied Polymer Solids	Total Samples	BEAST Classification		MD Classification	
		Acceptable	Unacceptable	Acceptable	Unacceptable
5%	6	2	4	3	3
6%*	6	6	0	4	2
7%	6	1	5	4	2
9%	6	1	5	3	3
10%*	6	6	0	3	3
11%	6	2	4	2	4
14%	6	1	5	2	4
15%*	6	5	1	4	2
16%	6	1	5	1	5

550mg/gram Pellets

Applied Polymer Solids	Total Samples	BEAST Classification		MD Classification	
		Acceptable	Unacceptable	Acceptable	Unacceptable
5%	6	1	5	2	4
6%*	6	6	0	3	3
7%	6	1	5	1	5
9%	6	0	6	3	3
10%*	6	6	0	3	3
11%	6	1	5	3	3
14%	6	1	5	2	4
15%*	6	6	0	4	2
16%	6	0	6	2	4

* Denotes Training Sample